TRANSPORTATION RESEARCH RECORD 810

Layered Pavement Systems

TRANSPORTATION RESEARCH BOARD

COMMISSION ON SOCIOTECHNICAL SYSTEMS
NATIONAL RESEARCH COUNCIL

NATIONAL ACADEMY OF SCIENCES
WASHINGTON, D.C. 1981

TRR 810

Contents

Effective Granular Modulus to Model Pavement Responses

RICHARD W. MAY AND MATTHEW W. WITCZAK

This report presents the results of a research study to further investigate the initial findings of an earlier research project concerning the prediction of pavement deflections. The principal objective of this study was to explore the consistent lack of agreement between field-measured deflections and those computed by using elastic-layered theory coupled with nonlinear dynamic modulus tests. During several periods of the year, surface deflections were measured with the Thumper testing vehicles on the same three Maryland flexible pavement sections that were previously studied. These field deflections were predicted mathematically for a large number of specific test conditions. Although these predicted deflections failed to match the measured values, a consistent trend in the ratio of the corresponding deflections was detected. As suggested in a previous study, an adjustment factor was applied to the granular base modulus to cause the deflection ratio to approach one. Linear log-log relationships were derived between this factor and increasing measured deflection values. From this analysis, it was surmised that current laboratory methods of granular material characterization appear to be inadequate for modeling in situ behavior, regardless of the measuring device. Based on the findings of recent seismic research, further analysis was made to determine whether a relationship exists between the adjustment factor and the induced shear strain in the granular layer. A clear curvilinear plot was produced, which indicated that the adjustment to the granular modulus is definitely related to the shear strain that develops in response to the surface loading. As a result, a procedure was presented for correcting for the effective in situ granular base modulus.

With the development of theory to model layered flexible pavement structure, researchers and designers realize the importance of obtaining accurate estimates of the actual field conditions. Laboratory testing of core samples taken from in-service highway pavements to estimate in situ strength characteristics is time consuming, destructive, and expensive. In contrast, surface deflection measurements are recognized as a valuable tool for obtaining quantitative information about a pavement structure because of its simplicity and nondestructive nature.

Currently, a large amount of research work that uses elastic-layered theory is involved in the determination of the in situ moduli of some or all of the layers that constitute a pavement system. The accuracy of these models is dependent on the manner in which the material properties are obtained and entered into the program. Adjustments to the models have been suggested (1-3) to incorporate the effects of test load frequency, temperature, and stress dependency on material behavior. Further improvement is advocated in the characterization of the granular base course material (4). Because of the large scatter that accompanies laboratory testing of remolded specimens, a better method is needed for evaluating the strength of this layer.

STUDY OBJECTIVE

This study (5) was initiated to further research results of a previous study (6) that observed a consistent trend in the analysis of deflections measured with a road rater and a Benkelman beam. The same three Maryland state highway sections were tested by measuring surface deflections by using the Federal Highway Administration (FHWA) pavement testing device called "Thumper." Measurements were made at three frequencies, four load magnitudes, and five times during the year to increase the data base obtained by using the other two deflection devices.

ANALYSIS PROCEDURE

The testing was conducted on field test sections of US-1, MD-97, and Interstate 695. At the time the data were taken, US-1 displayed extensive surface cracking, MD-97 had some minor surface cracking especially in the wheelpath, and I-695 was completely intact. For each of these sections, layer thicknesses and material characterizations were previously established (7) and are presented in Figure 1 and Table 1, respectively. The moduli of the asphalt-stabilized layers were obtained from Shell nomographs developed for these particular mix designs and are a function of pavement temperature and load frequency. The temperature within each asphalt layer for each Thumper test date was calculated from surface measurements and relationships developed by Southgate (8). As shown in Table 1, the moduli of the lower layers were determined in the laboratory

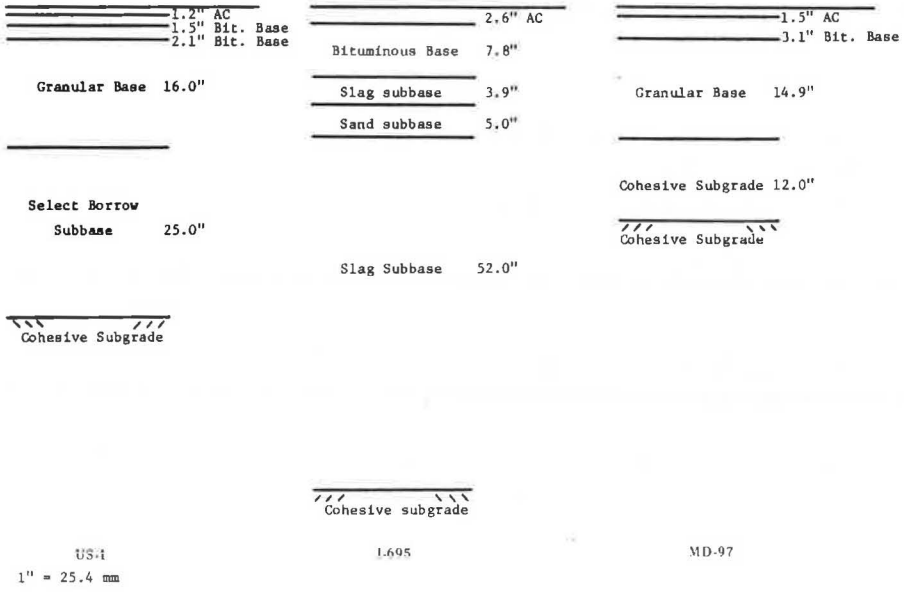

Figure 1. Average cross-sections of Maryland pavements.

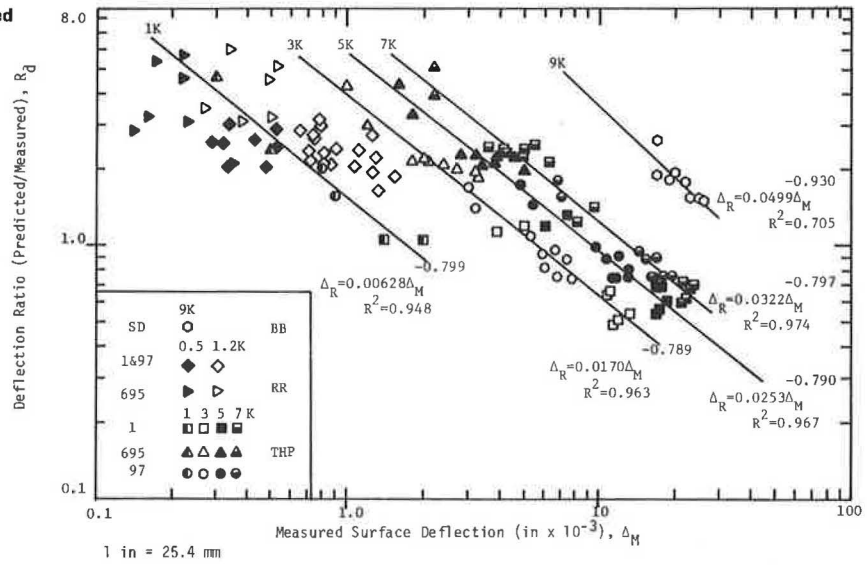

Figure 3. Deflection ratio versus measured deflection.

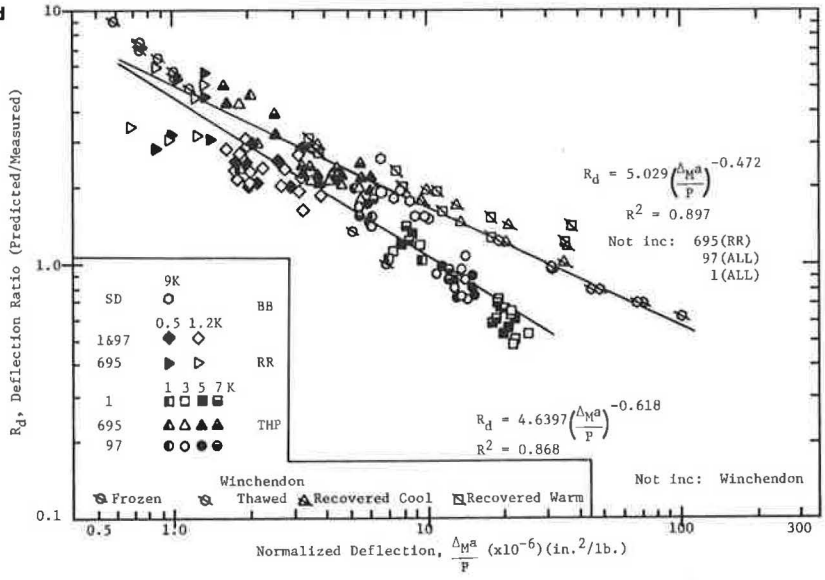

Figure 4. Deflection ratio versus normal measured deflection.

shown in Figure 4. In view of all the possible sources of error, the amount of scatter is extremely small. These data show that some consistent and rational cause appears to be responsible for the lack of agreement between measured and calculated deflections.

Data for the Winchendon test section appear to fall slightly out of line with the rest of points plotted in Figure 4. Although analysis of these data is still in progress, this deviation may be partly explained by a closer examination of the individual data points. MD-97 and especially US-1 had considerable surface cracking that was not taken into account in the characterization of the modulus of this layer. If the original asphalt concrete moduli for these sections were reduced to reflect the loss of structural integrity due to cracking, the predicted or computed deflection would increase and, in turn, increase the deflection ratio. This revision could conceivably cause the MD-97 and US-1 data to align more closely with the I-695, San Diego road test, and Winchendon data; however, further research must be conducted before conclusive results can be reached.

Granular Modulus Adjustment

Past research (4,11) has shown deficiencies in current methods for evaluation of granular material in the laboratory. In this study, because of these uncertainties in remolding and compacting granular material for modulus testing in the laboratory and the suggestions of other research results (6,12), the granular base modulus was modified to produce agreement between measured and computed deflections. Assuming that the multilayer elastic computer model is satisfactory and the modular inputs of the other layers are appropriate, the revised pavement layer system is believed to be compatible with field behavior.

The procedure used for adjusting the modulus of the granular layer was the same as that reported by D'Amato and Witczak (6). The resilient modulus equation obtained from dynamic laboratory testing is of the form

$$M_R = k_1 \theta^{k_2} \quad (1)$$

where k_1 and k_2 are laboratory-derived regres-

Figure 5. K_1-factor versus measured surface deflection for thumper data points only.

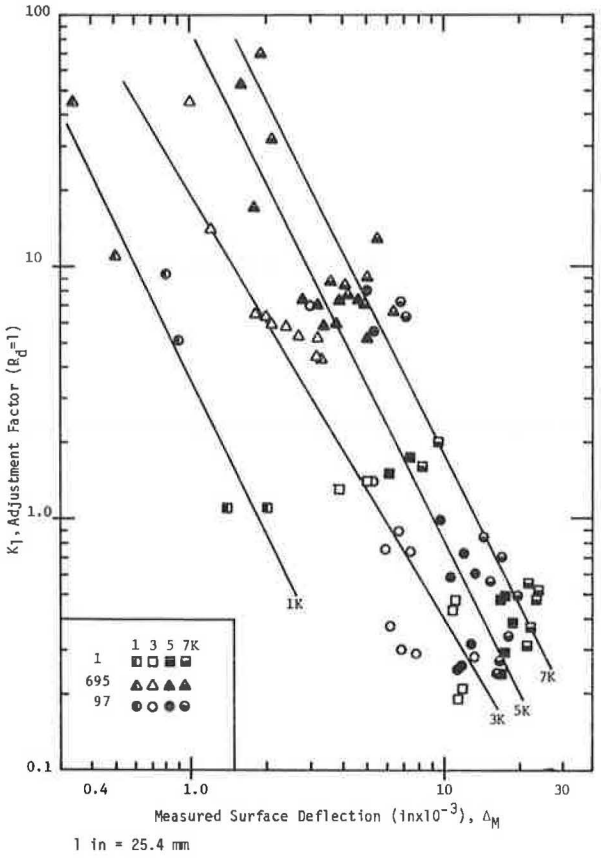

Figure 6. K_1-factor versus normal measured deflection.

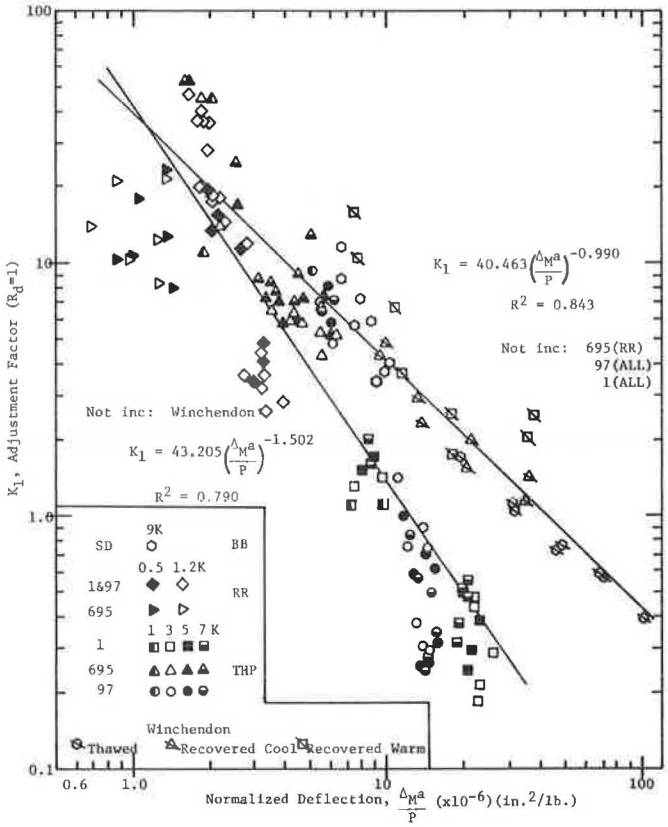

sion constants and θ represents the first stress invariant (bulk stress). In this study, the computed surface deflections were made to equate to the measured values (R_d = 1). The resulting equation used in this approach was

$$M_R = K_1 k_1 \theta^{k_2} \quad (2)$$

where K_1 is an empirical adjustment factor.

In the iterative procedure of the modified program, the combined coefficient K_1k_1 is entered into the program and changed repeatedly until the center deflections match those measured in the field.

A plot of the calculated K_1-values at a deflection ratio equal to one (R_d = 1) versus the deflections measured by using Thumper is shown in Figure 5. Although there is scatter in the data, a trend of decreasing K_1 with increasing surface deflection is clearly visible for each load magnitude. As before, the K_1-factor versus deflection data was made normal to eliminate the variables of load and surface contact and this is plotted in Figure 6 along with the results of the previous D'Amato and Witczak study. Again, the scatter is more pronounced with the I-695 road-rater data. The additional data from Winchendon continue to appear isolated when compared with the other data. However, if the US-1 and MD-97 data are revised to incorporate a reduced surface modulus as described previously, the entire data set may provide a good correlation. With a lower asphalt surface modulus, the K_1-factor necessary to obtain the same field-measured deflection would increase, which would cause all data points to tend to coincide along a unique relationship. Although this hypothesis is speculative, certain problems are unavoidable in the use of original material properties to model pavement responses with elastic layer theory when the existing surface is severely cracked.

Effective Base Modulus

The final iteration of the computer program analysis provided the final modulus for each sublayer at a deflection ratio of one (R_d = 1). The resulting moduli represent the effective response of the lower layers. These lower moduli of the sublayers were averaged together into one composite granular base modulus (E_B) and one composite subgrade modulus.

In Figure 7, the average granular base modulus was plotted against the measured deflection. The trend of increasing base modulus with decreasing surface deflection is intuitively correct; however, a lot of scatter is shown in these data. This scatter is expected because the surface deflection can result from varying amounts of displacement in the other layers as well. Again, definitive bands of data for each load magnitude demonstrate the linear elastic behavior of the material. These individual bands were blended together by using the same normalization process described earlier. A plot of these data along with the additional Winchendon data is shown in Figure 8. This extreme range of effective material moduli presented in Figure 8, for even the same pavement section, is not just an indication of the need to incorporate stress-dependent effects. It illustrates the necessity for further examination of the in situ characterization of granular material.

Once again, the Winchendon data plot above the data from US-1 and MD-97 in the lower portion of the figure. As before, if the cracking in the surface of these pavements was considered, by reducing the moduli of the existing material, the effective base

Figure 7. Average effective granular base modulus versus measured surface deflection.

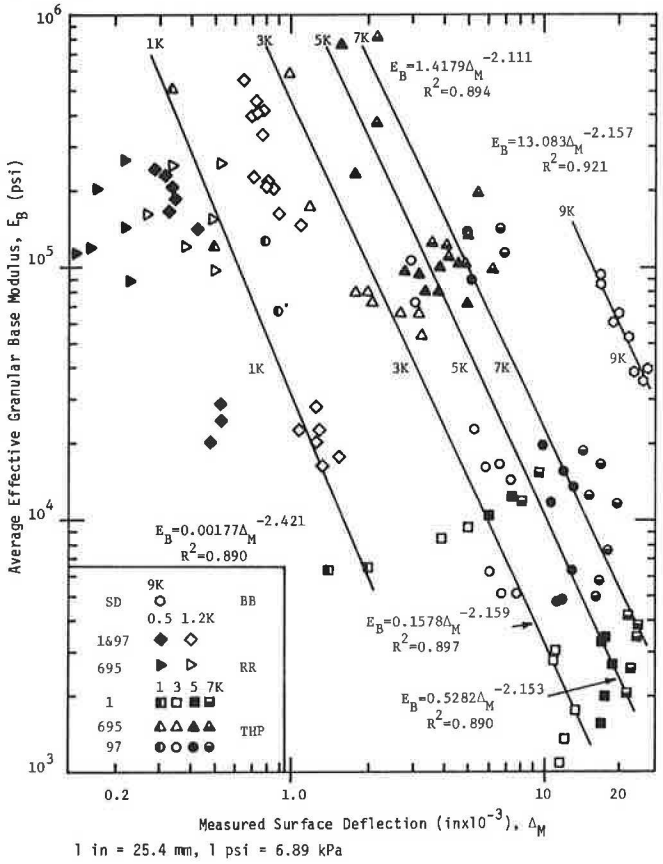

Figure 8. Base modulus versus normal measured deflection.

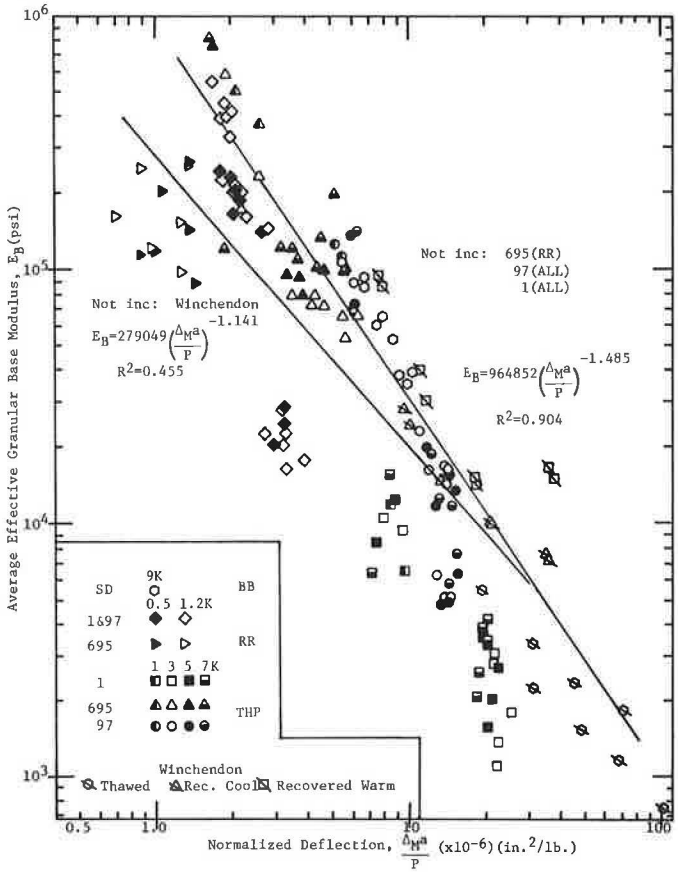

modulus necessary to produce the same deflection would certainly increase.

Associated Shear Strain

The modulus of granular material is a function of density, gradation, degree of saturation, angularity of the particles, and stress state (13). As such, duplication in the laboratory of the actual particle structure that exists in the field is impossible. Recent studies, directed toward development of better understanding of soil response under dynamic loading conditions, have indicated that the shear modulus (G) of a granular soil is dependent on both the level of shear strain and stress state. Ideal relationships have been developed that show that the shear modulus of a granular soil decreases with increasing shear strain (12), as shown in Figure 9, according to the equation:

$$G = 1000K_2(\sigma_m')^{0.5} \quad (3)$$

In this expression the K_2-value has been related to magnitude of the shear strain.

This equation is similar to the modified resilient modulus equation (Equation 2) if the elastic modulus (E) is substituted into the equation along with a typical Poisson ratio:

$$E = 2800K_2(\sigma_m')^{0.5} \quad (4)$$

By using the Chevron N-layer program to compute the principal strains at the middle of the adjusted granular base layer beneath the center of loading and the following Mohr circle of strain relationship, D'Amato and Witczak examined the hypothesis (6)

Figure 9. Shear modulus of granular soil related to shear strain.

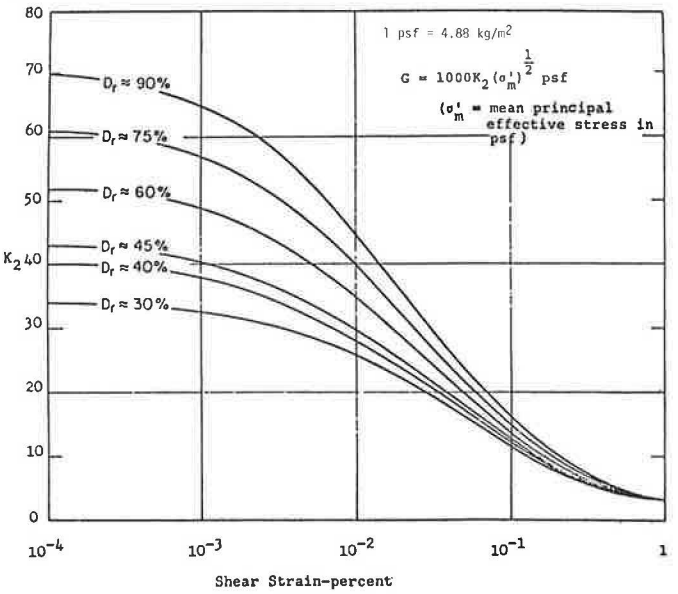

$$\gamma_{MAX} = \epsilon_1 - \epsilon_2 \quad (5)$$

where ϵ_1 and ϵ_2 are the principal strains. They found separate linear relationships for the road-rater and Benkelman beam data. The effect of shear strain also appeared to diminish when the strain was large and the slope of the Benkelman beam data was considerably flatter. This corresponded

conceptually with the change in slope of the ideal curves of Figure 9 (12).

The shear strain hypothesis was extended further by including the data determined from measurements of Thumper deflection. Plots of all the data for the three devices revealed a unique family of curves for each pavement section, depending on the magnitude of test load, as shown in Figures 10-12. These plots show that the K_1-factor appears to be a function of pavement structure, test load, and developed shear strain. The shear strain developed in the I-695 section was relatively low, as expected in a very stiff pavement that produced higher values for K_1. In the US-1 section, the induced shear strain was much higher. This is not only a result of a thinner cross section, but, the high strain in the granular layer is probably a consequence of a severely cracked surface course, which was not distributing the load. The MD-97 section, which is even thinner, falls in between the other two pavements with respect to shear strain and K_1-values. The San Diego road test data, plotted on Figure 10, had the highest shear strains and unusually high K_1-factors for these corresponding strains; this is partly explained by the heavy [9000-lb (40-kN)] load, applied through a flexible tire to very thin test sections.

Unfortunately, shear strain data for the Winchendon test sections are not available at this time. For all the sections analyzed, one general characteristic could be found: The deflection increased naturally with load and, consequently, the maximum shear strain also increased.

The in situ modulus of the granular layer [designated as $K_1 \times M_R$(laboratory)] can vary significantly from the original laboratory resilient modulus as shown in the figures. This variation may be caused by differences in the shear strain, which is mobilized under the triaxial simulation devices, from that induced in the field. Slight differences in shear strain may mean large differences between the two moduli (K_1), especially when measured de-

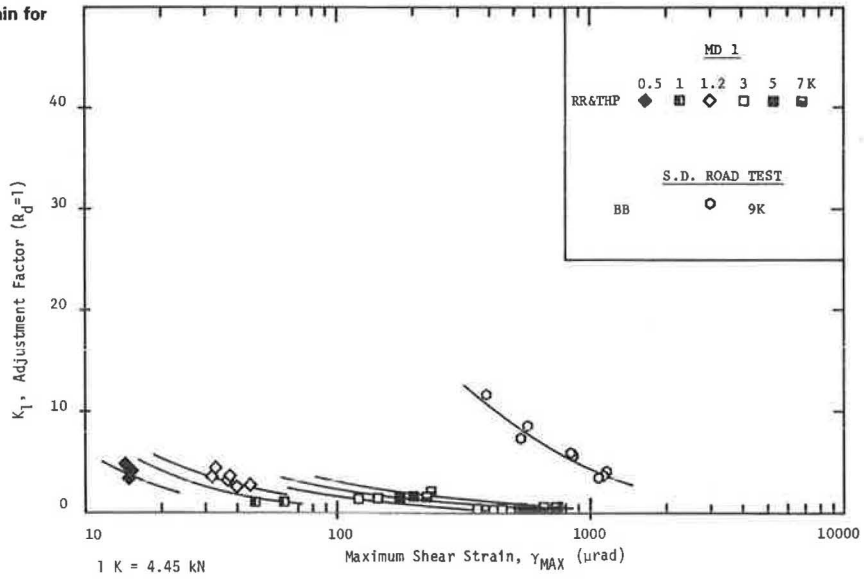

Figure 10. K_1-factor versus maximum shear strain for US-1 and San Diego data.

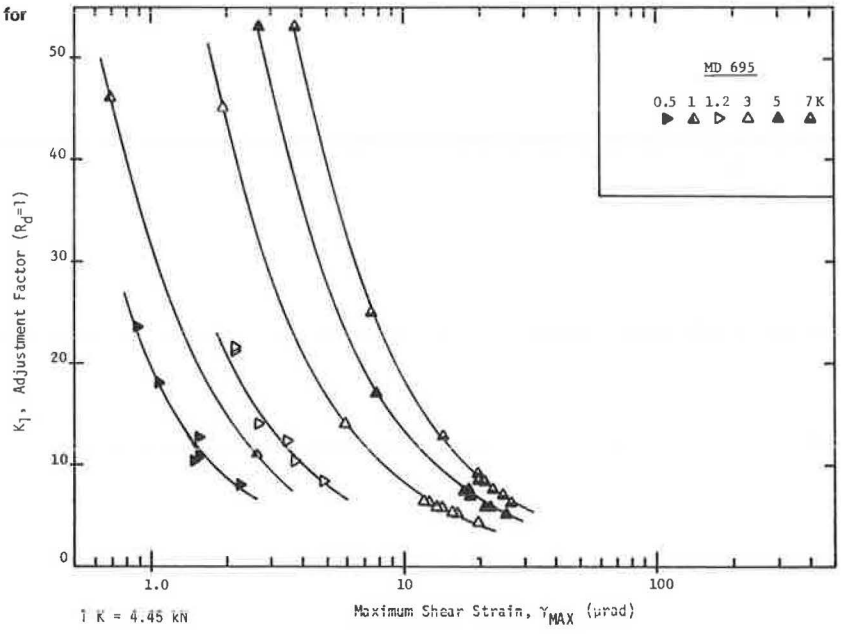

Figure 11. K_1-factor versus maximum shear strain for I-695 data.

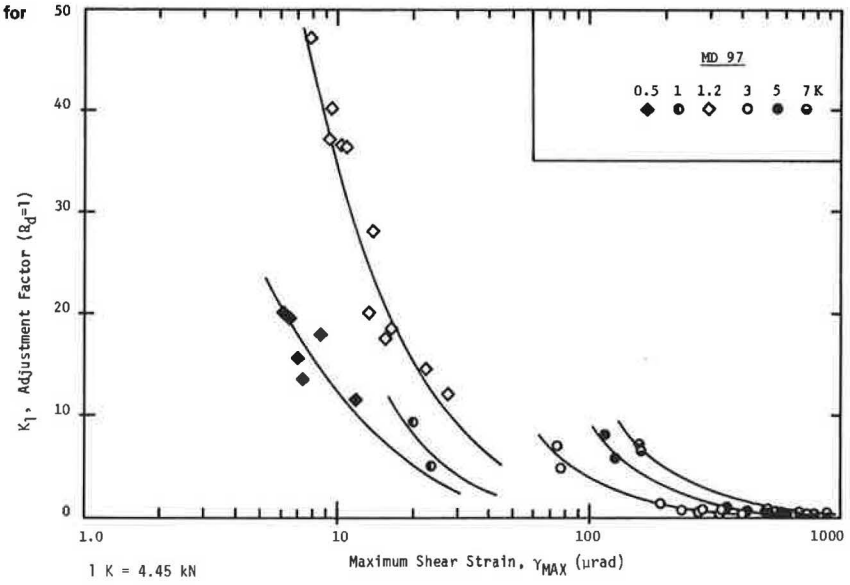

Figure 12. K_1-factor versus maximum shear strain for MD-97 data.

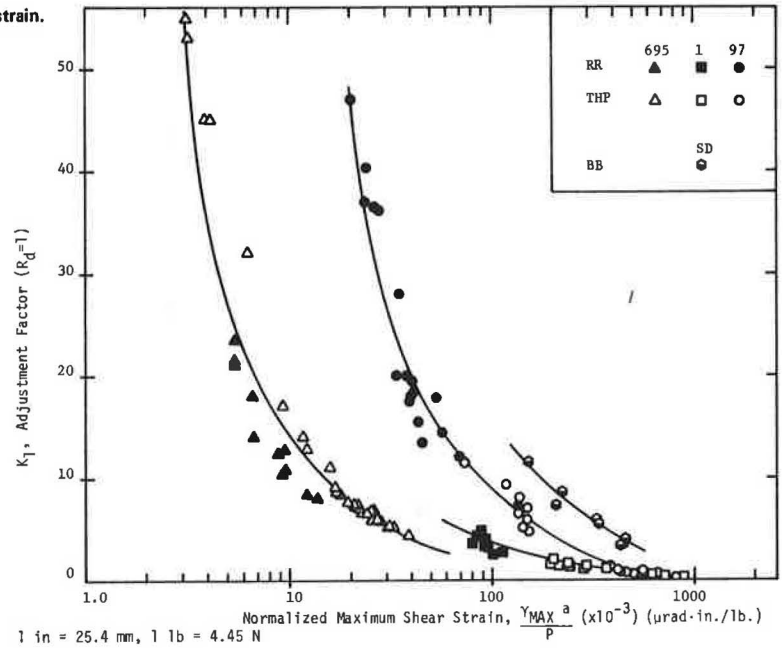

Figure 13. K_1-factor versus normal maximum shear strain.

flections or shear strains are relatively low. Granular materials, when recompacted in the laboratory to field density and moisture conditions, will probably not construct the same fabric or particle structure that exists in the pavement. Since the modulus of this layer is affected by so many variables, the values determined in the laboratory may not be completely accurate.

The amount of shear strain development in the granular layer, which apparently influences the magnitude of adjustment (K_1) required for the laboratory modulus, is naturally dependent on the structural characteristics of each particular pavement section. Close examination of Figures 10-12 shows that the shape of the curves are the same; however, each set of curves, for each pavement, appears to be shifted along the horizontal shear-strain axis. This idea is better illustrated in Figure 13; all the data have been normalized, as before, for test load and contact surface, and are shown in one plot. Here, four separate curves can be distinguished for the four different pavement sections that were used to produce the data. Again, the curvilinear trend of decreasing K_1 with increasing shear strain is shown; however, in this figure, a convergence of the curves at the high shear strains is clearly presented. This convergence closely resembles that shown in Figure 9, developed from the dynamic studies. Similarly, at the low end of the shear-strain scale, the curves are expected to flatten out when the deflections and shear strain become very small, although no data exist to verify such an extrapolation.

The separation of the data according to pavement structure can be partly compensated by accounting for the thickness of the granular base layer. When a load is imposed on the pavement surface, the shear strain will obviously vary with depth regardless of the type of material. In this study, the average depth of the granular layer or the approximate mid-

Figure 14. K_1-factor versus normal maximum shear strain times average base depth.

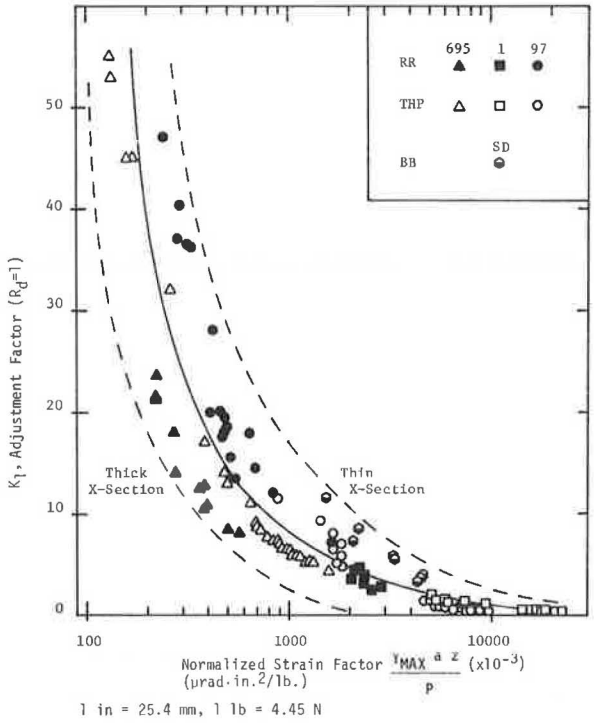

1 in = 25.4 mm, 1 lb = 4.45 N

point of the granular layer was simply figured into the normalized expression of maximum shear strain, as shown in Figure 14.

The spread of the data is greatly reduced; however, the scatter is still rather extensive, especially for logarithmic scales. This scatter has a clearly defined basis in the fact that the points blend from an extremely stiff pavement to a relatively weak pavement in going from left to right (outside to inside) across the band of data. For example, at a K_1 equal to 6, the normalized shear-strain expression is 1100, 1800, and 3300 for sections I-695, MD-97, and the San Diego test road, respectively. The stronger pavement naturally experiences the lesser shear strain. This grading aspect holds true at every level of K_1. From this analysis, there appears to be some basis for the K_1 modification of the granular layer modulus and this basis seems to be connected to the shear strain mobilized in this layer.

PROCEDURE FOR ESTIMATING SUBGRADE MODULUS

The most-important potential for testing pavement deflection is the possibility of evaluating the modulus of the subgrade without having to drill cores and take samples back to the laboratory. Subgrade response is extremely variable in the field and poses the most problems when designing the proper thickness of pavement overlay. This section presents a tentative procedure for obtaining an approximation of the subgrade modulus by using elastic layer theory and one of the relationships developed in this study.

The procedure is based on the premise that accurate information is available on the materials that were used in the construction of the upper layers of the existing pavement. The moduli of the asphalt surface layers are assumed to be known or obtainable from laboratory mix testing results. In addition, it is presumed that the coefficients of resilient modulus testing, performed on the base course materials, are accessible or can be approximated from experience.

Initially, the procedure requires the average field-measured deflection response (Δ_M) at the center of the applied test load. For these measurements, the temperature, test frequency, magnitude of the load, and time of day should be recorded. The asphalt surfacing moduli are adjusted for field conditions as a function of the test temperature and frequency.

In addition to deflection, the method employs the relationship shown in Figure 6. In the absence of further research regarding the effect of surface cracking on the US-1 and MD-97 data, a relationship closer to that found in the Winchendon data may be more accurate for preliminary use. The solution for subgrade modulus involves the following steps:

1. Compute the normalized deflection [$\Delta_M a/P(x10^{-6})$],
2. Determine the K_1-adjustment factor by using Figure 6,
3. Use elastic layered theory and the modified resilient modulus relationship for the granular material ($K_1 k_1 \theta^{k_2}$) to calculate the predicted deflection (Δ_p), and
4. Repeat this solution of Δ_p for various assumed subgrade modulus values until $\Delta_p = \Delta_M$.

Although the solution is based on purely empirical relationships, evidence is substantial that a rational explanation exists in the behavior of granular material. As discussed previously, the characterization of this material in the laboratory by using remolded specimens is highly questionable. In Figure 13, the curves that relate the computed maximum shear strain to the adjustment factor (K_1) necessary for matching deflections suggest that differences in shear strain development between laboratory and field situations are responsible.

CONCLUSIONS

In summary, the results presented in this report are preliminary because the data base is limited to only a few different pavement sections. However, based on the results obtained, we can unequivocably state that the type of device used in making the deflection measurements is independent from the relationships described. Further investigation is necessary to substantiate these findings with data obtained from other flexible pavement sections. The following is a list of conclusions reached as a result of this study:

1. The major factor that contributes to the discrepancy between measured and theoretically predicted surface deflections (from a layered-elastic program) lies in the current procedure for characterizing the resilient modulus (M_R) of granular materials in the laboratory.
2. The data produced from this research study with the FHWA Thumper exhibit complete agreement with earlier work, which demonstrates that an adjustment factor (K_1) must be applied to the value of the laboratory-resilient modulus in order to obtain equal measured and predicted deflections (by multilayer-elastic theory); this K_1 adjustment was found to vary linearly with surface deflections on a log-log scale.
3. Evidence is substantial that the in situ effective modulus ($K_1 M_R$) of the granular layer is a function not only of the stress state but also the magnitude of the shear strain induced in that layer by the surface loading. For low levels of shear

strain, the effective in situ modulus is much larger than at higher levels of shear strain.

4. The amount of shear-strain development in the granular layer appears to be related to the overall pavement strength in addition to loading magnitude, which is intuitively correct.

5. Since shear strain cannot be measured easily in the field, a provisional procedure was developed and outlined for estimating the granular base modulus adjustment factor (K_1) directly from field-measured deflection results by using an empirically derived relationship from this study.

6. With the bituminous surface and granular base layers of a conventional asphalt pavement accurately characterized, elastic-layered theory can be used to compute the subgrade modulus by matching surface deflections.

From the results of this study, the possibility of the behavior of granular material being related to mobilized shear strain seems entirely plausible. We recommend that this connection be further investigated over a broader range of pavement sections to incorporate different material types and climate conditions. In recognition of all the possible sources of error that could enter into the production of the data used in this study (e.g., field deflection measurement, laboratory material testing, mathematical manipulation, and existing natural variation), the amount of scatter exhibited in the relationships involving the proposed adjustment factor is simply too small to forego additional exploration.

ACKNOWLEDGMENT

We are indebted to the Maryland State Highway Administration for providing traffic control to assist the field testing performed under this study.

REFERENCES

1. B.S. Coffman. Pavement Deflections from Laboratory Tests and Layer Theory. Proc., 2nd International Conference on the Structural Design of Asphalt Pavements, Univ. of Michigan, Ann Arbor, Aug. 1967.
2. C.L. Monismith, H.B. Seed, F.G. Mitry, and C.K. Chan. Prediction of Pavement Deflections from Laboratory Tests. Proc., 2nd International Conference on the Structural Design of Asphalt Pavements, Univ. of Michigan, Ann Arbor, Aug. 1967.
3. L.H. Irwin. Determination of Pavement Layer Moduli from Surface Deflection Data for Pavement Performance Evaluation. Proc., 4th International Conference on the Structural Design of Asphalt Pavements, Univ. of Michigan, Ann Arbor, Vol. 1, Aug. 1977.
4. H.B. Seed, F.G. Mitry, C.L. Monismith, and C.K. Chan; University of California. Prediction of Flexible Pavement Deflections from Laboratory Repeated-Load Tests. National Cooperative Highway Research Program, Rept. 35, 1967, 117 pp.
5. R.W. May. Interpreting Dynamic Surface Deflections in the Granular Base Layer of the Pavement Structure. FHWA, Staff Study Rept. FHWA/RD-80/149, Feb. 1981.
6. P.A. D'Amato and M.W. Witczak. Analysis of In Situ Granular-Layer Modulus from Dynamic Road-Rater Deflections. TRB, Transportation Research Record 755, 1980, pp. 20-30.
7. M.W. Witczak and K.R. Bell. Remaining-Life Analysis of Flexible Pavements. Proc., Assn. of Asphalt Paving Technologists, Lake Buena Vista, FL, Vol. 47, 1978.
8. H.F. Southgate. An Evaluation of Temperature Distribution Within Asphalt Pavements and Its Relationship to Pavement Deflections. Kentucky Department of Highways, Frankfort, Rept. KYHPR-64-20, 1968.
9. M.W. Witczak. A Study of the Deflection Behavior of the Ikalanian Sand Winchendon Test Section. U.S. Army Cold Regions Research and Engineering Laboratory, Hanover, NH, Jan. 1980.
10. M.P. Jones and M.W. Witczak. Subgrade Modulus on the San Diego Test Road. TRB, Transportation Research Record 641, 1977, pp. 1-6.
11. S.F. Brown. Repeated Load Testing of a Granular Material. Geotechnical Engineering Journal of ASCE, Vol. 100, No. GT7, July 1974, pp. 825-841.
12. Bechtel Power Corporation. Seismic Analysis of Structures and Equipment for Nuclear Power Plants. Bechtel Power Corporation, San Francisco, CA, Rept. BC-TOP-4-A, Rev. 3, Nov. 1974.
13. R.G. Hicks and C.L. Monismith. Factors Influencing the Resilient Response of Granular Materials. HRB, Highway Research Record 345, 1971, pp. 15-31.

Publication of this paper sponsored by Committee on Flexible Pavement Design.

Prediction of Subgrade Moduli for Soil that Exhibits Nonlinear Behavior

JAN MOOSSAZADEH AND MATTHEW W. WITCZAK

The main objective of this report is to develop a simple and accurate procedure to predict an equivalent one-layer subgrade modulus for a soil that exhibits nonlinear behavior in a flexible highway pavement system. The analysis is predicated on developing such a modulus that would yield identical values of either vertical strain or deflection at the top of the subgrade compared with results obtained from a stress-dependent iteration technique that accounts for the stress-dependent (nonlinear) behavior of the subgrade. Use of a modified elastic layered computer program was made to determine equivalent subgrade modulus values for nearly 3900 separate layered pavement problems. By using the results obtained, multiple regression techniques were used to determine predictive equations for the equivalent subgrade modulus values as a function of the nonlinear subgrade and layered pavement properties. Use of partial model regressions techniques allowed predictive equations to be obtained that had correlation coefficients in excess of 0.95 and residual errors less than 10 percent. Both analytical and nomographic solutions are presented to demonstrate the simplicity of the approach. It was found that values of deflection-based equivalent mod-

ulus are larger than or equal to values of strain-derived modulus for a given set of load, pavement, and nonlinear subgrade properties. Although the vertical subgrade-strain-derived subgrade moduli are generally independent of the incorporation of overburden stresses, equivalent subgrade moduli based on deflection criteria, without overburden considered, were almost always larger than equivalent deflection based moduli developed with overburden incorporated into the analysis.

Until recently, the moduli of unbound flexible pavement layer materials have been treated as parameters of constant magnitude. However, recent research in dynamic materials characterization has indicated that many pavement materials are stress dependent. Due to the importance of the subgrade modulus in the overall performance of the flexible pavement, the most accurate assessment of modulus is essential to the successful design of a pavement system. Such assessment is also required in calculation of any stress, strain, or deflection in the pavement system.

Several mathematical forms have been suggested by researchers to model the nonlinear behavior of fine-grained subgrade soil. One such useful, but simple, model is

$$M_r = K_1(\sigma_d)^{K_2} \quad (1)$$

where

M_r = resilient modulus,
K_1 and K_2 = constants dependent on material type and physical soil properties, and
σ_d = deviator stress.

This relation is illustrated in Figure 1 for two different soils that show marked differences in nonlinear behavior. The most important aspect illustrated in Figure 1 is that, since the deviator stress varies with depth in the subgrade, the modulus must likewise change with depth. Clearly, the magnitude of this change is most significantly affected by changes in the slope or K_2-value. This parameter indicates, to a large degree, the nonlinearity of a given material.

STUDY OBJECTIVE

The general purpose of this research was to develop a simple and accurate method of evaluating a single (one-layer) modulus value for the entire subgrade layer that would yield identical values of selected critical parameters to those found by using an iterative multilayer systems approach to account for the nonlinear behavior. The critical parameters selected for this study were the vertical strain (ε) and deflection (δ) at the top of the subgrade layer. Both of these parameters are performance indicators of the pavement system. The two resulting moduli will be referred to as the equivalent strain [$E(\varepsilon)$] and equivalent deflection moduli [$E(\delta)$], respectively.

This study follows a similar research effort by Smith (1) on the stress-dependent modulus of granular base material. However, there are few, if any, studies on the stress-dependent solutions for the subgrade modulus value. The closest technique is the one developed by Treybig and others (2). However, this method is only applicable for overlay analysis. Furthermore, the method mentioned only accounts for adjustments in the state of stress at the top of subgrade layer, and, therefore, the change with depth of these parameters is neglected.

In a layered pavement system, there are three major parameter groups that affect the deviator stress in the subgrade, and hence the variation of moduli within this layer. They are as follows:

1. Nonlinear subgrade properties (K_1 and K_2),
2. Pavement layer properties (E_i, h_i, and μ_i), and
3. Vehicle load properties (P, p, and spacing).

Study on Values of K_1 and K_2

In order to arrive at typical values for K_1 and K_2, available test data in the literature were used. Three sets of data were used in this study: the results of the San Diego County Test Road (3), the results of a subgrade study by the Illinois Department of Transportation (4-6), and the data from a study conducted for the Maryland State Highway Administration (7). Altogether, 137 sets of nonlinear moduli results were analyzed.

Through linear regression techniques, values of K_1 and K_2 were determined for each set of data. A summary of these values is shown in Table 1. This table shows that the majority of K_1 values fall between 0 and 200 kips/in^2, and K_2 ranges from 0 to -1.0.

The above study also afforded some insight into the effect of soil parameters on K_1 and K_2 values. Although very general, the important findings of this study were as follows:

1. K_1 increases and K_2 decreases as the dry density increases or the moisture content decreases;
2. The value of K_1 is directly proportional to the liquid limit and plasticity index, but inversely proportional to the plastic limit; K_2 is relatively insensitive to the Atterberg limits; and
3. K_1 and K_2 are relatively independent of each other.

Arrangement of Factorial Matrix

In order to relate the equivalent subgrade modulus values to other pavement system parameters, a factorial study was conducted. A selected number of each parameter was chosen to encompass the whole range of values of such parameters encountered in design. Use was made of available data concerning the ranges of each variable, as well as the K_1-K_2 study mentioned above. Thickness values for the asphalt and base layers (h_1 and h_2) were selected from an examination of typical highway pavement sections encountered in practice. The load used in this study was a 9-kip single wheel load and a tire pressure of 70 lbf/in^2 to approximately model the effects of an 18-kip single-axle load. Because of this load selection, the results of this study are considered applicable only for typical highway pavements. Table 2 illustrates the values of each variable used in the factorial study. As observed, a matrix of 972 combinations was evaluated.

METHOD ANALYSIS

Equivalent Moduli

As mentioned earlier, determination of a stress-dependent subgrade modulus value with elastic layered theory involves an iterative procedure. In this study the subgrade was subdivided into four 12-in sublayers and a semi-infinite lower layer. The values of the deviator stress at the top of each sublayer were calculated by the Chevron N-layer computer program (8). The predicted values of σ_d found were then substituted in Equation 1 and a new value was calculated for each sublayer modulus. This new value of the sublayer modulus was then compared with the original value and the iteration procedure continued until a difference of ±5

Figure 1. Typical nonlinear modulus results for subgrade soils.

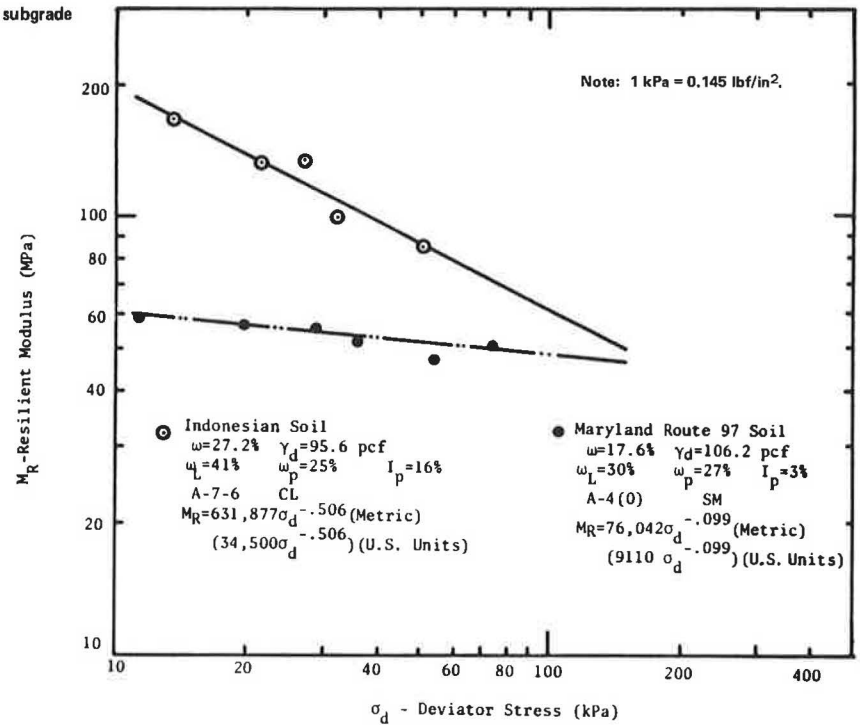

Table 1. Summary of nonlinear soil parameters.

	San Diego Study		Illinois Study		Maryland Study	
Parameter	K_1	K_2	K_1	K_2	K_1	K_2
Mean	60.6 kips/in^2	-0.37	16.5 kips/in^2	-0.42	47.7 kips/in^2	-0.51
SD	89.3 kips/in^2	0.264	8.3 kips/in^2	0.156	37.8 kips/in^2	0.290
Coefficient of variance (%)	147	71	51	37	79	57
Range	5.0 to 684 kips/in^2	-1.17 to 3.93	3.0 to 34.0 kips/in^2	-0.74 to -0.17	8.0 to 125.0 kips/in^2	-1.13 to -0.04
Total no. of samples	79		39		19	
No. of samples that have K_1 between 0 and 200 kips/in^2	76[a]		39[b]		19[b]	
No. of samples that have K_2 between 0 and -1.0	75[c]		39[b]		18[d]	

[a]This represents 96.2 percent of the samples.
[b]This represents 100 percent of the samples.
[c]This represents 94.9 percent of the samples.
[d]This represents 94.7 percent of the samples.

percent occurred between the two values. Because of the large size of the factorial matrix analyzed, we modified the Chevron N-layer program to perform this iterative sequence internally.

After the stress-dependent sublayer moduli were found, the multilayer pavement system was reduced to a three-layer system. This three-layer system had the same top two layers as did the original multilayer pavement but one subgrade layer was added that had a unique modulus value. The end product of this analysis was to determine what one-layer subgrade modulus would yield the same critical parameters as the stress-dependent sublayer moduli system.

As mentioned before, the two selected parameters (critical criteria) used in this study were the values of vertical strain and deflection at the top of the base-subgrade interface. These two parameters would, as expected, result in two different E_3 values [$E(\varepsilon)$ and $E(\delta)$]. In addition, the effects of both ignoring and including the pavement overburden stresses on the E_{eq} values were also studied. Thus, four separate E_{eq} parameters were investigated.

The procedure used to determine the E_{eq} value consisted of examining the effect of subgrade modulus on the desired parameter (ε or δ) for a particular three-layer pavement system. As it turned out, these relations were virtually linear on a log-log scale. The value of the equivalent subgrade modulus was then determined as that modulus yielding the same strain (or deflection) as that found from the multilayer stress-dependent iteration study. Figure 2 depicts one such solution for the $E_{eq}(\varepsilon)$ and $E_{eq}(\delta)$ value. Although the figure denotes a graphical solution, the above steps in the equivalent subgrade study were computerized to save time and increase the accuracy of the solution.

Statistical Data Analysis

For each combination of pavement and soil parameters examined (i.e., h_1, E_1, h_2, E_2, K_1, and K_2) a unique E_{eq} value for a given critical criterion was obtained. The next study step was to examine whether a relation existed between the

mentioned variables and E_{eq}. The use of multiple regression techniques was employed to determine the best model (highest correlation coefficients). In this phase of the study, 10 different model combinations were analyzed. The best model (highest R^2) form was found to be a total log model. In order to reduce the number of independent variables in the prediction equations, the individual thickness and moduli parameters were combined into one unique parameter by the concept of equivalent layers. One such equivalent layer technique is that recommended by Palmer and Barber (9). In this method, it is assumed that the upper layer of thickness (h_1), modulus (E_1), and Poisson's ratio (ν_1), may be replaced by an equivalent thickness (h_1) of the base material, with E_2 and ν_2, as follows:

$$h_1' = h_1 [E_1(1 - \nu_2^2)/E_2(1 - \nu_1^2)]^{1/3} \quad (2)$$

Table 2. Summary of study parameters.

Parameter	Value Used	Levels
Tire load, single wheel	9 kips	1
Tire pressure	70 lbf/in^2	1
Asphalt layer		
Thickness (h_1)	4, 8, and 12 in	3
Modulus (E_1)	50, 100, 500, and 1000 kips/in^2	4
Density (γ_1)	145 lb/ft^3	1
Poisson's ratio (μ_1)	0.3	1
Granular base layer		
Thickness (h_2)	4, 10, and 16 in	3
Modulus (E_2)	20, 50, and 80 kips/in^2	3
Density (γ_2)	130 lb/ft^3	1
Poisson's ratio (μ_2)	0.4	1
Subgrade layer		
Thickness	Semi-infinite	1
K_1	10, 50, and 200 kips/in^2	3
K_2	-0.1, -0.3, and -1.0	3
Density (γ_3)	110 lb/ft^3	1
Poisson's ratio (μ_3)	0.45	1

Note: Total matrix size is 972 combinations.

Thus, the new equivalent layer has a modulus (E_2), Poisson's ratio (ν_2), and thickness of $h_e = h_1' + h_2$. A relative stiffness value for the equivalent layer was defined as follows:

$$D = E_2 h_e^3 \quad (3)$$

where D is termed the equivalent pavement stiffness value.

Thus, the entire pavement system could now be identified by only three parameters: D, K_1, and K_2. Further multiple regressions proved that virtually the same predictive values of E_{eq} were obtained from expressions of the following form:

$$\log E_{eq} = f(\log D, \log K_1, \log K_2) \quad (4)$$

compared with the use of log h_1, log E_1, log h_2, and log E_2 individually. The correlation coefficients of the predictive models stayed almost the same with R^2 values that ranged between 0.906 and 0.938. Finally, although not discussed in this report, the equivalent layer approach developed by Barros (equivalent moduli) (9) was also analyzed and found to yield identical solutions.

Partial Models

The regression models developed resulted in very high correlation coefficients; however, a study of residuals from Equation 4 showed some large numerical differences between the actual and regression-predicted E_{eq} values. In order to overcome this problem, separate predictive models were developed by holding constant the least-significant parameter (i.e., the variable that had the smallest correlation value). This parameter turned out to be K_2. The results were improved correlations and lower residuals. The models were of the general form:

$$\log E_o \text{ or } \log E_{eq} = f(\log D, \log K_1) \quad (5)$$

where K_2 is a constant.

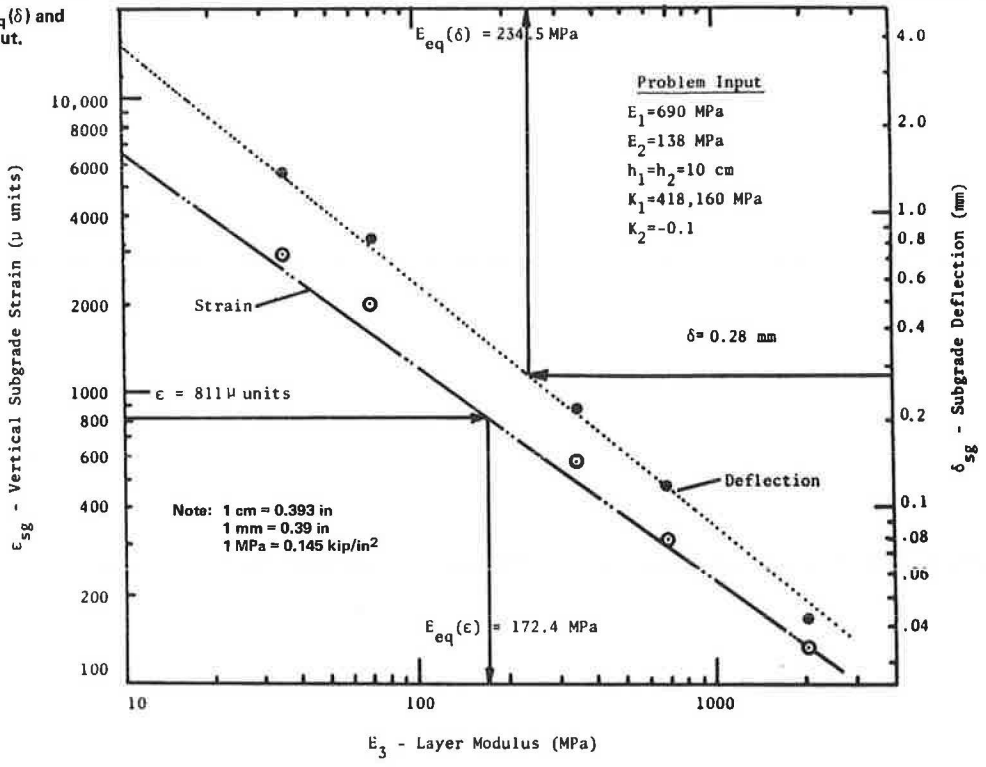

Figure 2. Determination of $E_{eq}(\delta)$ and $E_{eq}(\epsilon)$ for specific problem input.

Table 3. Summary of regression models.

Equation	Total Model (K_2 included) $\log E_{eq(or\ o)} = A_0 + A_1 \log D + A_2 \log K_1 + A_3 \log \lvert K_2 \rvert$					Partial Model (K_2 = constant) $\log E_{eq(or\ o)} = B_0 + B_1 \log D + B_2 \log K_1$				
	A_0	A_1	A_2	A_3	R^2	K_2	B_0	B_1	B_2	R^2
$E_{eq}(\delta)$	-1.3262	+0.2011	+0.8316	-0.3211	0.9350	-0.1	-0.4986	+0.0592	+0.9823	0.9971
						-0.3	-1.0069	-0.1543	+0.8965	0.9967
						-1.0	-1.9840	+0.3897	+0.6160	0.9941
$E_o(\delta)$	-0.9897	+0.1029	+0.9012	-0.5035	0.9723	-0.1	-0.3944	+0.0373	+0.9955	0.9977
						-0.3	-0.7043	+0.0887	+0.9389	0.9974
						-1.0	-1.1036	+0.1827	+0.7692	0.9853
$E_{eq}(\epsilon)$	-1.3058	+0.1563	+0.8224	-0.6111	0.9074	-0.1	-0.9361	+0.0464	+1.0708	0.9841
						-0.3	-1.1224	+0.1373	+0.9026	0.9794
						-1.0	-0.9284	+0.2852	+0.4937	0.9702
$E_o(\epsilon)$	-1.2189	+0.1372	+0.8437	-0.5955	0.9129	-0.1	-0.9447	+0.0423	+1.0816	0.9842
						-0.3	-1.0862	+0.1213	+0.9267	0.9779
						-1.0	-0.7188	+0.2479	+0.5229	0.9592

DEVELOPMENT OF PREDICTIVE MODELS

Table 3 summarizes the regression models developed for prediction of E_{eq} (without overburden) or E_o (with overburden). Both total and partial regression equations for $E_{eq}(\epsilon)$ and $E_{eq}(\delta)$ parameters, with and without overburden stress, are shown. An examination of the tabulated R^2 values in the table clearly supports the accuracy of all model combinations--the lowest R^2 value found was 0.9074.

The increase in accuracy provided by using the partial models (k_2 = constant) can be observed to yield regression equations that have R^2 values of 0.96-0.99. A study of the residual errors between the total and partial models also greatly supports the partial model approach. The total models resulted in residuals in excess of 100 percent of the actual values for some cases, and the partial models reduced the maximum residuals to less than 20 percent; the majority of points were within the 1-10 percent limit.

Example Solution

The mechanics of using any of the models in Table 3 is quite direct. Units for the input values are as follows:

D in inch-pounds (h_e = inches and E_2 = pounds per square inch),
K_1 in pounds per square inch, and
K_2 is dimensionless.

The resulting E_{eq} value is then expressed directly in units of pounds per square inch. For example, consider if the E_{eq} value is desired for the conditions noted below.

For the total model with overburden, equivalent deflection criteria are as follows:

h_1 = 4 in, E_1 = 100 000 lbf/in^2, and v_1 = 0.3;
h_2 = 8 in, E_2 = 40 000 lbf/in^2, and v_2 = 0.4; and
$h_3 = \infty$ and $E_3(M_r) = 25\ 000\ \sigma_d^{-0.4}$.

From Table 3, the appropriate A_i coefficients for the total model $-E_o(\delta)$ are shown. Thus,

$$E_o(\delta) = -0.9897 + 0.1029 + \log D + 0.9012 \log K_1 - 0.5035 \log \lvert K_2 \rvert$$

$$h_1' = h_1 [E_1(1 - v_2^2)/E_2(1 - v_1^2)]^{1/3}$$

$$= 4[(100\ 000/40\ 000)(1 - 0.16)/(1 - 0.09)]^{1/3} = 5.29 \text{ in}$$

$$h_e = h_1' + h_2 = 5.29 + 8 = 13.29 \text{ in}$$

$$D = E_2 h_e^3 = 40\ 000(13.29)^3 = 9.38 \times 10^7 \text{ in} \cdot \text{lb}$$

for

$$D = 9.38 \times 10^7,\ K_1 = 25\ 000, \text{ and } K_2 = -0.4$$

$$\log E_o(\delta) = -0.9897 + 0.8203 + 3.9634 + 0.2004 = 3.9944$$

$$E_o(\delta) = 9872 \text{ lbf/in}^2$$

Nomographic Solutions

The simplicity afforded by nomographic solutions in practical analysis problems is appealing. Moossazadeh (10), presents nomographs (and their specifications for construction) for solutions of D as well as all 16 equations shown in Table 3. Figures 3 and 4 are solutions for the total model equations, with and without overburden effects considered for both deflection and strain-based equivalent modulus. If the more accurate partial model solutions are desired, refer to Moossazadeh (10). The use of the partial model equations or nomographs requires that an interpolation procedure be employed for the actual $\lvert K_2 \rvert$ value of the subgrade soil. The accuracy of the nomograph can be easily verified with the example problem previously presented.

DISCUSSION OF RESULTS

Effect of Parameters

An examination of the equations in Table 3 indicates that the value of E_{eq} is directly dependent on all pertinent parameters. These parameters, in order of importance, were K_1, K_2, h_1, E_1, and h_2. The value of E_{eq} was almost independent of E_2. The results confirm the logic that, as the value of h_1, h_2, E_1, or E_2 increases (an increase in D), the pavement system approaches the condition of a rigid slab, which in turn, results in a decrease of σ_d due to the external loads within the subgrade layer. This decrease, in turn, results in an increase in E_{eq}.

The value of K_1, however, had the strongest effect on E_{eq}. In almost all cases, the variation in K_1 contributed to more than 80 percent of the variation in E_{eq}, as measured by the correlation coefficient.

Comparison of Equivalent Subgrade Modulus Types

The values of $E_{eq}(\epsilon)$ versus $E_{eq}(\delta)$ are presented in Figure 5. As seen, all values of $E_{eq}(\delta)$ are larger than or equal to the corresponding values of $E_{eq}(\epsilon)$. The influence of

Figure 3. Nomographs for $E_{eq}(\delta)$ and $E_{eq}(\epsilon)$ without overburden for total model.

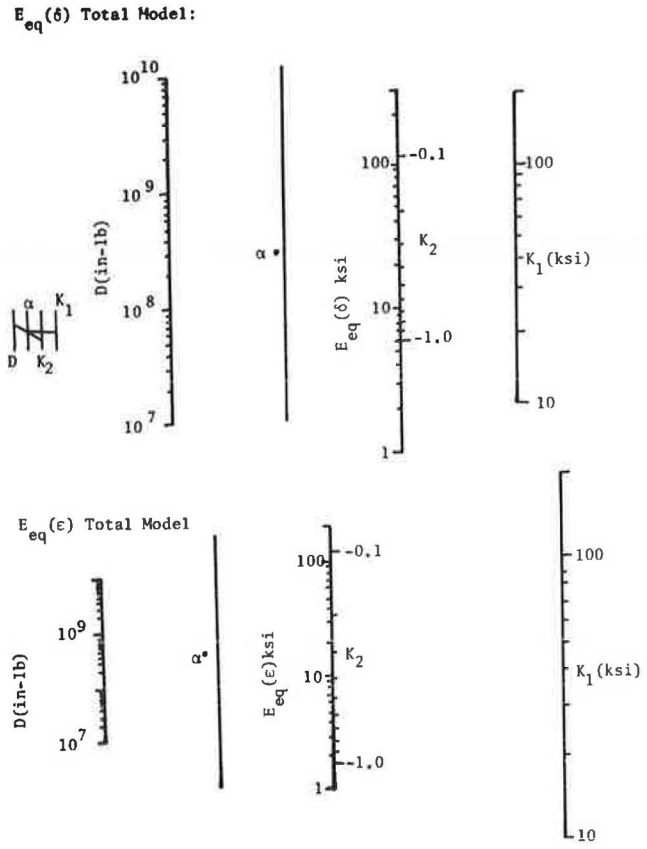

Figure 4. Nomographs for $E_o(\delta)$ and $E_o(\epsilon)$ with overburden for total model.

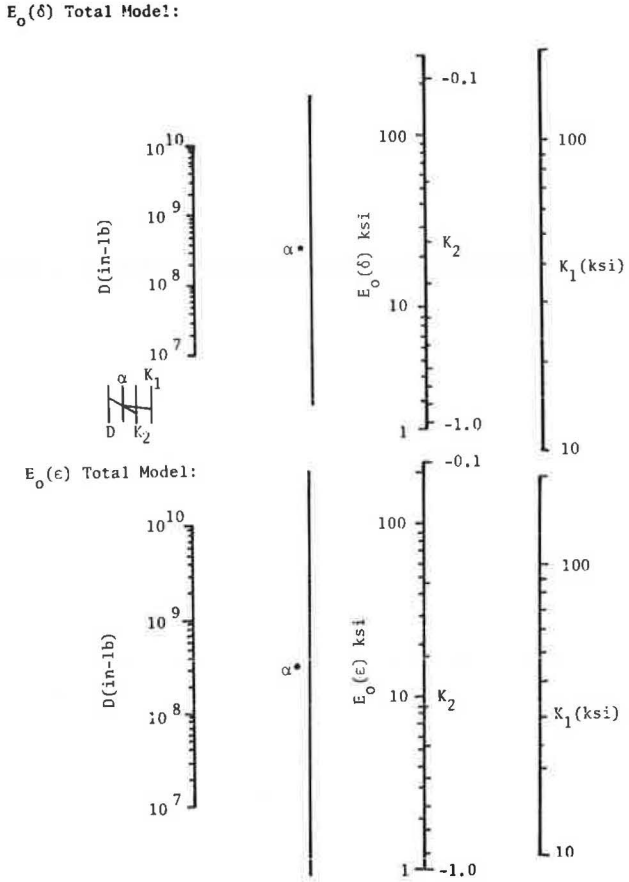

Figure 5. Relation between $E_{eq}(\delta)$ and $E_{eq}(\epsilon)$ without overburden.

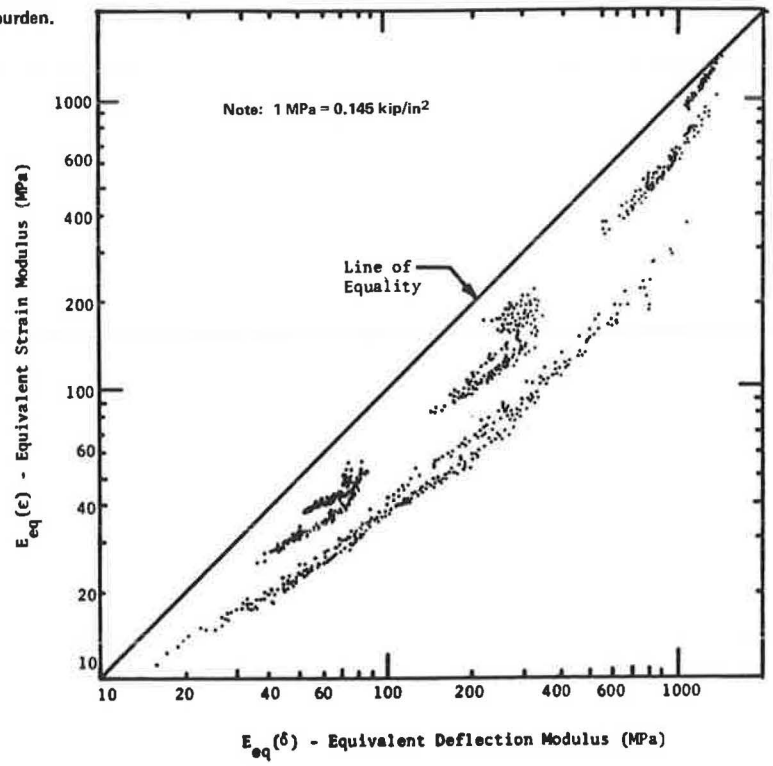

Figure 6. Comparison of equivalent one-layer subgrade modulus with and without overburden.

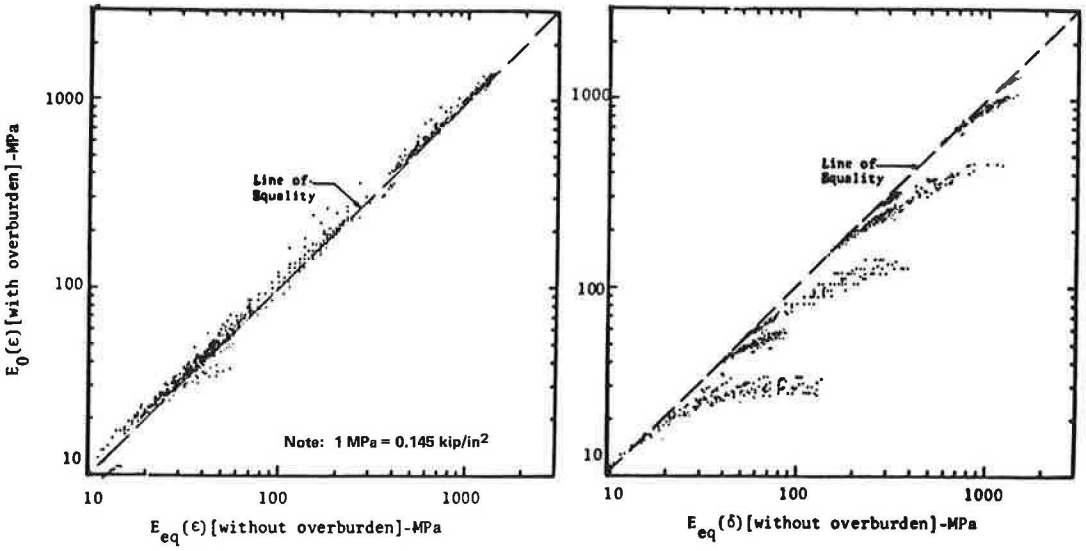

K_1-K_2 combinations are reflected by the banding effect on the plot. Notice that, in general, there is close agreement between the two types of equivalent modulus for small values of K_1 and K_2. However, as the absolute values of K_1 and K_2 increase, the difference between the two groups becomes larger. This can be explained by recognizing that, for small values of K_1 and $|K_2|$, the subgrade modulus is less sensitive to changes in deviator stress (more linear) and thus does not vary greatly with depth. On the other hand, large combinations of K_1 and $|K_2|$ are indicative of highly sensitive (nonlinear) subgrade modulus.

The value of the vertical strain at the top of the subgrade is highly sensitive to the value of the subgrade modulus near the top (first sublayer) and not so much on the subsequent sublayers. However, subgrade deflection is a function of the moduli of the total subgrade layer. Thus, the value of $E_{eq}(\delta)$ will generally always be larger than $E_{eq}(\epsilon)$, especially when the subgrade is highly nonlinear.

Effect of Overburden Stress

As previously noted, equivalent subgrades were analyzed under two sets of assumed deviator stress conditions (with and without overburden stresses). Obviously, the effect of including overburden resulted in changes in regression coefficients as shown in Table 3. However, all of the relative comparisons and results of the E_{eq} models (without overburden) were identical to those of the E_o models (with overburden). For example, the K_1 factor had the highest influence and E_2 the least on the regression; partial regression models greatly decreased the residual error; and the deflection-based equivalent subgrade modulus $[E_o(\delta)]$ was always greater than the strain-based modulus $[E_o(\epsilon)]$.

Figure 6 shows the comparison between equivalent modulus for models with and without overburden considered. A comparison of E_{eq} and corresponding E_o values showed that $E_{eq}(\delta)$ was always larger than or equal to $E_o(\delta)$. The values of $E_{eq}(\epsilon)$ and $E_o(\epsilon)$, on the other hand, were virtually equal all the time. The reason is that, at shallow depths, the value of overburden stress is small enough so that the difference in the σ_d value used by the two methods is quite small. Therefore, the values of $E_3(\epsilon)$, which are heavily influenced by the state of the top layers, stay close to each other.

At deep locations in the subgrade the inclusion of the overburden stress causes the deviator stress not to vary as much. This, in turn, prevents the subgrade modulus from increasing as rapidly. This fact causes the $E_o(\delta)$ value, which is a function of the total subgrade layer, to be smaller than $E_{eq}(\delta)$.

RECOMMENDATIONS FOR IMPLEMENTATION

Based on the previous discussion, general recommendations regarding the type model to use (δ or ϵ, with or without overburden) can be made. One of the more important implications of this study is that the subgrade moduli may be a function of its intended use. If the analysis is to be used in design situations with limiting subgrade strain as a distress criteria, the equivalent strain model should be used. However, if the models are to be used with in situ deflection tests (e.g., nondestructive testing) to determine in situ subgrade response, the deflection-based model should be used. This appears to be critical, especially if highly nonlinear soils are anticipated (large $|K_2|$).

In either case, the most probable and realistic estimate of modulus can be obtained with the overburden effect included. Recall that, for the equivalent strain models, the $E_o(\epsilon)$ was approximately equal to the $E_{eq}(\epsilon)$, and the $E_o(\delta)$ was less than the $E_{eq}(\delta)$ for the equivalent deflection model. Thus, inclusion of the overburden effect will result in either equivalent moduli or values slightly conservative for practice regardless of the criterion selected.

SUMMARY

This study has presented a highly accurate and simple technique to determine the equivalent subgrade moduli for soils that exhibit nonlinear dynamic behavior. There are several major advantages to this approach.

The solution technique offers the potential for a significant savings in time and cost by not having to conduct detailed iterative nonlinear elastic layered computerized solutions. The solution also

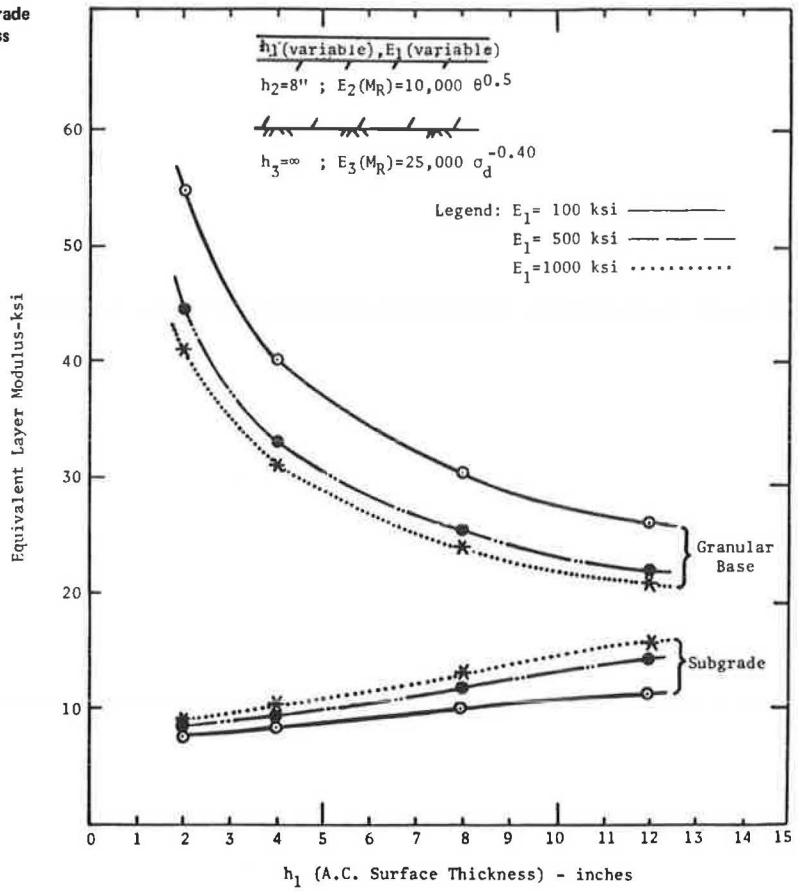

Figure 7. Summary of equivalent granular base and subgrade modulus as functions of asphalt concrete surface thickness and modulus.

provides a basis for quick determination of single subgrade modulus values for nonlinear soils for use in pavement design charts such as found in the Shell Oil, the Asphalt Institute, or even American Association of State Highway and Transportation Officials (AASHTO) design schemes. The results of this study can also be used to evaluate the influence of various layer pavement parameters (h_i and E_i) on the equivalent subgrade modulus.

This study on nonlinear subgrade soils followed the study concepts used by Smith (1) to predict equivalent granular base moduli. The results of the two studies were intended to allow the combination of their predictive equations to quickly and accurately determine the simultaneous solution of both unbound granular and subgrade soil nonlinear moduli problems. Figure 7 shows the results of such a sample solution by using nonlinear moduli properties for both the granular base and subgrade from predictive equations developed in this study and Smith's work (1). Note that the values shown in the figure were computed manually for the sample pavement cross section noted.

Finally, the solution presented allows examination of the probable levels of the subgrade deviatoric stress for any given pavement structure. The technique for this is best illustrated by referring to the example problem previously worked. For a K_1 = 25 000 and K_2 = -0.4, the $E_o(\delta)$ was found to be 9872 lbf/in². Because

$$M_r = E_o(\delta) = K_1 \sigma_d^{K_2} \quad (6)$$

the deviator stress (σ_d) can be easily computed to be σ_d = 10.2 lbf/in².

ACKNOWLEDGMENT

We are indebted to the Asphalt Institute, through the B. Gray grant, for making this research study possible. In addition, a generous grant provided by the University of Maryland Computer Science Center, which allowed the computer study to be conducted, is greatly appreciated.

REFERENCES

1. B.E. Smith. Prediction of Equivalent Granular Base Moduli Incorporating Stress Dependent Behavior in Flexible Parameters. Univ. of Maryland, College Park, M.S. thesis, 1970.
2. H.J. Treybig, B.F. McCullough, F.N. Finn, R. McComb, and W.R. Hudson. Design of Asphalt Concrete Overlays Using Layer Theory. Proc., 4th International Conference on Structural Design of Asphalt Pavements, Univ. of Michigan, Ann Arbor, Vol. 1, 1977.
3. M.P. Jones. Analysis of the Subgrade Modulus and Pavement Fatigue on the San Diego Test Road. Univ. of Maryland, College Park, M.S. thesis, 1975.
4. M.R. Thompson and Q.L. Robnett. Final Report--Data Summary: Resilient Properties of Subgrade Soils. Univ. of Illinois, Urbana, Rept. UILU-ENG-76-2009, 1976.
5. M.R. Thompson and Q.L. Robnett. Final Report: Resilient Properties of Subgrade Soils. Univ. of Illinois, Urbana, Rept. UILU-ENG-76-2009, 1976.
6. M.R. Thompson and Q.L. Robnett. Interim Report: Resilient Properties of Subgrade Soils, Phase I--Development of Testing Procedure.

Univ. of Illinois, Urbana, Rept. UILU-ENG-73-2010, 1973.
7. K.R. Bell. Predicted Flexible Pavement Remaining Life Interpreted from Various Analytical Procedures. Univ. of Maryland, College Park, M.S. thesis, 1976.
8. J. Michelow. Analysis of Stresses and Displacements in an N-Layered Elastic System Under a Load Uniformly Distributed on a Circular Area. California Research Corp., Richmond, CA, 1963.
9. H.G. Poulos and E.H. David. Elastic Solutions for Soil and Rock Mechanics. Wiley, New York, 1972.
10. J. Moossazadeh. Determination of Equivalent Subgrade Moduli for Soil Exhibiting Non-Linear Dynamic Behavior. Univ. of Maryland, College Park, M.S. thesis, 1978.

Publication of this paper sponsored by Committee on Flexible Pavement Design.

Analysis of Pavements with Granular Bases

S.F. BROWN AND J.W. PAPPIN

The nonlinear stress-strain response of unbound granular materials has to be modeled satisfactorily when numerical analysis is used for pavement structures that contain significant quantities of such material. The simple model, which has been used widely for the purpose of relating resilient modulus to the sum of the principal stresses, has serious limitations. This is because the triaxial tests used in its development do not cover an adequate range of stress paths when compared with the situation in the pavement. A more complex and accurate model is described that has been developed from extensive laboratory repeated load testing. It is expressed in terms of shear and volumetric stress-strain relationships. The need for better modeling of cohesive soils for analysis is also discussed and the importance of the principle of effective stress is emphasized. A new finite-element program is described and its main features are explained. It uses a secant modulus approach, has been specifically developed to deal with nonlinear materials, and is called SENOL for secant modulus nonlinear. The use of the new granular material models for the three-dimensional stress system in a pavement is discussed and results from analyses with SENOL are compared with in situ measurements from a test pavement.

Most of the development work concerned with the use of theoretical analysis in flexible pavement design has concentrated on accurate modeling of the asphalt layer. Simplifying assumptions are often made concerning the mechanical properties of the unbound granular layer and the subgrade soil. This situation is a reflection of the relative states of knowledge concerning the various materials together with a need to produce design methods that are not unduly complex.

The existence of nonlinear stress-strain characteristics for granular materials and soils has been well known for many years, and numerous papers have reported experimental data, mainly from laboratory repeated load tests (e.g., 1,2). The increasing use of finite-element analysis has provided a means of more accurate modeling of nonlinear materials within pavement structures, but the full potential of the method has often not been realized. Recent work at the University of Illinois (3) represents an improvement to the finite-element approach since the analysis considers failure conditions and has been used to generate data for use in simplified design charts (4). However, the nonlinear stress-strain relations that have been used are not really adequate for analysis of a three-dimensional system, even an axisymmetric one. The approach reported here describes a more-detailed method of characterizing granular materials and discusses the use of this in a finite-element, secant modulus nonlinear (SENOL) program, which has been recently developed.

CHARACTERIZATION OF GRANULAR MATERIALS

In general, an element of material in the granular layer of a pavement is subjected to three principal stresses: σ_1, σ_2, and σ_3, where $\sigma_1 > \sigma_2 > \sigma_3$. Each stress consists of two components, a constant value due to overburden and a transient value due to the passing wheel load.

Use of the repeated load triaxial test to obtain data on the resilient characteristics of granular materials implies that two of the stresses are equal because of axial symmetry. If, however, the stresses are expressed in invariant form, this difficulty can be partly overcome (5).

Most research in this field has involved tests with a constant confining stress and a deviator stress applied repeatedly by pneumatic or servohydraulic actuators between zero and a peak value. Various peak values have been used at a range of confining stresses and a well-established relationship has emerged to relate resilient modulus (M_r) to stress level:

$$M_r = K_1 \theta^{K_2} \tag{1}$$

in which

$$M_r = q_r/\epsilon_{ar} \tag{2}$$

where q_r is a repeated stress given by $\sigma_{ar} - \sigma_c$ and ϵ_{ar} is resilient (recoverable) axial strain.

$$\theta = \sigma_{ar} + 2\sigma_c = 3\sigma_c + q_r \tag{3}$$

where

σ_{ar} = peak axial stress,
σ_c = constant confining stress, and
K_1 and K_2 = material constants.

Confusion has often arisen over the use of Equation 1 because the factor K_1 is not dimensionless. Furthermore, distinction is rarely made between total stress and effective stress. Although this is of no consequence for dry materials, it is of fundamental importance when pore water is present.

Figure 1 shows a typical stress path in triaxial stress space for a test of the type described above. The parameters used are mean normal effective stress [$p' = (1/3)(\sigma_a' + 2\sigma_c')$] and the deviator stress (q). The tests are assumed to have been carried out on dry material, so that no pore pressures are generated and, hence, the path in Figure 1 represents effective stress.

Figure 1. Typical stress path for a constant confining stress test.

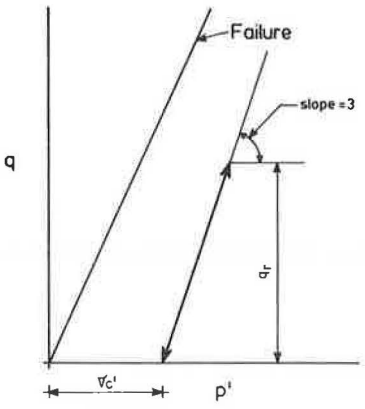

Figure 2. Typical repeated load stress path.

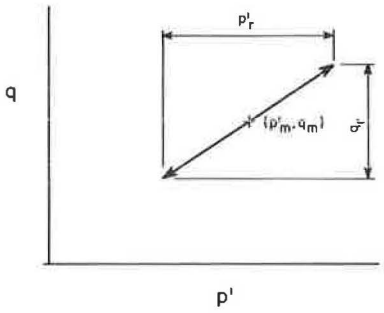

Figure 3. Stress paths applied to test specimens at one value of p_m'.

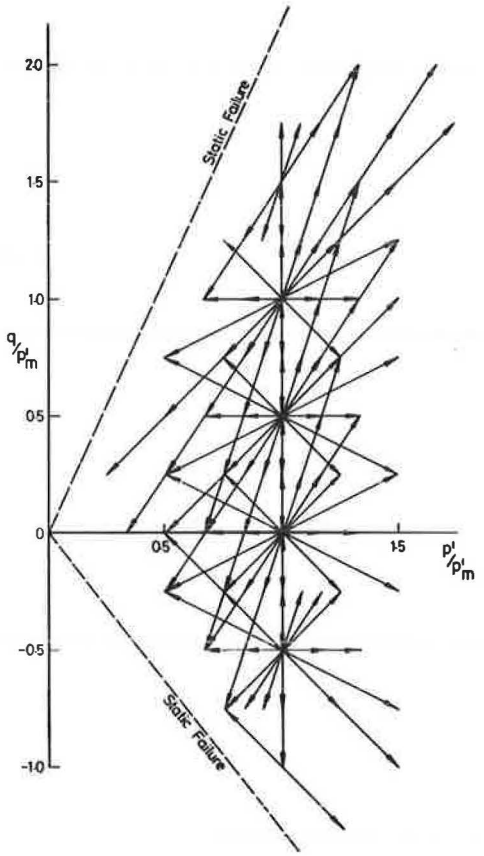

Figure 4. Resilient strain contours: (left) normalized shear strain and (right) volumetric strain.

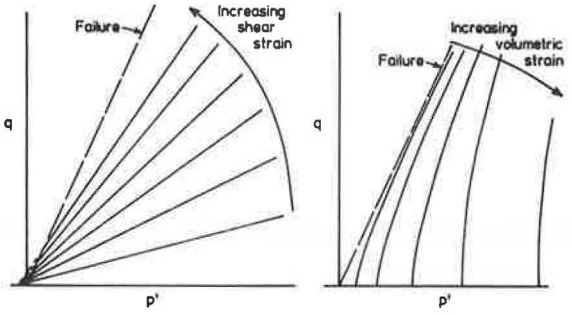

From the definitions of p' and q it is apparent that:

$$p' = \sigma_c' + (1/3)q \tag{4}$$

Hence the stress path in Figure 1 has an intercept on the p' axis equal to the effective confining stress and has a slope of 3. Figure 1 also shows the position of the failure line for which q/p' equals M, a constant. This is related to the angle of shearing resistance (ϕ') (6) by

$$M = 6 \sin\phi'/(3 - \sin\phi') \tag{5}$$

Experiments have shown (3) that the expression for resilient modulus (Equation 1) applies even for stress paths that approach failure, but most tests have involved stress paths well short of this condition so that specimens are not subjected to significant permanent strains.

Tests of the type represented in Figure 1 are restrictive because they do not investigate the influence of the mean value of deviator stress nor do they allow any variation in slope of the stress path. Both of these factors are likely to occur in the pavement situation and can be reproduced with triaxial test equipment.

Figure 2 shows a more general stress path that requires facilities to cycle the confining stress and operate from a nonzero minimum stress. The path is defined by the mean and peak to peak values of p' and q (i.e., p_m', q_m and p_r', q_r, respectively).

Servohydraulic equipment to apply these general stress paths has been developed at Nottingham in recent years (7,8) and used to investigate the behavior of crushed limestone. In these tests, large numbers of stress paths were applied both in triaxial compression and extension (negative deviator stress), as shown in Figure 3 for one value of p_m'. Results for well-graded material have been presented by Pappin and Brown (9) and for uniformly graded specimens by Shaw and Brown (10). A general pattern of behavior has emerged both from these tests and from similar ones conducted by Mayhew at the Transport and Road Research Laboratory.

Figure 4 shows the way in which the compression results were expressed in terms of contours of resilient shear strain (ϵ_r) (Figure 4, left) and volumetric strain (v_r) (Figure 4, right),

$$\epsilon_r = (2/3)(\epsilon_{ar} - \epsilon_{rr}) \tag{6}$$

and

$$v_r = \epsilon_{ar} + 2\epsilon_{rr} \tag{7}$$

where ϵ_{rr} is the resilient radial strain.

For a particular material, Figure 4 (right) can be used directly to determine the resilient volumetric strain for a stress path simply by subtracting the contour value for one end of the path from that at the other. The contour values v_{rc} are given by an equation of the form:

$$v_{rc} = (p'/A)^m [1 - B(q/p')^n] \quad (8)$$

where A, B, m, and n are material constants and p' and q are the coordinates of the stress point concerned.

For shear strain, the situation is slightly more complicated because the results were dependent on the stress path (9). In practice, this meant that the resilient shear strain not only depended on the end points of the stress path but also on its length. The pattern of contours shown in Figure 4 (left) is for normalized values of shear strain (ϵ_{rn}); a correction was introduced to allow for the path length [see Pappin and Brown (9)].

The contour value is given by an equation of the form:

$$\epsilon_{rn} = Cq/(p' + D) \quad (9)$$

where C and D are material constants and D is the negative value of p' through which all the contours pass. The actual resilient strain for a stress path between the points (p_1', q_1) and (p_2', q_2) is calculated from:

$$\epsilon_r = C\{[q_1/(p_1' + D)] - [q_2/(p_2' + D)]\} (\ell_r/p_m')^r \quad (10)$$

where ℓ_r is path length equals $\sqrt{p'_r{}^2 + q_r{}^2}$ and r is a material constant.

Values of the various constants for two gradings of crushed limestone are given in Table 1.

Pappin (11) performed some drained and undrained tests on saturated specimens of well-graded crushed limestone. He showed that the model established for dry material was applicable provided that effective stresses were used. Tests on partially saturated specimens, which required estimates to be made of the negative pore pressures, confirmed this conclusion as did the data of Smith and Nair (12).

This approach to the characterization of resilient behavior for granular materials is more flexible and potentially more accurate, though more complex, than the frequently used combination of Equation 1 for stress-dependent resilient modulus and a constant Poisson's ratio of, typically, 0.3.

In pavement analysis, a wide range of stress paths is encountered and, hence, the simple model does not provide a satisfactory basis for computations. Similarly, the full model, which was only developed for axisymmetric triaxial stress conditions, may be inapplicable to the general three-dimensional system that occurs in a pavement layer under wheel loading. The results from triaxial tests carried out in extension provided a basis for dealing with the general case.

Figure 5 shows a view down the space diagonal ($\sigma_1' = \sigma_2' = \sigma_3'$) in a plot that has orthogonal axes for the three principal stresses. All triaxial tests take place on the vertical line F_e-0-F_c, with compression tests above zero and extension tests below. The resilient-response model was developed for stress paths such as AB in Figure 5. The extension tests (9) showed that a path A'B' could be defined that gave the same resilient strains. The relationship between these corresponding points was based on the Mohr-Coulomb failure criterion, which states that:

$$\sigma_1'/\sigma_3' = \text{constant} \quad (11)$$

For a particular value of p', corresponding failure values of q can be obtained in both compression and extension, shown in Figure 5 as F_c and F_e, respectively. The same procedure was used to relate stress conditions below failure in compression and extension.

Since the three principal stress axes are interchangeable, all the arguments concerning the vertical line on Figure 5 can be equally applied to the other principal axes. This results in the familiar hexagonal shape for the Mohr-Coulomb failure surface in this view. It also means that points that correspond to A and B can be identified, as shown, on the corners of similar hexagons. A general three-dimensional stress path such as XY, for instance, can be related back to points in the compression region such as AB and appropriate resilient strains can be predicted by using the material model.

Typical data for both the simple and the new model are given in Table 1 for two gradings of a crushed limestone.

CHARACTERIZATION OF COHESIVE SOILS

A simple nonlinear model, analogous to that for granular materials, has been used for fine-grained soils. It is based on tests similar to that illustrated by the stress path in Figure 1, except that the tests were generally carried out undrained, the materials were usually partly saturated, and hence the pore pressure was not known so that only the total stress path was defined. However, it has become clear from tests on both saturated and partly saturated soils (13) that it is the initial effective stress that influences resilient characteristics (i.e., σ_c' in Figure 1). This stress is the one to which elements of soil are subjected prior to the application of wheel loading. The mag-

Table 1. Material constants for different gradings of crushed limestone.

Item	Constant	3-mm Uniform Grading	Continuous Grading 40-mm Maximum Size
Volumetric strain	A(kPa)	12.3 billion	1.9 trillion
	B	0.033	0.08
	m	0.5	0.33
	n	3.5	2.0
Shear strain	C	0.000 55	0.000 24
	D(kPa)	130	13
	r	0.45	0.4
Simple model	K_1[a]	19 454	8634
	K_2[a]	0.5	0.69

[a]Use of these values in Equation 1 gives M_r in kilopascals.

Figure 5. View down the space diagonal in three-dimensional stress space.

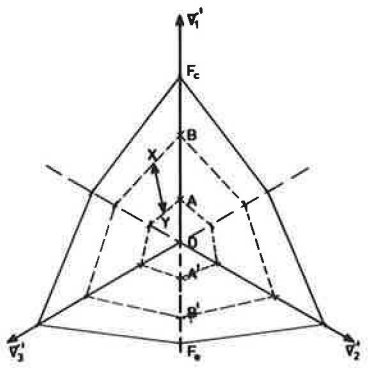

nitude of this stress depends on the position of the water table and the depth of the element. For deep water tables, high suctions will develop and the magnitude of suction may be taken as equal to the effective stress. Dehlen (14) and others (e.g., 15) have shown that resilient modulus is related to soil suction. For high water tables, it is possible to estimate the negative pore pressure and hence effective stress in the held water zone. Several workers have noted (2,15) that confining stress has little influence on the resilient modulus of cohesive soils. This results from tests where the soil suction is high in relation to the range of confining stresses and hence the effective stress, which controls the behavior, is relatively unaffected. Tests with saturated soils by using a range of stress histories, and hence initial effective stresses, have illustrated this point (16).

The simple models for cohesive soils relate resilient modulus, as defined by Equation 2, to repeated deviator stress, which shows a stress-softening effect. A more-detailed model that shows subsequent stiffening at higher deviator stresses has been developed at the University of Illinois (17).

The relation developed at Nottingham takes the form:

$$M_r = K(p_o'/q_{max})^s \quad (12)$$

where p_o' is initial effective stress, equals σ_c', and K and s are material constants.

Since all triaxial tests to date have pulsed q from zero to a peak, it is not clear whether the deviator-stress parameter in Equation 12 should be q_{max} or q_r (i.e., the peak value or the repeated value). Brown (13) has demonstrated that the basic relation of Equation 12 seems to apply to a range of soils and moisture conditions but that further testing is needed to properly establish it.

SENOL PROGRAM

A new finite-element program named SENOL has been developed specifically to analyze pavements made of nonlinear materials, though it has a range of other capabilities. A detailed description of the program is available elsewhere (18) and it is only necessary to summarize here its major characteristics.

Either plane strain or axisymmetric analysis may be performed, the latter being used for resilient response of pavements. Figure 6 shows a typical arrangement of elements and boundary conditions. In order to use the nonlinear resilient-response model developed for granular materials, it was found advantageous to use a secant modulus approach.

An important part of the overall analysis was the initial computation of stresses due to overburden, which provides a correct starting point with appropriate values of modulus before superposition of the wheel loading. This was applied in 10 gradually increasing steps until the full load was applied in the last one. At each step the element stresses were computed and new values of modulus determined. An iterative process was then carried out by using a variable damping factor, if necessary, to assist convergence. The procedure is summarized in the flow diagram of Figure 7. The convergence error was calculated from

$$\text{Error} = \Sigma(E_n - E_o)^2/\Sigma E_n^2$$

where E_o is the current value of Young's modulus and E_n is that from the previous iteration. The summation took place over all nonlinear elements and convergence was considered satisfactory when the error was below 0.002.

The values of secant modulus for the granular material were determined from the models described in the previous section of the paper. The bulk modulus (K) at any point in p',q stress space was calculated from the contour value of volumetric strain (Equation 8) by using

$$K = p'/v_{rc} \quad (13)$$

Figure 6. Typical finite-element layout.

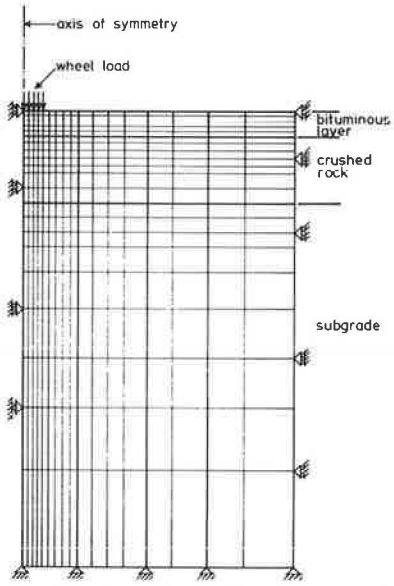

Figure 7. Flow diagram of SENOL finite-element program.

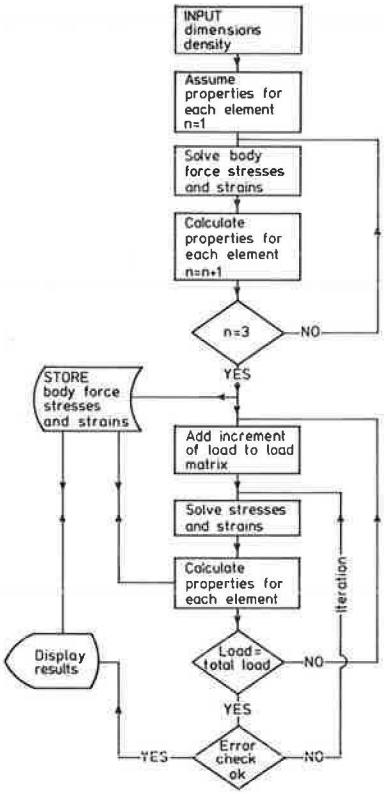

Shear modulus (G) was more difficult to determine because the contours in Figure 4 (left) were based on normalized values of shear strain and hence the zero in that figure does not correspond to zero strain. The procedure, therefore, was to estimate an initial value of shear strain (ϵ_1) and deviator stress (q_1) based on overburden stress conditions (p_1',q_1). Then:

$$G_1 = q_1/3\epsilon_1 \quad (14)$$

For a particular stress path from (p_1',q_1) to (p_2',q_2), the value of ϵ_r was obtained from Equation 10 so that

$$\epsilon_2 = \epsilon_1 + \epsilon_r \quad (15)$$

and

$$G_2 = q_2/3\epsilon_2 \quad (16)$$

A similar procedure was adopted for all successive stress paths.

Since the model for fine-grained soils was less detailed than that for the granular material, certain approximations were used while basically following the procedures outlined above for shear modulus.

In the absence of radial strain measurements on silty clay material, an assumption had to be made so that the shear strain could be determined. For $\nu \simeq 0.5$, the shear strain is equal to the axial strain in the triaxial test because

$$\epsilon_r = (2/3)(\epsilon_{ar} - \epsilon_{rr}) = (2/3)(\epsilon_{ar} + 0.5\epsilon_{ar}) = \epsilon_{ar} \quad (17)$$

By using the expression for the tangent resilient modulus (Equation 12),

$$\epsilon_r = \epsilon_{ar} = (q_r/M_r) = (q_r/K)(q_{max}/p_o')^s \quad (18)$$

This expression was then used in the same way as Equation 10 for the granular material by following Equations 14-16.

The bulk modulus was calculated from an assumed constant Poisson's ratio and the correct value of G by using:

$$K = [2(1 + \nu)/3(1 - 2\nu)]\,G \quad (19)$$

Clearly, K equals ∞ if ν equals 0.5. The asphalt layer has been treated as linear elastic in all analyses to date, the value of Young's modulus was taken as the dynamic stiffness (19,20), and Poisson's ratio was 0.4.

No special provisions are made in the SENOL program to prevent elements from going beyond a failure condition. A stress-adjustment procedure was used by Raad and Figueroa (3) to ensure that no element exceeded the Mohr-Coulomb failure condition. By using the detailed granular material model in SENOL, the need for a failure correction is less necessary as large strains will develop when stresses approach failure. This results in an automatic redistribution of stresses. This will not be the case when the simple model adopted by Raad and Figueroa is used and, hence, their correction procedure is necessary. The fact that elements in some analyses by SENOL did go slightly beyond failure in practice is a reflection of the inaccuracy of the resilient model at high stress levels and an indication of a weak pavement. Ideally, the model should be of a form that can deal with all stress conditions and cope with the onset of failure.

The use of stress invariants to specify stress conditions avoids the problems encountered in other finite-element analyses due to tensile stress in a particular direction. So-called tension corrections have been applied, perhaps unnecessarily, since failure of granular material depends on the relative values of p' and q and hence on the complete stress system at a point. If at any stage in the computation procedure of SENOL a tensile value of p' occurred, then a very low modulus (E = 100 kPa) was assigned to the element concerned. This only occurred under very severe loading conditions when, in most cases, a convergent solution was unobtainable, which indicates pavement failure.

The SENOL program has been used in computing the response of test pavements (18) to moving wheel loads. Typical results are given in Figures 8 and 9. The structure comprised 50 mm of hot rolled asphalt and 170 mm of well-graded crushed limestone over a silty-clay subgrade. A moving wheel load of 8 kN was applied at a contact pressure of 530 kPa and a speed of 14.5 km/h. The test temperature was 25°C. The resilient strains (Figure 8) were generally better predicted than the transient stresses (Figure 9). Note that the check against measured values is thorough and involves vertical, radial, and tangential directions at different depths in the three-layered structure and includes variations in radial distance from the wheel-load center. The horizontal axis of each plot in Figures 8 and 9 is located at the relevant depth in the structure determined from the left-hand vertical scale.

We have also used the program in an extensive parameter study to examine the effects of thickness and stiffness of the asphalt layer, thickness of the granular layer, and stiffness of the subgrade on the stresses and strains of interest for pavement design. These data are proving extremely useful in formulating simplified procedures for use in design.

CONCLUSIONS

1. The simple nonlinear model ($M_r = K_1\theta^{K_2}$), frequently used for the characterization of granular materials in pavement analysis, is likely to lead to inaccurate results because it has been established from data that used a very limited range of stress paths;
2. A more complex model that gives a better description of resilient response has been developed for crushed rock and can be used in numerical analyses that involve three-dimensional stress systems;
3. Whenever possible, characteristics of soil and granular material should be expressed in terms of effective stresses;
4. More research is required on the resilient properties of fine-grained soils in order to establish reliable stress-strain relationships based on effective stress; and
5. A finite-element program, called SENOL, has been developed for the analysis of problems that involve nonlinear materials.

ACKNOWLEDGMENT

We are grateful for the assistance rendered by P. Shaw in providing data for this paper. The contents are based on research carried out for the Transport and Road Research Laboratory, the European Research Office of the U.S. Army, and British Rail. The sponsorship of these organizations is gratefully acknowledged. The work was carried out in the Department of Civil Engineering, University of Nottingham. Facilities were provided through the courtesy of R.C. Coates. The interest and advice of P.S. Pell was also much appreciated.

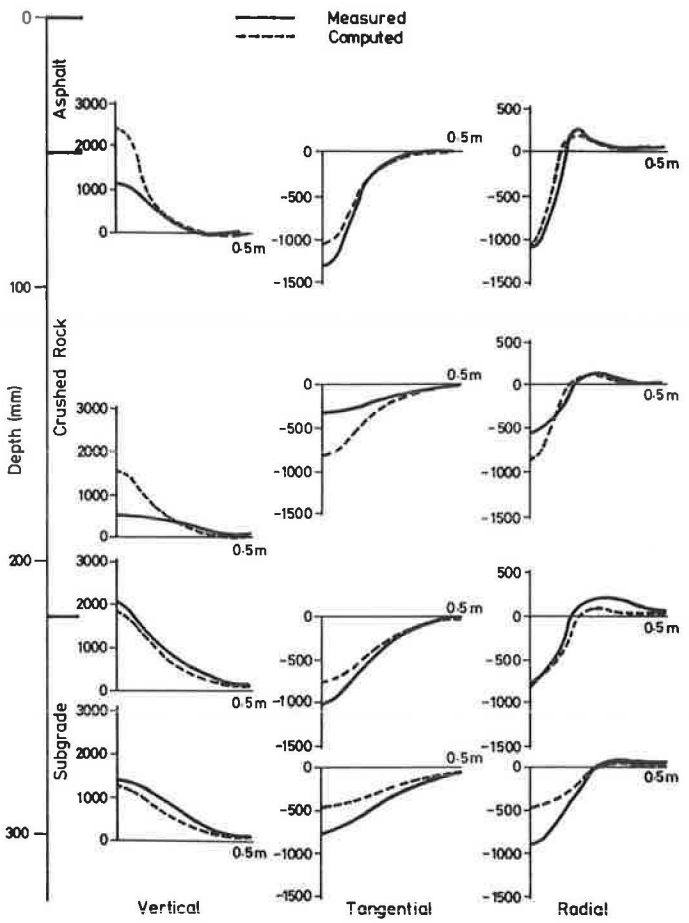

Figure 8. Comparison of resilient strains in microstrain with values computed by SENOL.

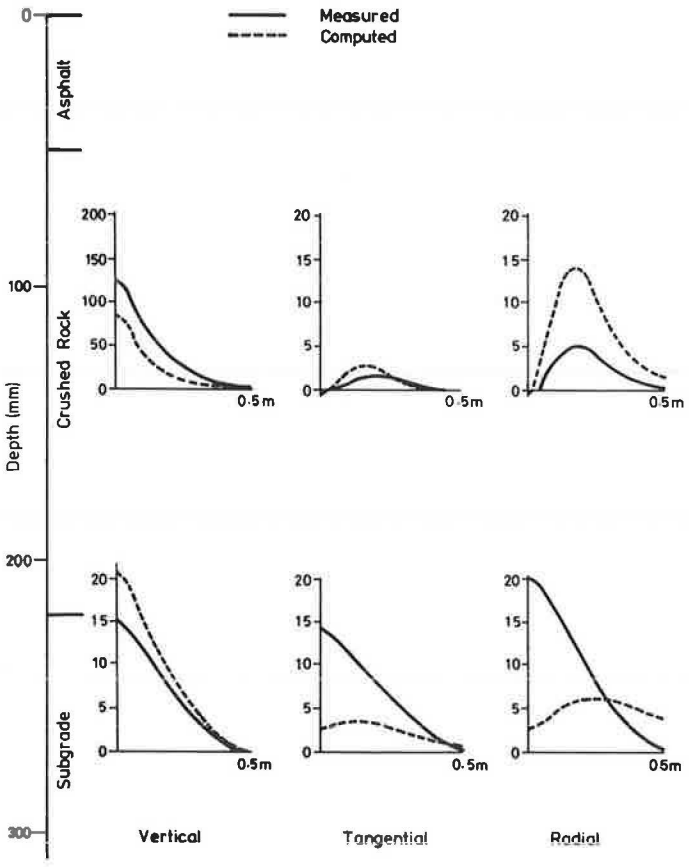

Figure 9. Comparison of transient stresses in kilopascals with values computed by SENOL.

REFERENCES

1. R.G. Hicks and C.L. Monismith. Factors Influencing the Resilient Response of Granular Materials. HRB, Highway Research Record 345, 1971, pp. 15-31.
2. H.B. Seed, C.K. Chan, and C.E. Lee. Resilience Characteristics of Subgrade Soils and Their Relation to Fatigue Failures in Asphalt Pavements. Proc., International Conference on the Structural Design of Asphalt Pavements, Ann Arbor, MI, 1962, pp. 611-636.
3. L. Raad and J.L. Figueroa. Load Response of Transportation Support Systems. Transportation Engineering Journal, ASCE, Vol. 106, No. TE1, 1980, pp. 111-128.
4. J.L. Figueroa and M.R. Thompson. Simplified Structural Analyses of Flexible Pavements for Secondary Roads Based on Illi-Pave. TRB, Transportation Research Record 766, 1980, pp. 5-10.
5. S.F. Brown. Improved Framework for Predicting Permanent Deformation in Asphalt Layers. TRB, Transportation Research Record 537, 1975, pp. 18-30.
6. A.N. Schofield and C.P. Wroth. Critical State Soil Mechanics. McGraw-Hill, New York, 1968.
7. J.R. Boyce, S.F. Brown, and P.S. Pell. The Resilient Behaviour of a Granular Material Under Repeated Loading. Proc., Australian Road Research Board, Vol. 8, 1976, pp. 8-19.
8. J.R. Boyce and S.F. Brown. Measurement of Elastic Strain in Granular Material. Geotechnique, Vol. 26, No. 4, 1976, pp. 637-640.
9. J.W. Pappin and S.F. Brown. Resilient Stress-Strain Behaviour of a Crushed Rock. Proc., International Symposium on Soils Under Cyclic and Transient Loading, Swansea, Great Britain, Vol. 1, 1980, pp. 169-177.
10. P. Shaw and S.F. Brown. Further Developments of Test Equipment for Shear Reversal on Granular Materials. Univ. of Nottingham, Nottingham, England, Rept. PS/2, Feb. 1980.
11. J.W. Pappin. Characteristics of a Granular Material for Pavement Analysis. Univ. of Nottingham, Nottingham, England, Ph.D. thesis, June 1979.
12. W.S. Smith and K. Nair. Development of Procedures for Characterization of Untreated Granular Base Course and Asphalt-Treated Base Course Materials. FHWA, FHWA-RD-74-61, 1973.
13. S.F. Brown. The Characteristics of Soils for Flexible Pavement Design. Proc., 7th European Conference on Soil Mechanics and Foundation Engineering, Brighton, England, Vol. 2, 1979, pp. 15-22.
14. G.L. Dehlen. The Effect of Nonlinear Material in the Behavior of Pavements Subjected to Traffic Loads. Univ. of California, Berkeley, Ph.D. thesis, 1969.
15. D.G. Fredlund, A.T. Bergan, and P.K. Wong. Relations Between Resilient Modulus and Stress Conditions for Cohesive Subgrade Soils. TRB, Transportation Research Record 642, 1977, pp. 73-81.
16. S.F. Brown, A.K.F. Lashine, and A.F.L. Hyde. Repeated Load Triaxial Testing of a Silty Clay. Geotechnique, Vol. 25, No. 1, 1975, pp. 95-114.
17. M.R. Thompson and Q.L. Robnett. Resilient Properties of Subgrade Soils. Transportation Engineering Journal, ASCE, Vol. 105, No. TE1, 1979, pp. 71-89.
18. S.F. Brown, J.W. Pappin, and B.V. Brodrick. Permanent Deformation of Flexible Pavements. European Research Office, U.S. Army, Univ. of Nottingham, Nottingham, England, Final Rept., 1980.
19. C. Van der Poel. A General System Describing the Visco-Elastic Properties of Bitumens and Its Relation to Routine Test Data. Journal of Applied Chemistry, No. 4, 1954, pp. 221-236.
20. W. Heukelom and A.J.G. Klomp. Road Design and Dynamic Loading. Proc., Assoc. of Asphalt Paving Technologists, Vol. 33, 1964, pp. 92-123.

Publication of this paper sponsored by Committee on Strength and Deformation Characteristics of Pavement Sections.

Comprehensive Evaluation of Laboratory Resilient Moduli Results for Granular Material

GONZALO RADA AND MATTHEW W. WITCZAK

A comprehensive evaluation of nonlinear resilient modulus test results on granular materials is presented. A total of 271 test results obtained from 10 different research agencies were used as the data base. The main objectives of the study were to (a) determine whether typical M_r relations exist for various granular materials; (b) develop a comprehensive summary of factors that affect the M_r response and determine whether predictive equations or typical relations could be stated; and (c) investigate whether a correlation exists between laboratory-measured M_r and laboratory-measured California bearing ratio (CBR) values. The results indicate that there appears to be an inverse relationship between K_1 and K_2 ($M_r = K_1\theta^{K2}$) for all granular materials. Six unique K_1 and K_2 relations are proposed for six different granular material types (silty sands, sand gravels, sand aggregate blends, crushed stone, limerock, and slag). Predictive equations are developed to relate the primary variables that influence the M_r response of six different aggregates (used by the Maryland State Highway Administration). The equations use bulk stress, degree of saturation, and percentage of modified compaction. Typical M_r equations are also stated to reflect probable influences of the K_1 and K_2 values due to compaction and moisture for the Maryland aggregates. Based on an analysis of nearly 100 data pairs, a general, but variable, correlation was found between laboratory-measured M_r and CBR values. However, the constant that relates these variables is a function of stress state. For typical bulk stress values anticipated in highway pavement structures, the coefficient (constant) value is significantly lower than the 1500-value suggested by Huekelom and Foster.

The resilient modulus test of unbound granular materials has been used for several years as a means of evaluating the response of granular material in the laboratory. The modulus (M_r) is a dynamic test response defined as the ratio of repeated axial

Table 1. Summary of M_r test results evaluated.

Research Agency	Reference	No. of Tests	Material
Asphalt Institute	(1-6)	36	Sands, silty sand, sand gravels, gravels, crushed gravel, crushed stone, and limerock
University of California at Berkeley	(7-9)	41	Sand gravels, gravels, and crushed gravels
Georgia Institute of Technology	(10)	19	Sand gravels, soil-aggregate blends, and crushed stone
National Crushed Stone Association	(11)	6	Crushed stone
University of Illinois	(12)	18	Crushed stone and gravels
Pennsylvania State University	(13)	2	Crushed stone
Florida Department of Transportation	(14)	5	Limerock and sands
U.S. Army Corps of Engineers	(12, 15-17)	11	Silty sand, sand gravels, and crushed stone
Woodward Clyde	(18, 19)	6	Sand gravels, crushed gravels, and crushed stone
University of Maryland, previous studies	(20)	26	Sands, soil-aggregate blends, sand gravels, crushed stone, limerock, and slag
Subtotal		170	
University of Maryland, MSHA project	MSHA study	101	Sand gravels, soil-aggregate blends, crushed stone, and slag
Total		271	

Figure 1. K_1-K_2 relation for all aggregate M_r results.

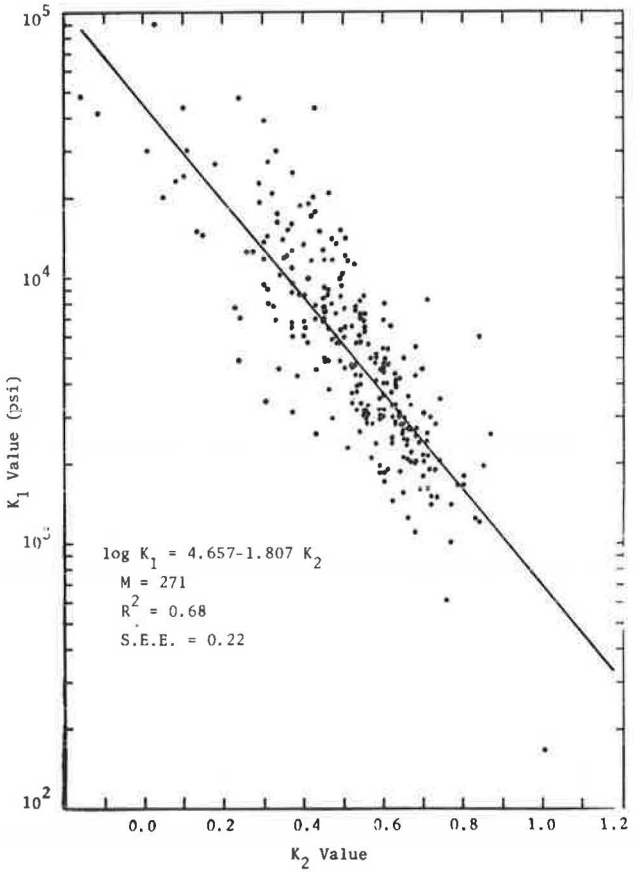

deviatoric stress (σ_d) to the recoverable or resilient axial strain (ϵ_r) or

$$M_r = \sigma_d/\epsilon_r \quad (1)$$

In general, the test is conducted in a triaxial cell that is equipped to monitor repetitive load conditions (pneumatic or electrohydraulic loading system) on cylindrical samples, usually 4-6 in in diameter. Both dynamic load and deformations [through linear variable differential transformers (LVDTs)] are measured continuously during the test. Previous studies have indicated that resilient deformations generally stabilize after 200 repetitions of load and, as such, the M_r value is usually computed at this level of repetition.

Because of the known nonlinear (stress-dependent) properties of most granular materials, the test is conducted at combinations of confining pressure (σ_c and σ_1/σ_3) ratios. Results of a single test are usually presented in a mathematical form that directly incorporates the stress sensitivity of the M_r value in terms of either σ_c or bulk stress (first stress invariant) (θ) by

$$M_r = K_1\theta^{K_2} = K_1'\sigma_c^{K_2'} \quad (2)$$

The constants (K_1', K_2' or K_1, K_2) are obtained from regression analysis of the test results and depend on the type of material and physical properties of the specimen during the test.

STUDY OBJECTIVES

Since the development of the M_r test, numerous individual research studies have investigated the dynamic response of granular materials. However, in general, each study was directed toward a specific type of material or a particular parameter on the M_r response for a given material. In view of this, an extensive laboratory study was initiated in 1978 at the University of Maryland for the Maryland State Highway Administration (MSHA) to develop M_r responses for typical base and subbase materials used in pavement systems. The combined evaluation of previous results and the Maryland study afforded the opportunity to assess various questions not previously addressed by other researchers.

Based on the relatively large data base collected, the following specific objectives were studied in this project:

1. Investigate whether typical limits of M_r relations exist for various granular material classes (types),
2. Investigate the feasibility of developing predictive M_r equations from physical properties of the granular materials,
3. Develop a comprehensive evaluation of factors that affect the M_r response of granular materials, and
4. Investigate whether accurate correlations between M_r and the California bearing ratio (CBR) exist for granular materials.

Data Sources

As noted, a comprehensive literature review of the M_r results of granular material reported by other researchers was conducted. Table 1 is a summary of the agencies, number of tests, materials studied, and references obtained from this literature review. As noted, a total of 170 individual M_r tests was found in the literature from 10 different

Figure 2. Effects of K_1 and K_2 on the resilient modulus.

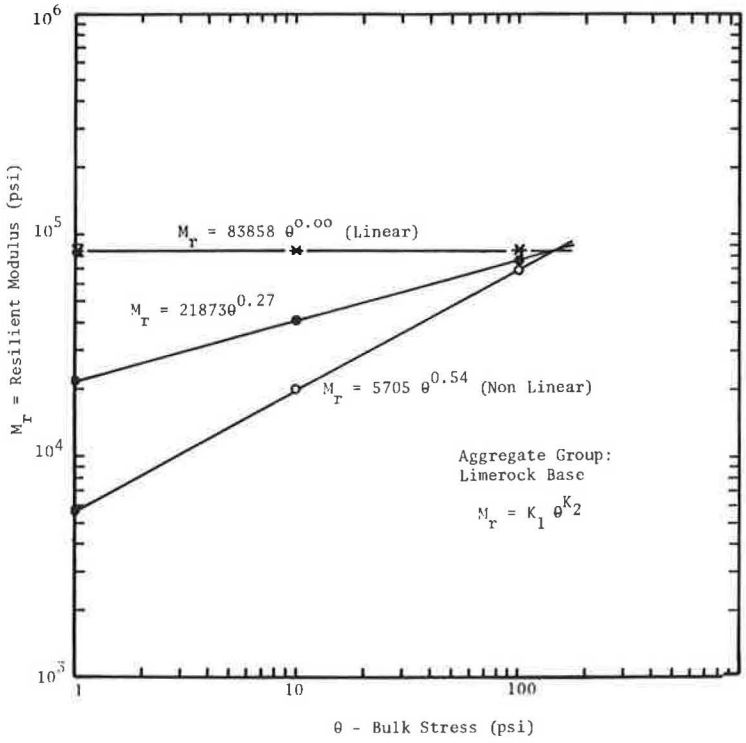

agencies. The results obtained were summarized for only the form that used the bulk stress (θ) equation (i.e., K_1 and K_2 values).

University of Maryland Study

Also shown in Table 1 is information regarding the M_r study on MSHA base and subbase materials. As noted, 101 separate M_r tests were conducted in this project. Thus, the combined number of individual granular material M_r results used in this report was 271.

Specific Testing Program

Although 271 combined M_r test results were available, not all of the previous studies contained information that could be used in all phases of the study objectives. The testing program of the MSHA study was thus developed to fill information gaps concerning the M_r response of various materials.

The study for MSHA involved testing six different aggregate types [two limestones that meet MSHA and dense-graded aggregate (DGA) specifications; a crushed stone and slag that meet MSHA crusher run (CR) 6 specifications; a bank-run gravel that meets MSHA specifications; and a sand-aggregate subbase blend]. For each aggregate investigated, three hand-blended gradations were used. On each aggregate-gradation combination, three compaction energies (low, standard, and modified) were used to develop moisture-density relations. In addition to developing compaction curves, as-molded and soaked CBR tests (588) were conducted.

The resilient modulus phase of the test program involved the testing of 18 specimens per aggregate. In general, for each aggregate-gradation combination, three M_r tests were conducted at modified compaction effort (optimum and ±2 percent optimum moisture), two tests at standard compaction effort (optimum and +2 percent optimum moisture), and one at optimum for a low (2200 pound•ft/ft³) compaction effort. The above M_r test program theoretically should have yielded 108 M_r data points, but 7 specimens failed or were unable to be tested.

TYPICAL M_r RESULTS FOR AGGREGATES

The analysis of all 271 individual M_r test results (from all agencies) led to an interesting observation relative to the overall behavior of all granular materials as a group. Figure 1 shows the relation between K_1 and K_2 for the entire data set. Observe that a definite correlation exists between increasing K_1 and decreasing K_2 for granular materials. Although the R^2 value of 0.68 is not exceptionally high from a statistical viewpoint, recognize that the results shown represent extremely variable physical properties as well as aggregates that range from fine silty sands to slag and limerock materials.

The significance of this relation may also be used to denote the relative degree of material nonlinearity. Recall the form of equation 2: As K_2 approaches a value of $K_2 = 0$, the material is truly linear, whereas larger K_2 values imply a greater degree of nonlinearity. This is illustrated in Figure 2, which shows M_r equations developed on a single limerock material tested under three differing sets of physical properties. The relative changes in the K_1 and K_2 values and their respective influence on the degree of nonlinearity can be observed.

Aggregate Class Analysis

In order to determine whether the scatter of points shown in Figure 1 could be reduced, a study was undertaken to determine whether relatively unique K_1-K_2 relations existed among various types (classes) of granular materials. Although not presented in this report, groupings of data based on both American Association of State Highway and Transportation Officials (AASHTO) and Unified Soil Classification System (USCS) systems were evaluated and found to yield poor correlations. By far, the

Table 2. Summary of K_1 and K_2 statistics by aggregate class.

Aggregate Class	No. of Data Points	K_1 Parameter			K_2 Parameter		
		Mean	SD	Range	Mean	SD	Range
Silty sands	8	1 620	780	710 to 3830	0.62	0.13	0.36 to 0.80
Sand gravel	37	4 480	4 300	860 to 12 840	0.53	0.17	0.24 to 0.80
Sand-aggregate blends	78	4 350	2 630	1880 to 11 070	0.59	0.13	0.23 to 0.82
Crushed stone	115	7 210	7 490	1705 to 56 670	0.45	0.23	-0.16 to 0.86
Limerock	13	14 030	10 240	5700 to 83 860	0.40	0.11	0.00 to 0.54
Slag	20	24 250	19 910	9300 to 92 360	0.37	0.13	0.00 to 0.52
All data	271	9 240	11 225	710 to 92 360	0.52	0.17	-0.16 to 0.86

Table 3. K_1-K_2 regression models by aggregate class.

Aggregate Class	Regression Constants of Form: $\log K_1 = A_0 + A_1 K_2$		R^2	Standard Error of Estimate
	A_0	A_1		
Silty sands	4.183	-1.666	0.75	0.14
Sand gravel	4.613	-2.100	0.82	0.17
Sand-aggregate blends	4.345	-1.308	0.56	0.15
Crushed stone	4.515	-1.492	0.68	0.19
Limerock	4.924	-2.162	0.92	0.08
Slag	4.965	-1.917	0.50	0.26
All data	4.657	-1.807	0.68	0.22

best grouping of the 271 data points occurred when the granular materials were divided qualitatively into the following six categories:

1. Silty sands;
2. Sand gravels;
3. Sand-aggregate blends, including shell-stabilized sands and crushed gravels;
4. Crushed stones;
5. Limerocks; and
6. Slags.

The resulting population of K_1 and K_2 values for a given group was analyzed to determine the typical limits associated with each group. Table 2 summarizes the results of this study by aggregate class. Regression studies between K_1 and K_2 for each class were conducted and the results summarized in Table 3. Figure 3 illustrates the resulting K_1 and K_2 relations found in the analysis. The limits of each line shown in this figure represent the actual limits of test results found.

Based on these results, the following observation can be made. Each class of aggregates appears to have its own relatively unique K_1-K_2 relation that distinguishes it from other groups. Although the R^2 values range from 0.50 to 0.92, much of the variation is due to material variations within a class (e.g., crushed limestone versus crushed gneiss) as well as the physical properties of each specimen during the test. The overall mean values, for all granular materials, of K_1 = 9240 and K_2 = 0.52 are generally in excellent agreement with typical values assumed in many design situations.

However, although this may be true from a global viewpoint, the range of K_1 (and hence K_2) within a given class appears to be significant. The largest range shown occurs for the crushed stone group, which has a range of K_1 values from 1700 to 57 000. Because of this, the influence of the specific type and moisture-density conditions are critical to accurate evaluation of the proper K_1-K_2 value to be used in design. In fact, the use of typical K_1-K_2 values to represent a specific granular material such as crushed stone or sand gravels may be more misleading in design.

Finally, observe from Table 2 that the average K_1 and K_2 values by aggregate class appear reasonable. In general, the order in which the aggregate classes are stated coincides with increasing K_1 order (decreasing K_2). This indicates that the overall degree of linearity increases from the silty sand category to the slag group. The order shown also corresponds generally to what one would associate with increasing shear strength behavior by the aggregate classes noted.

Loading Conditions

The effect of loading conditions in the M_r test for granular materials is generally well understood from previous research investigations. The most-significant loading factor that affects the modulus is the stress level (8,9,11,12,19,21-25). In general, it is customary to relate either θ and σ_c to the modulus. In this study, the M_r relation that uses θ was used because of its ease of adaptation into nonlinear solutions in layered pavement systems.

Other load factors, such as stress duration, stress frequency, sequence of load, and number of stress repetitions necessary to reach an equilibrium-resilient strain response have been covered adequately in the literature (9,11,12,21,23,24). In general, these factors have little, if any, effect on the M_r response. In the testing at the University of Maryland, a haversine pulse load (0.1-s load duration) at 30 repetitions/min was used. Modulus values were computed with resilient strains after 200 load repetitions.

Degree of Saturation

Based on previous studies (9,12,19,21,26), the degree of saturation (for a given aggregate) plays a major role in the M_r response. Repeated load triaxial tests, conducted by Haynes and Yoder (12,19,26) on gravels and crushed stone, indicated that there was a critical degree of saturation near 80-85 percent, above which granular materials became unstable and deteriorated rapidly under repeated loading. Seed and others (12,19,26) found that, for well-graded gravels, K_1 was reduced and K_2 unchanged with increasing saturation (S_r) values. This was also substantiated in work conducted by Kallas, Riley, Shifley, Hicks, and Finn (12,19,26).

Figure 4 shows the general effect of S_r on the K_1 and M_r values (at θ = 10 lbf/in^2) for 159 separate test results on a variety of aggregates. From this global viewpoint, the marked reduction in the K_1 value and modulus with increasing saturation is clearly evident. In general, the effects of moisture can change the typical K_1 values from 30 000 (dry) to 1000 (saturation), with resultant changes in modulus from 40 000 to 10 000 lbf/in^2 or less.

Although the above is true in a general sense, the exact influence of saturation appears to be

Figure 3. Typical K_1-K_2 relations by aggregate class.

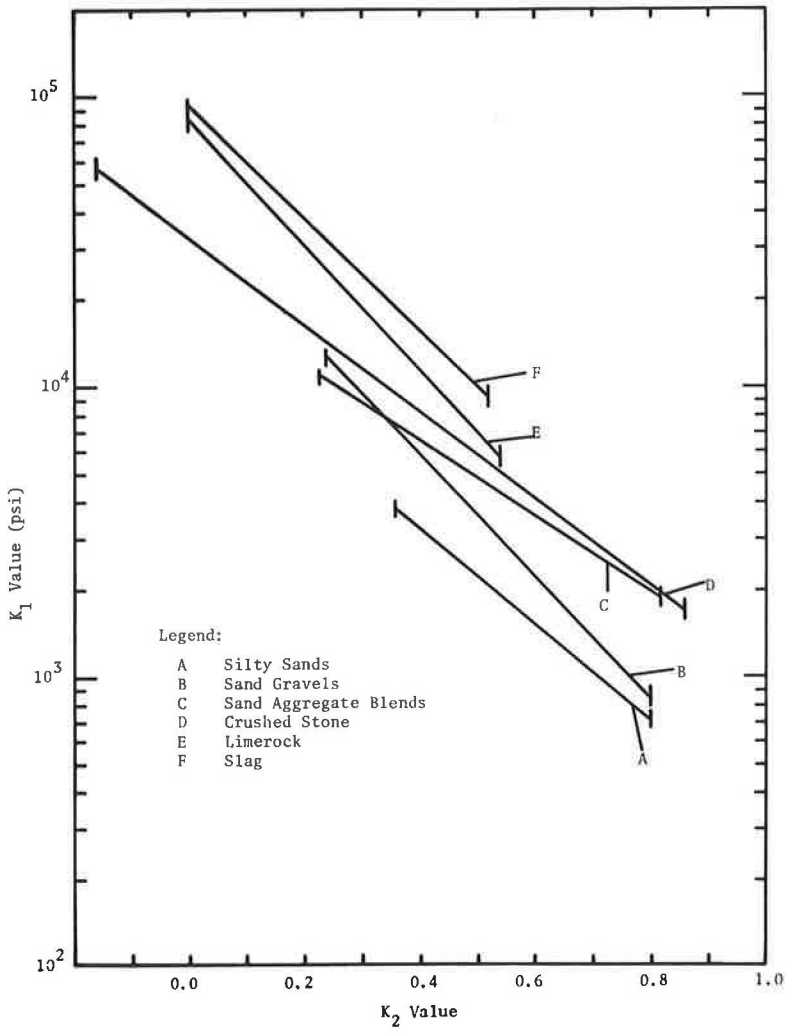

Figure 4. Effect of degree of saturation on K_1 and M_r.

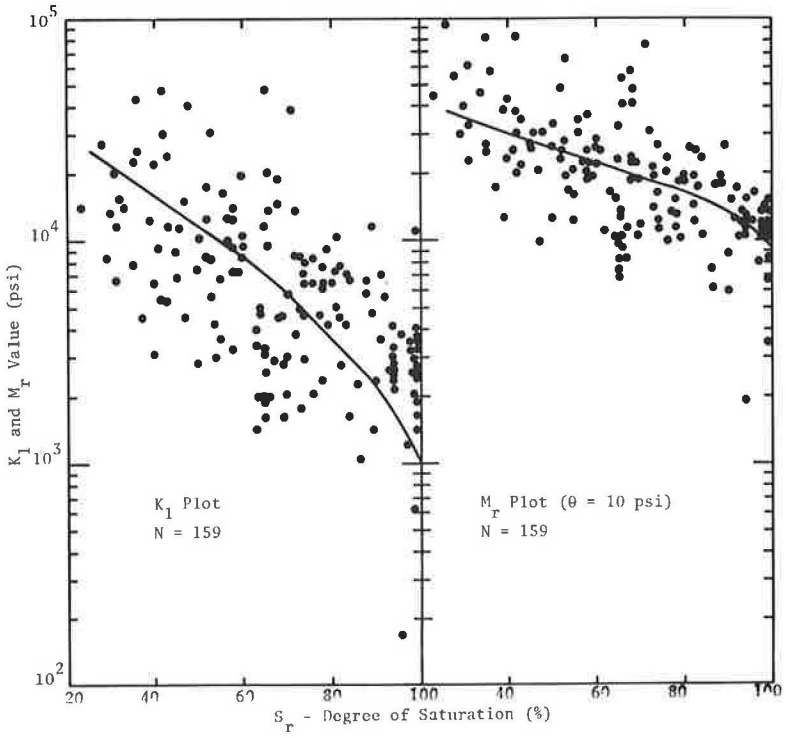

Figure 5. Effect of degree of saturation on K_2.

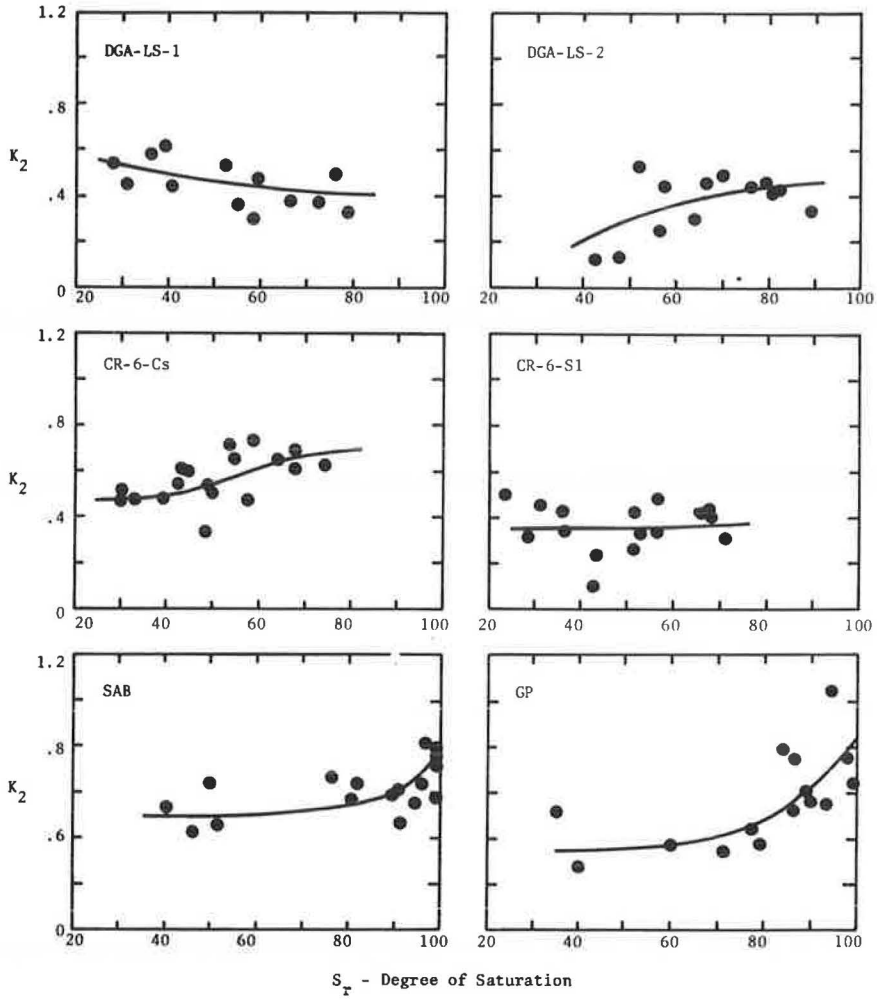

dependent on the aggregate type. The following acronyms for the aggregate are used in Figures 5-9:

LS--limestone,
CS--crushed stone,
Sl--slag,
SAB--sand-aggregate blend, and
GP--bank-run gravel.

Figure 5 illustrates the influence of S_r on K_2 for the six aggregates investigated in the MSHA study. Observe that, although changes in K_2 may not be large, various trends are recognizable from the plots. There is, however, no uniform trend among all aggregates. For example, a comparison of the K_2 values for the two different crushed limestone materials (DGA-limestone-1 and DGA-limestone-2) show decreasing and increasing K_2 trends with increased S_r, respectively. However, in general, the increase in K_2 for S_r values near saturation is very pronounced for the subbase materials (sand-aggregate blend and bank-run gravel). For these materials, a definite increase in K_2 at high saturations is clearly evident. Finally, the analysis of K_2 and S_r showed no distinctive pattern relative to the influence of compactive effort and aggregate gradation on the results.

In contrast to the relatively minor influence of S_r on K_2, the influence of S_r on the K_1 values may be significant. Figure 6 shows the results for three of the six aggregates investigated in the MSHA study (two crushed limestone-DGA and the bank-run gravel). For the two crushed stone materials, the influence of S_r on the K_1 value is seen to vary even within a common aggregate class. The DGA-limestone-1 material is a relatively hard, dense (low-abrasion) limestone and appears to exhibit less of a sensitivity in K_1 to the effects of moisture. This contrasts to the softer (high-abrasion) DGA-limestone-2 material that yields a greater influence of K_1 to S_r.

Although the two crushed limestones may exhibit differing degrees of moisture sensitivity, we can also see that they exhibit less sensitivity compared with the bank-run gravel results, especially near the critical 80-85 percent level suggested by Haynes and Yoder. The resulting decrease in modulus for these materials, with increasing S_r values, is clearly shown in Figure 6.

Percentage Compaction

Several studies have been conducted by previous researchers into the effects of density on the M_r response of granular material (8,9,12,21-23,26). These studies have indicated that, although increase in density results in an increase in modulus, the effect is relatively small compared with changes caused by stress level and moisture. The results of the MSHA study generally confirm this over a wide range of aggregate types.

Figure 7 is a plot of the average K_1 and K_2 values (by aggregate) as a function of the unit volumetric compaction energy (E_c). As previously noted, three levels of compaction energy were studied. The low compactive effort was E_c = 2200

Figure 6. Influence of degree of saturation on K_1 and M_r for several aggregates.

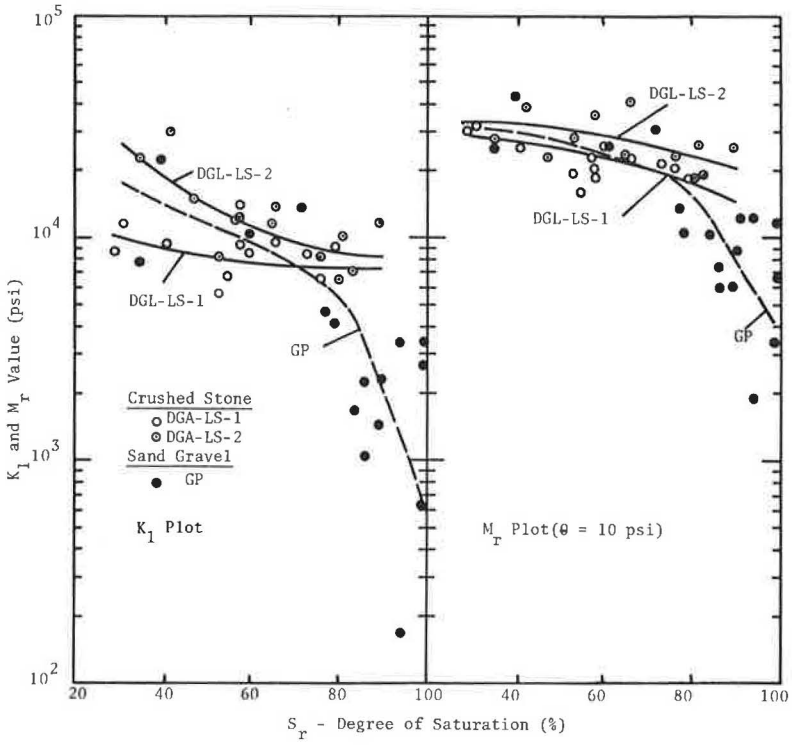

Figure 7. Influence of compaction energy on K_1 and K_2.

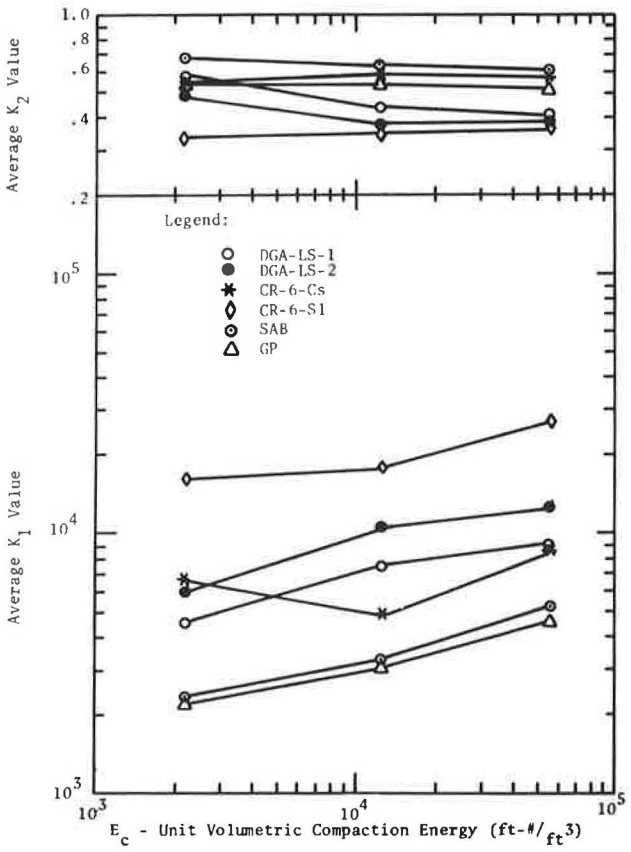

ft•lb/ft³, although the remaining two levels were standard and modified (12 300 and 56 200 ft•lb/ft³, respectively). From this figure, observe that K_1 increases gradually with increasing compaction and the K_2 value remains essentially constant. The average increase in K_1, from standard to modified compaction energy, was nearly 48 percent: the DGA aggregates averaged 25 percent, CR-6 averaged 62 percent, and the subbase materials (sand-aggregate blends and bank-run gravel) averaged 58 percent. Based on these results, the influence of compaction in improving the modulus (K_1) cannot be ignored.

Aggregate Gradation

Previous research investigations of the effect of aggregate gradation have indicated no general trend regarding the influence of fines (percentage that passes no. 200) on the M_r response (8,9,12.21-23, 26). In general, the degree of influ- ence of this parameter appears to be related to the aggregate investigated.

In the MSHA study, hand-blended gradations were used to investigate the effect of the p_{200} variable. All of the six aggregates studied had a D_{max} = 1.0 in. The four base materials (DGA and CR-6) were graded according to

$$p = (d/D_{max})^n \quad (3)$$

with n values of 0.30, 0.45, and 0.6. The selection of these values resulted in gradations that progressed from dirty (17 percent), dense (7 percent), to lean or open (3 percent) type. Because of difficulties involved in obtaining enough fines (p_{200}) for the subbase materials, the sand-aggregate blend used three gradations that had p_{200} values of 3.2, 4.3, and 5.8 percent, and the bank-run gravel material used p_{200} values of 5.1, 10, and 15 percent.

Figure 8 illustrates the results of this study phase. We can see that there is no general or uniform trend applicable for all aggregate types, although several observations can be made. For the angular base materials (DGA and CR-6 aggregates), there appears to be little change in either K_1 or K_2 for p_{200} values in the dense to dirty range

Figure 8. Influence of percentage fines on K_1 and K_2.

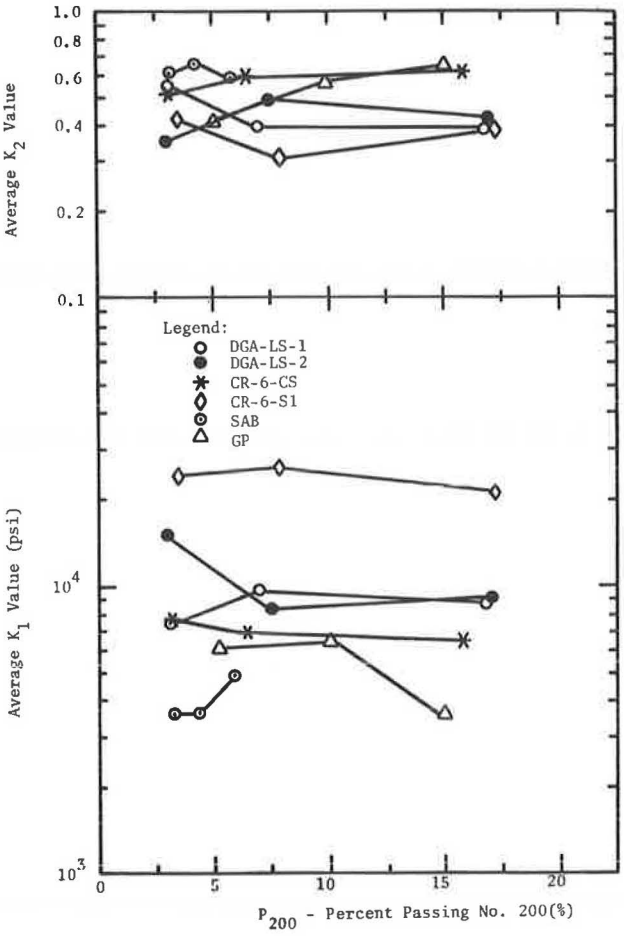

(around 7-17 percent). This is not the case, however, for the bank-run gravel. For this material, an optimum K_1 value is apparent near the dense condition and a marked decrease in K_1 occurs as the P_{200} value increases. In contrast, the K_2 value for the bank-run gravel series appears to increase with an increase in fines. Thus, just like the results for S_r effect, the relative sensitivity for the sand-gravel material is more pronounced than for crushed, angular aggregate. Finally, although no pronounced changes occur in K_1 and K_2 for the base materials, it would be intuitively obvious that increases in P_{200} beyond the 16-18 percent range would eventually have pronounced changes in the M_r response for these materials.

M_r Predictive Equations

The previous discussion has focused on the relative influence of loading and physical properties on the M_r response of various aggregates. In general, the most-significant factors found to affect M_r are the stress state, degree of saturation, and compactive effort (density). In addition, the general changes in the K_1 and K_2 values were noted with changes in several variables.

Based on the results of the MSHA study, predictive equations were investigated to develop accurate M_r predictions from the significant variables. Several forms and variables were considered in this analysis. The most accurate (highest R^2 and lowest standard error) model was found to be of the form shown in Table 4. Also shown in the table are regression constants for each aggregate type and for the model by using all aggregate types combined. The form of the model used implies that no interaction effect of the primary variables are considered for the K_2 value (note that $C_3 = K_2$). Further work is being conducted to determine whether increased accuracy will result if C_3 has various functions of the input values.

The major input variables are bulk stress (θ), degree of saturation (S_r), and percentage compaction relative to modified compactive effort (PC). Table 5 shows the influence of variables in the predictive equations studied as measured by the R^2 value. Observe that the addition of the P_{200} variables added little to the predictive accuracy; however, the elimination of the PC term lowered the R^2 values significantly for all aggregates except DGA-limestone-1 and sand-aggregate blend.

Typical Relations

Based on the MSHA study, typical $M_r = f(\theta)$ relations for the six aggregate types studied have been developed and are summarized in Table 6. This classification scheme reflects the relative influence of the significant variables on the K_1-K_2 values.

Modulus-CBR Comparison

Although recent research has focused on the use of laboratory determined moduli in design procedures, empirical correlations to existing routine tests are frequently used. One of the most-widely used correlations is the one developed by Huekelom and Foster (25), which relates dynamic modulus to CBR. The relation established

$$E = 1500\ CBR \quad (E \text{ in lbf/in}^2)$$

was found from extensive dynamic (wave propagation)

Table 4. Summary of M_r predictive equations, physical properties.

Aggregate	Regression Constants in $\log M_r = C_0 + C_1 S_r + C_2 PC + C_3 \log\theta$						
	No. of Data Points	C_0	C_1	C_2	C_3	R^2	Standard Error
DGA-limestone-1	14	3.4060	-0.005 289	0.011 94	0.004 843	0.79	0.13
DGA-limestone-2	17	-0.3017	-0.005 851	0.050 54	0.004 445	0.60	0.21
CR-6-crushed stone	18	1.0666	-0.003 106	0.035 56	0.006 469	0.81	0.15
CR-6-slag	17	3.2698	-0.003 999	0.016 63	0.003 840	0.59	0.18
Sand-aggregate blend	18	4.1888	-0.003 312	0.021 38	0.006 785	0.83	0.15
Bank-run gravel	17	0.9529	-0.012 07	0.041 17	0.006 035	0.84	0.17
All data	101	4.022	-0.006 832	0.007 055	0.005 516	0.61	0.23

Note: S_r = degree of saturation (%), PC = percentage compaction relative to modified density (%), and θ = bulk stress or first stress invariant (lbf/in^2).

field tests and not laboratory resilient moduli. Although the equation is important, note that their data showed a wide range of scatter and had a band width of roughly ±2. Although the equation has been used frequently for predicting subgrade moduli for materials that have CBR of 20 or less, the original Huekelom and Foster data uniformly covered a range of CBR from 2 to 200.

In the MSHA study, recall that complete moisture-density strength curves (CBR, as molded and soaked) were established for each aggregate type (six), gradation (three), and compactive energy (three) combination. Thus, for each compacted M_r test specimen studied, it was possible to establish the laboratory measured CBR value. This allowed for the comparison of laboratory derived M_r values to laboratory measured CBR values for each modulus specimen.

Because the M_r value from the resilient tests is stress dependent, there cannot be a unique relation between M_r and CBR. Figure 9 is a summary plot that compares CBR to M_r values at bulk stress levels of 10 and 100 lbf/in^2. As can be seen from both diagrams, a general correlation between modulus and CBR does exist. However, the results indicate that a wide range of scatter exists for the relation. In general, the scatter bands shown on each diagram (±1σ) are roughly equivalent to a 50 percent relative difference in residual error. This band is also very similar to the ±2 band width defined by Heukelom and Foster.

The results of this study were analyzed by using the relation:

$$M_r(\theta) = F(CBR) \quad (4)$$

Table 5. Influence of variables on R^2 values for M_r predictive equations.

Aggregate	No. of Data Points	S_r, P_{200}, PC, θ	S_r, PC, θ	S_r, θ
DGA-limestone-1	14	0.79	0.79	0.78
DGA-limestone-2	17	0.61	0.60	0.41
CR-6-crushed stone	18	0.82	0.81	0.46
CR-6-slag	17	0.59	0.59	0.46
Sand-aggregate blend	18	0.85	0.83	0.83
Bank-run gravel	17	0.84	0.84	0.76
All data	101	0.61	0.61	0.60

Table 6. Typical M_r relations for MSHA aggregates.

	Dry, S_r < 60 Percent				Wet, S_r > 85 Percent			
	Standard CE		Modified CE		Standard CE		Modified CE	
Aggregate	K_1	K_2	K_1	K_2	K_1	K_2	K_1	K_2
DGA-limestone-1[a]	8 500	0.5	10 500	0.5	7000	0.4	9000	0.4
DGA-limestone-2[a]	11 500	0.3	15 000	0.3	6000	0.5	7500	0.5
CR-6-crushed stone[a]	6 000	0.5	9 000	0.5	3500	0.7	5000	0.7
CR-6-slag[a]	12 500	0.35	20 000	0.35	5600	0.35	9000	0.35
Sand-aggregate blends[b]	3 800	0.5	6 000	0.5	1900	0.7	3000	0.7
Bank-run gravel[b]	5 000	0.4	8 000	0.4	1250	0.7	2000	0.7

[a] K_1-K_2 values are typical for fines percentage (no. 200) of less than 15-18 percent.
[b] K_1 value should be decreased and K_2 value increased if fines percentage is greater than 10 percent.

Figure 9. Comparison of laboratory-measured M_r values to laboratory-measured CBR values.

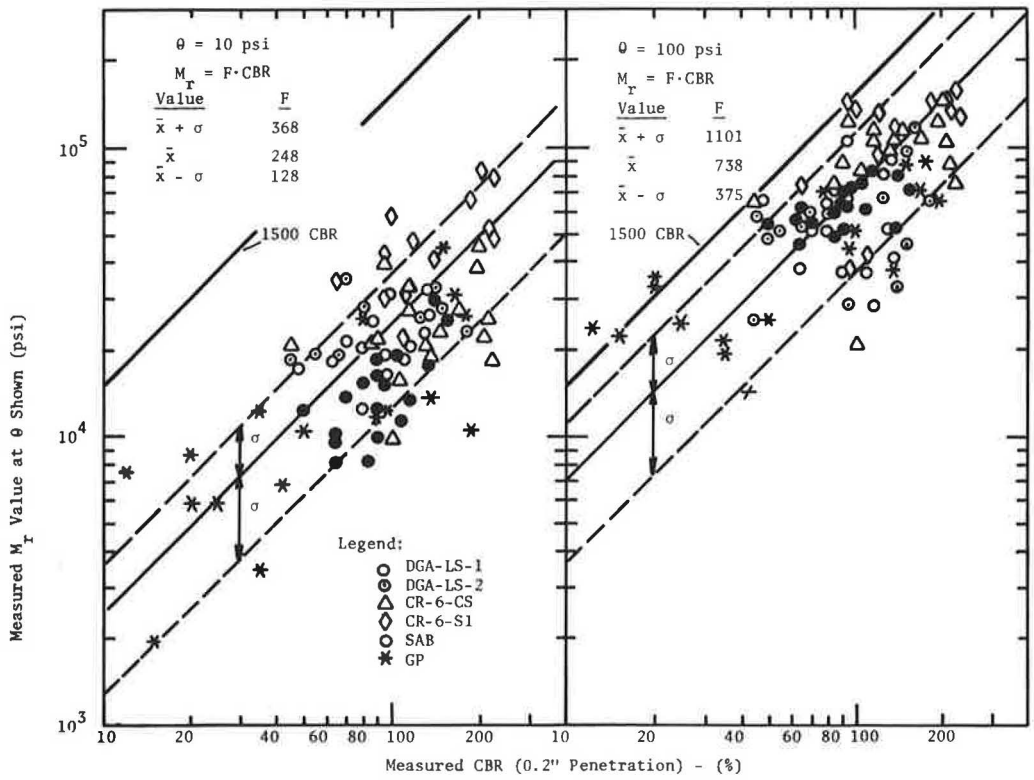

Table 7. F-value summary statistics: $M_r = F(CBR)$.

Aggregate	$\theta = 10$ lbf/in^2 $\bar{F}$	σ_F	CV (%)	90 Percent Confidence Range	$\theta = 100$ lbf/in^2 $\bar{F}$	σ_F	CV (%)	90 Percent Confidence Range
DGA-limestone-1	240	68	28.1	±111	727	296	40.7	±487
DGA-limestone-2	318	170	53.4	±279	635	373	58.7	±613
CR-6-crushed stone	201	121	60.3	±200	772	322	41.7	±530
CR-6-slag	358	120	33.5	±197	837	343	41.0	±565
Sand-aggregate blends	165	43	25.9	±70	699	171	24.5	±281
Bank-run gravel	232	146	62.9	±240	822	559	68.0	±920
All data	248	120	48.6	±198	738	363	49.2	±597

where F is the adjustment factor necessary for equivalence (comparable to the 1500 value of Huekelom and Foster). Table 7 is a summary of the F-values by type of aggregate studied. It can be seen that, even within an aggregate type, the variation (σ_F) may be quite large. However, note that not all of the deviations shown in Figure 9 can be related to variations in the M_r value. This is because unavoidable errors in determining the correct CBR value may occur due to the extremely high sensitivity of moisture to CBR for most granular materials.

As shown in both Figure 9 and Table 7, the average F-values for θ = 10 lbf/in^2 and 100 lbf/in^2 were F = 248 and F = 738, respectively. By using a linear relation between F and log θ, the following general relation that relates M_r to θ and CBR is

$$M_r = (490 \log\theta - 243)CBR \quad (5)$$

Finally, because most highway design structures result in bulk stress values near θ = 10 lbf/in^2 (for subbase) and θ = 20-40 lbf/in^2 (for bases), the resulting correlations developed in this study differ significantly from that established by Huekelom and Foster. In order for the F-value to be equal to 1500, a θ = 350-400 lbf/in^2 would be required. Although this discrepancy cannot be fully explained until further research is conducted, we hypothesize that this difference can be attributed to shear strain differences caused by the dynamic wave propagation field tests of Huekelom and Foster and those found in laboratory specimens that undergo M_r testing.

SUMMARY

This study was based on resilient modulus test results of granular materials obtained from both a comprehensive literature review and extensive laboratory study. Based on this analysis, the following conclusions were obtained.

An analysis of more than 270 separate M_r test results on granular materials indicated that an inverse correlation between K_1 and K_2 (constants in $M_r = K_1\theta^{K_2}$) exists for the global class of all granular materials. Relatively unique K_1-K_2 relations were found to exist for six different aggregate classes or types. These categories were silty sands, sand gravels, sand-aggregate blends, crushed stones, limerocks, and slags.

An analysis of the results indicated that the primary variables that influence the M_r response of granular materials are the stress state, degree of saturation, and degree of compaction. For crushed, angular materials, an increase in moisture leads to a small to moderate decrease in the K_1 value and relatively minor changes in the K_2 magnitude. These results contrast with those of sand gravels, which showed a marked decrease in K_1 and increase in K_2 with increasing moisture.

The influence of compaction (density) on all granular materials results in an increase in the K_1 term, and the K_2 value remains essentially constant. The gradation and its influence on the K_1-K_2 parameters are dependent on the type of material considered. For crushed, angular materials there was little, if any, change in either parameter over a range of 3 to 17 percent that passes the no. 200 sieve. However, for sand-gravel material, the K_1 parameter had a maximum value near optimum fines and then a marked decrease in K_1 with increasing fines content. This change concurrently led to an increase in the K_2 value with increasing fines.

By using the results of the M_r-physical property study, predictive equations that relate the specimen properties to the M_r-value were developed for six different aggregate types used in the laboratory study. Typical K_1-K_2 relations were stated for these aggregate types to reflect the relative influence of moisture, compaction, and gradation on their M_r response.

The final phase of the study dealt with investigating whether general correlations exist between laboratory measured resilient modulus and laboratory measured CBR results. An analysis of nearly 100 data sets indicated that a very general, but variable, correlation does exist. However, because the M_r test is stress dependent, the coefficient that relates M_r to CBR must be stress dependent and not a unique or constant value such as has been noted by previous investigators. The average coefficient values found at a bulk stress of 10 and 100 lbf/in^2 (F = 248 and F = 738) is significantly lower than the 1500 value proposed by Huekelom and Foster.

REFERENCES

1. M.P. Jones. Analysis of the Subgrade Modulus and Pavement Fatigue on the San Diego Test Road. Univ. of Maryland, College Park, M.S. thesis, Dec. 1975.
2. B.F. Kallas and J.C. Riley. Mechanical Properties of Asphalt Materials. Proc., 2nd International Conference on the Structural Design of Asphalt Pavements, Ann Arbor, MI, Aug. 1967.
3. B.F. Kallas and J.F. Shook. San Diego Experimental Base Project. Asphalt Institute, College Park, MD, Final Rept. 77-1 (RR-77-1), Nov. 1977.
4. R.I. Kinghan and B.F. Kallas. Laboratory Fatigue and Its Relationship to Pavement Performance. Proc., 3rd International Conference on the Structural Design of Asphalt Pavements, London, England, Sept. 1972.
5. M.W. Witczak. Design Analysis--Asphalt Concrete Overlay Requirements for Runway 18-36, Washington National Airport. Asphalt Institute, College Park, MD, Research Rept., Dec. 1971.
6. M.W. Witczak. Asphalt Pavement Performance at Baltimore-Washington International Airport. Asphalt Institute, College Park, MD, Research

Rept. 74-2(RR-74-2), 1974.
7. R.G. Hicks and C.L. Monismith. Prediction of the Resilient Response of Pavements Containing Granular Layers Using Non-Linear Elastic Theory. Proc., 3rd International Conference on the Structural Design of Asphalt Pavements, London, England, Sept. 1976.
8. C.L. Monismith, H.B. Seed, F.G. Mitry, and C.K. Chan. Prediction of Pavement Deflections from Laboratory Tests. Proc., 2nd International Conference on the Structural Design of Asphalt Pavements, Ann Arbor, MI, Aug. 1967.
9. C.L. Monismith, R.G. Hicks, and Y.M. Salam. Basic Properties of Pavement Components. Federal Highway Administration, Berkeley, CA, Final Rept. FHWA-RD-72-19, Sept. 1971.
10. R.D. Barksdale. Laboratory Evaluation of Rutting in Base Course Materials. Proc., 3rd International Conference on the Structural Design of Asphalt Pavements, London, England, Sept. 1972.
11. I.V. Kalcheff. Rational Characterization of Granular Bases. Proc., 1st Federally Coordinated Program on Research Progress Review, San Francisco, CA, Sept. 1973.
12. Y.T. Chou. Engineering Behavior of Pavement Materials--State of the Art. Federal Aviation Administration; U.S. Army Engineer Waterways Experiment Station, Vicksburg, MS, Final Rept. FAA-RD-77-37, Feb. 1977.
13. M.G. Sharma and W.J. Kenis. Evaluation of Flexible Pavement Design Methodology. Proc., Association of Asphalt Paving Technologists, Technical Sessions, Phoenix, AZ, Feb. 1975.
14. J. Sharma, L.L. Smith, and B.E. Ruth. Implementation and Verification of Flexible Pavement Design Methodology. Proc., 4th International Conference on the Structural Design of Asphalt Pavements, Ann Arbor, MI, Aug. 1977.
15. W.R. Barker and R.C. Gunkel. Structural Evaluation of Open-Graded Bases for Highway Pavements. U.S. Army Engineer Waterways Experiment Station, Vicksburg, MS, Final Rept., Miscellaneous Paper GL-79, May 1979.
16. E.E. Chisolm and F.C. Townsend. Behavioral Characteristics of Gravelly Sand and Crushed Limestone for Pavement Design. Federal Aviation Administration; U.S. Army Engineer Waterways Experiment Station, Vicksburg, MS, Final Rept. FAA-RD-75-177, Sept. 1976.
17. M.W. Witczak. A Study of the Deflection Behavior of the Ikalanian Sand Winchendon Test Section. U.S. Army Corps of Engineers, Cold Regions Research and Engineering Laboratory, Hanover, NH, Jan. 1980.
18. F. Finn, C. Saraf, B. Kulkarni, K. Nau, W. Smith, and A. Abdullah. The Use of Distress Prediction Subsystems for the Design of Pavement Structures. Proc., 4th International Conference on the Structural Design of Asphalt Pavements, Ann Arbor, MI, Aug. 1977.
19. W.S. Smith and K. Nair. Development of Procedures for Characterization of Untreated Granular Base Course and Asphalt-Treated Base Course Materials. Federal Highway Administration, Oakland, CA, Final Rept. FHWA-RD-74-61, Oct. 1973.
20. M.W. Witczak and K.R. Bell. Determination of Remaining Flexible Pavement Life-Predicted Flexible Pavement Remaining Life Interpreted from Various Analytical Procedures. Maryland Department of Transportation, College Park, Res. Rept. FHWA-MD-R-79-3, Vol. 3, Oct. 1978.
21. E.J. Barenberg. Response of Subgrade Soils to Repeated Dynamic Loads--State of the Art. Proc., Allerton Park Conference on Systems Approach to Airfield Pavements, Champaign, IL, March 1970.
22. Y.T. Chou. Evaluation of Nonlinear Resilient Module of Unbound Granular Materials from Accelerated Traffic Test Data. U.S. Army Engineer Waterways Experiment Station, Vicksburg, MS, Final Tech. Rept. S-76-12, Aug. 1976.
23. I.V. Kalcheff. Characteristics of Graded Aggregates As Related to Their Behavior Under Varying Loads and Environments. Proc., Conference on Utilization of Graded Aggregate Base Materials in Flexible Pavements, Oak Brook, IL, March 1974.
24. I.V. Kalcheff and R.G. Hicks. A Test Procedure for Determining the Resilient Properties of Granular Materials. Journal of Testing and Evaluation, ASTM, Vol. 1, No. 6, Nov. 1973.
25. E.J. Yoder and M.W. Witczak. Principles of Pavement Design, 2nd ed. Wiley, New York, 1975.
26. T.C. Johnson. Is Graded Aggregate Base the Solution in Frost Areas? Proc., Conference on Utilization of Graded Aggregate Base Materials in Flexible Pavements, Oak Brook, IL, March 1974.

Publication of this paper sponsored by Committee on Strength and Deformation Characteristics of Pavement Sections.

Use of Pressuremeter Test to Predict Modulus and Strength of Pavement Layers

JEAN-LOUIS BRIAUD AND DONALD H. SHIELDS

Most airport pavements are designed or evaluated on the basis of a plate test. This article shows how a pressuremeter test can replace plate tests to advantage. A 1-in diameter hole is made through the pavement and pressuremeter tests are run every foot down to a depth of 6 ft. Each test yields a deformation modulus, so that a modulus profile is obtained at each hole location. The results of a comparison between 93 pavement pressuremeter tests and 11 plate tests performed at two airport sites indicate that the pavement pressuremeter can be used for pavement design; the plate tests performed were standard for the design of airport pavements in Canada. A chart for the design of flexible airport pavements by using the results of pavement pressuremeter tests is presented. A procedure based on multilayer elastic theory is also discussed. This procedure uses the pressuremeter modulus as the elastic modulus of each layer. The multilayer elastic procedure makes more thorough use of the pressuremeter test results than does the chart procedure.

Most airport pavements are designed or evaluated on the basis of a plate test. This article shows how a

Figure 1. Pavement pressuremeter test.

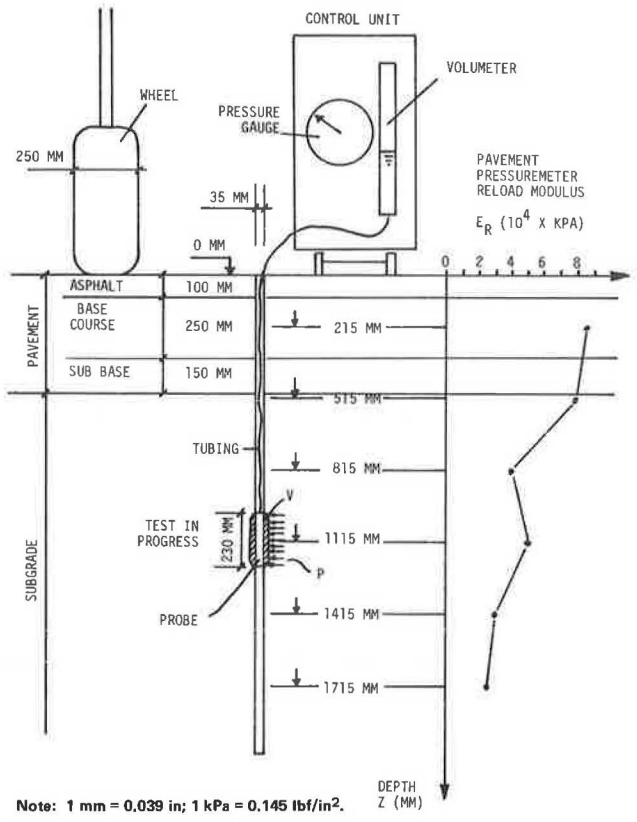

Note: 1 mm = 0.039 in; 1 kPa = 0.145 lbf/in^2.

pressuremeter test can replace advantageously plate-bearing tests and how a pavement can be designed or evaluated on the basis of pressuremeter tests results.

A pressuremeter test (1) (Figure 1) consists of placing a cylindrical expandable probe in a borehole and then inflating the probe. A control unit on the ground surface generates the pressure necessary to inflate the probe. The pressure against the wall of the borehole (p) and the expansion of the cavity (v) are recorded, and a p-v curve is plotted (Figure 2). A modulus of deformation is obtained from the slope of the curve (A to B on Figure 2) and, in the standard test used for foundation design, a limit pressure is read at large strains (E on Figure 2). In the case of pavement design and evaluation, only the modulus of deformation is of interest, and the test can be terminated as soon as point B is reached. This simplifies considerably the design of the pressuremeter.

Pressuremeters for foundation engineering are available commercially, but the commercial models are unsuitable for the tests described here. Both the recommended apparatus and the test procedure have been described in detail elsewhere (2,3).

For pavement engineering, pressuremeter tests have to be performed at very shallow depth, and some concern was expressed initially that a lack of confining pressure at shallow depth would lead to deformation moduli values that were too low. It was shown (2) that, even very close to the ground surface, the pressuremeter-derived deformation modulus is consistent with the pressuremeter-derived deformation modulus measured at larger depth.

Two ways in which deformation information can be used to design new pavements (subbase, base, and surface course) or to evaluate existing pavements are as follows:

1. An empirical approach in which a correlation is found among deformation moduli, design, and performance, and
2. A theoretical approach where moduli are entered into a mathematical model of a pavement.

Both approaches were used in the work covered by this article. For the empirical approach, use was made of existing design charts based on plate-bearing tests by converting pressuremeter data, in effect, to an equivalent plate-bearing test result; the conversion procedure was obtained from the results of comparison tests between the standard plate test, which is used for airport pavement design in Canada, and pressuremeter tests. Multilayer elastic theoretical representation of a pavement appears ideally suited to the theoretical approach to design by using pressuremeter data. This theoretical approach offers an advantage over the empirical approach in that each pressuremeter test result can be used directly.

PAVEMENT PRESSUREMETER TEST

The pavement pressuremeter (Figure 3) (2,3) consists of a probe, tubing, and a control unit. The probe is a cylinder 32.5 mm (1.33 in) in diameter that is inflatable to a diameter of 39.5 mm (1.61 in). The inflatable part of the probe is 230 mm (9.1 in) long. The tubing is made of nylon, 6 mm (0.24 in) in outside diameter, and 2 mm (0.08 in) in inside diameter. It is about 5 m (16.4 ft) long.

The control unit (Figure 3) is housed in a plywood box 1.2 m (47.2 in) long, 0.6 m (23.6 in) wide, and 0.3 m (11.8 in) deep. The control unit serves three purposes:

1. It generates the pressure necessary to inflate the probe,

Figure 2. Typical pavement pressuremeter curve.

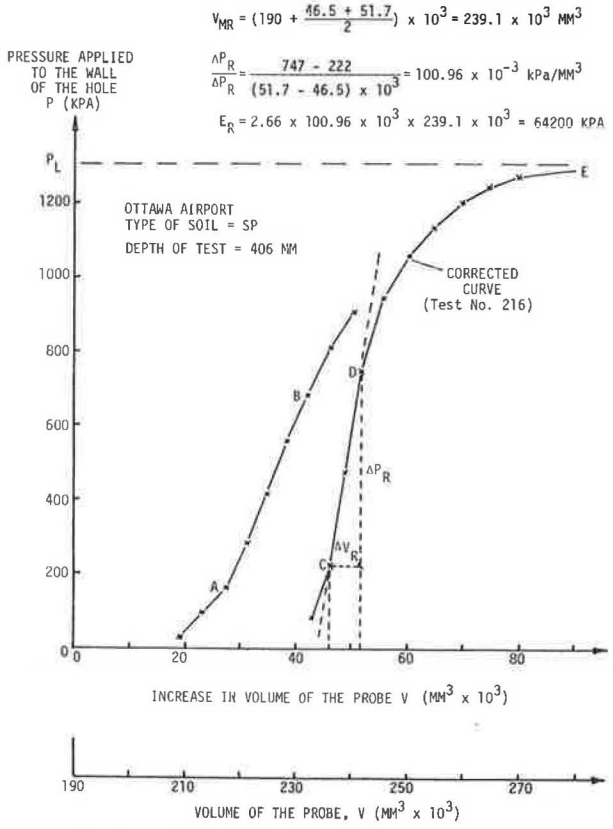

Note: 1 mm = 0.039 in; 1 kPa = 0.145 lbf/in^2.

Figure 3. Components of pavement pressuremeter.

2. It indicates on a pressure gauge what this pressure is at any time, and
3. It indicates on a volumeter what volume of liquid has been sent to the probe.

A hand pump is used to generate the pressure. By rotating the wheel of the hand pump, a piston advances and forces water through the volumeter. This water displaces a column of red kerosene in two parallel plexiglass tubes. The kerosene-water interface facilitates the reading, on a scale, of the volume of water sent to the probe. The control unit was designed specifically for the execution of strain-controlled tests and for imposing unloading-reloading cycles during the test.

The box that houses the control unit is also used to transport the probe, tubing, penetration rods, and necessary accessories (Figure 3). When filled with equipment, the box weighs about 0.5 kN (110 lb) and can be pulled along on its two wheels by one person.

To evaluate the base, subbase, and subgrade of an existing pavement or the subgrade for a new pavement, with the pavement pressuremeter, a hole is made from the surface down to a depth of 2000 mm (78.7 in) by driving a 35 mm (1.38 in) diameter steel rod. Immediately after the steel rod is withdrawn, the short pressuremeter probe is inserted in the hole, and tests are performed every 3000 mm (11.8 in) of depth (Figure 1). The making of the hole takes from 2 to 10 min, and one pavement pressuremeter test takes an average of 6 min. Therefore, a test station that consists of one hole and six tests can be completed in an hour.

A pavement pressuremeter test consists of inflating the probe at a constant rate of strain; both pressure and volume are recorded. An unloading-reloading cycle is performed during each test toward the end of the AB portion of the curve (Figure 2). The pressure and volume readings are corrected for membrane resistance and tubing expansion, respectively (3). The corrected curve is plotted, and two moduli values are calculated, as explained below.

The modulus (E) is obtained from the slope of the AB portion of the test curve (Figure 2) by using the linear elastic, cylindrical expansion theory of Lamé and Poisson's ratio of 0.33 (1). The reload modulus (E_r) is obtained from the reloading portion of the cycle (CD on Figure 2) by using the same assumptions:

$$E = 2.66\, V_m(\Delta p/\Delta v) \quad (1)$$

$$E_r = 2.66\, V_{mr}(\Delta p_r/\Delta v_r) \quad (2)$$

$$V_m = V_c + [(v_o + v_f)/2] \quad (3)$$

$$V_{mr} = V_c + [(v_{or} + v_{fr})/2] \quad (4)$$

where, referring to Figure 2,

$\Delta p/\Delta v$ = slope of AB,
$\Delta p_r/\Delta v_r$ = slope of CD,
V_c = initial volume of the probe = 1.9 x 10^5 mm³,
v_o = volume injected at A,
v_f = volume injected at B,
v_{or} = volume injected at C, and
v_{fr} = volume injected at D.

The method used to prepare the borehole (driving of the rod) disturbs the soil. This disturbance seems to result in a change in E-value of about 30 percent (2) and seems to be particularly important in silt and loose soils. However, the method of borehole preparation outlined here is recommended in all types of soils for the following reasons: The use of one standard method for all soils avoids errors due to the wrong choice among several recommended methods. Augering, sampling, and selfboring are not feasible because of the small diameter of the hole. The recommended method is simple, fast, and leaves a well-calibrated hole that has smooth sidewalls that rarely cave in. The standardization of the method allows any deviation from an ideal hole to be absorbed in correlations between the test and observed pavement behavior. Other researchers have used similar methods with success (4). Even though disturbance has an influence on the first loading modulus, it has less influence on the reload modulus (E_r). As shown here, the pressuremeter test and the plate test correlate reasonably well. Since preparations for the plate test do not disturb the soil, we can conclude that disturbance involved in the preparation of the hole for the pavement pressuremeter is not a major concern.

CORRELATION WITH A PLATE TEST

McLeod Plate Test

The McLeod plate test is widely used in Canada for the evaluation of airport pavements. When the pressuremeter test is correlated to the McLeod plate test, use can be made of the existing design and evaluation procedures associated with the McLeod test.

The McLeod plate test (5) consists of loading a 762-mm (30-in) diameter steel plate placed on the pavement surface (Figure 4). Usually, a trailer loaded with a huge rubber container filled with water is used as a reaction (Figure 4). The test consists of applying to the plate a load (S) that, repeated 10 times, will cause a 12.5 mm (0.5 in) deflection of the surface at the tenth repetition. If the plate test is performed on the pavement surface, S is the pavement bearing strength (S_p); if performed on the subgrade surface, S is the subgrade bearing strength (S_s).

The subgrade bearing strength (S_s) is the basic design parameter for airport pavements in Canada at the present time. In general, S_s is not measured directly but is deduced from the measurement of S_p. A relation has been established between S_s and S_p (5):

$$S_s = S_p \times 10^{-(t/165)} \quad (5)$$

where t is the equivalent granular thickness of the pavement in centimeters (1 cm of base course equals 1 cm of equivalent granular thickness; 1 cm of asphalt concrete equals 2 cm of equivalent granular thickness).

Testing Program

Pavement pressuremeter tests and McLeod plate tests were performed at two airport sites selected by Transport Canada: Sarnia Airport and Ottawa International Airport.

At Sarnia Airport, the pavement of the main runway is made up of 60 mm (2.4 in) of asphalt concrete and 280 mm (11 in) of moist, medium-sized, sandy gravel. The testing program took place while the runway pavement was being overlaid. After the overlay the total asphalt concrete thickness was about 140 mm (5.6 in). The subgrade is a silty clay that has a natural water content of 13 percent, a liquid limit of 29 percent, and a plastic limit of 15 percent.

Five McLeod plate tests were run along the center line of the runway; S_p was measured and then S_s was calculated. The results are shown in Table 1. The McLeod plate tests at locations (holes) 3, 5, and 6 were performed before the overlay, and tests at 7 and 15 were performed just after the overlay.

Pavement pressuremeter tests were performed in a total of five holes located a few feet from where the plate tests had been performed. Each hole was prepared by driving the 35-mm (1.35-in) rod to a depth of 1800 mm (6 ft), withdrawing the rod, and then inserting the pressuremeter to the 1800-mm depth. Pressuremeter tests were run at 1-ft intervals from the bottom of the hole up to a depth of 1 ft. For each test, only the first loading modulus (E) was calculated because, at the time of the Sarnia tests, the standard procedure for running a pressuremeter test that involved an unloading-reloading cycle (3) had not been established. Figure 5 shows a typical profile of pavement pressuremeter moduli and Table 2 summarizes the pressuremeter results for Sarnia Airport.

Ottawa International Airport has two parts: an older, smaller airport and a more recent airport. The pavement of the older airport is made up of 50 mm (2 in) of asphalt concrete and 100 mm (4 in) of base course; the subgrade is a moist, uniform, medium-to-fine sand. The pavement of the more recent airport is made up of 100 mm (4 in) of asphalt concrete and 300 mm (12 in) of base course. The subgrade is a dense, silty sand that has 20 percent silt, 60 percent sand, and 20 percent gravel.

Six McLeod plate tests were run at Ottawa International Airport: Two were run on the more recent pavement and four were run on the older pavement. S_p was measured in each case and then S_s was calculated. The results are shown on Table 3. Pavement pressuremeter tests were performed in six holes a few feet away from where the plate tests had been performed. Each hole was prepared and the tests were run as described for Sarnia Airport, with the exception that, at Ottawa International Airport, unloading and reloading cycles were performed. By the time of the Ottawa tests, the standard procedure to run a pavement pressuremeter test (3) had been

Figure 4. McLeod plate test.

Figure 5. Sarnia Airport: pressuremeter modulus profile of hole 7.

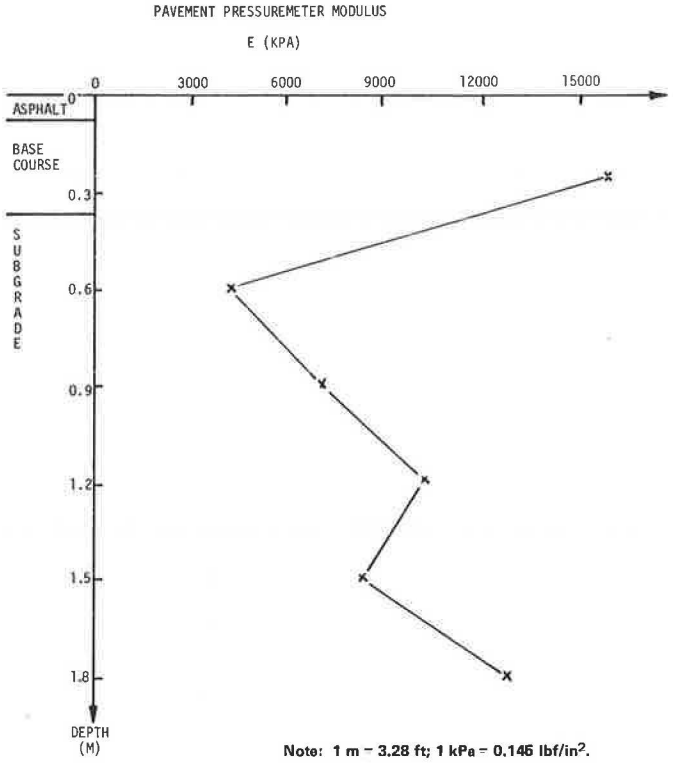

Note: 1 m = 3.28 ft; 1 kPa = 0.145 lbf/in^2.

Table 1. Sarnia Airport: summary of McLeod plate test results.

Hole	Pavement Bearing Strength, S_P (kN)	Base Course Thickness, T_B (cm)	Asphalt Thickness, T_A (cm)	Equivalent Pavement Thickness, T (cm)	Subgrade Bearing Strength, S_S (kN)
3	196	20	5	30	129
5	186	23	7	37	111
6	243	24	6	36	147
7	265	29	14.5	58	118
15	208	24	14.5	53	100

Note: 1 cm = 0.393 in; 1 kN = 0.224 klp.

Table 2. Sarnia Airport: summary of pressuremeter moduli profiles.

Depth (m)	Pavement Pressuremeter Modulus, E (MPa)				
	Hole 3	Hole 5	Hole 6	Hole 7	Hole 15
0.23	6.6	6.4	10.1	16.8	15.3
0.6	1.4	5.8	2.8	4.2	7.5
0.9	2.2	17.9	10.3	7.2	5.6
1.2	7.9	28.2	14.2	10.2	13.1
1.5	9.2	21.2	9.0	8.4	17.8
1.8	7.7	18.2	9.1	12.8	10.5

Note: 1 m = 3.28 ft; 1 MPa = 145.037 lbf/in^2.

established. Therefore, both E and E_r values are available for the Ottawa tests. Figure 6 shows an E and E_r profile and Table 4 summarizes the pressuremeter results.

Comparison

At each test location, the McLeod plate gives one unique value of S_p, and the pressuremeter gives two profiles of six moduli (Figure 6) [one profile in the case of Sarnia (Figure 5)]. It is the profiles of stiffness that give the pressuremeter test a major advantage over the plate test; the engineer can now see where weak layers exist in a pavement or if soft soil exists over a particular depth in a subgrade. In order to make a comparison between the two tests, the pressuremeter moduli had to be reduced to one average or equivalent modulus by using an appropriate averaging method.

The chosen method involves the following steps:

1. The pavement and the subgrade are divided into layers with the boundary between layers considered to be at the midpoint between two consecutive pressuremeter tests;
2. A pressuremeter modulus is assigned to each layer;
3. The rigid McLeod plate is placed on this multilayer soil, and the plate is loaded with the bearing strength that has been measured in the field;
4. The settlement (s) of the rigid plate is calculated by using multilayer elastic theory and the finite element method (2); and
5. The equivalent pressuremeter modulus is obtained from the formula that gives the settlement of a rigid plate on a linear elastic homogeneous half space:

$$E_e = (\pi/4)(1 - \nu^2)(Q/sB) \quad (6)$$

where

E_e = the equivalent modulus;
ν = Poisson's ratio, considered as 0.33 in all cases;
Q = the load (S_p or S_s depending on the case);
B = the plate diameter [762 mm (30 in)]; and
s = the settlement calculated by using multilayer elastic theory.

A total of four equivalent pressuremeter moduli was calculated. The four are

1. The pavement equivalent pressuremeter modulus (E_{ep}), the modulus of a fictitious homogeneous material that is equivalent to the layered pavement and subgrade that have six pressuremeter moduli (E) as layer moduli;
2. The pavement equivalent pressuremeter reload modulus (E_{rep}), the modulus of a fictitious homogeneous material that is equivalent to the layered pavement and subgrade that have six pressuremeter reload moduli (E_r) as layer moduli;
3. The subgrade equivalent pressuremeter modulus (E_{es}), the modulus of a fictitious homogeneous soil that is equivalent to the layered subgrade that have pressuremeter moduli (E) as layer moduli; and

Table 3. Ottawa International Airport: summary of McLeod plate test results.

Hole	Old or New Airport	Pavement Bearing Strength, S_P (kN)	Asphalt Thickness, T_A (cm)	Base Course Thickness, T_B (cm)	Equivalent Granular Thickness, T (cm)	Subgrade Bearing Strength, S_S (kN)
1	New	1709	10	30	50	851
2	New	1728	10	30	50	860
3	Old	412	5	10	20	312
4	Old	405	5	10	20	306
5	Old	601	5	10	20	455
6	Old	614	5	10	20	464

Note: 1 kN = 0.224 kip; 1 cm = 0.393 in.

Figure 6. Ottawa International Airport: pressuremeter modulus profile of hole 7.

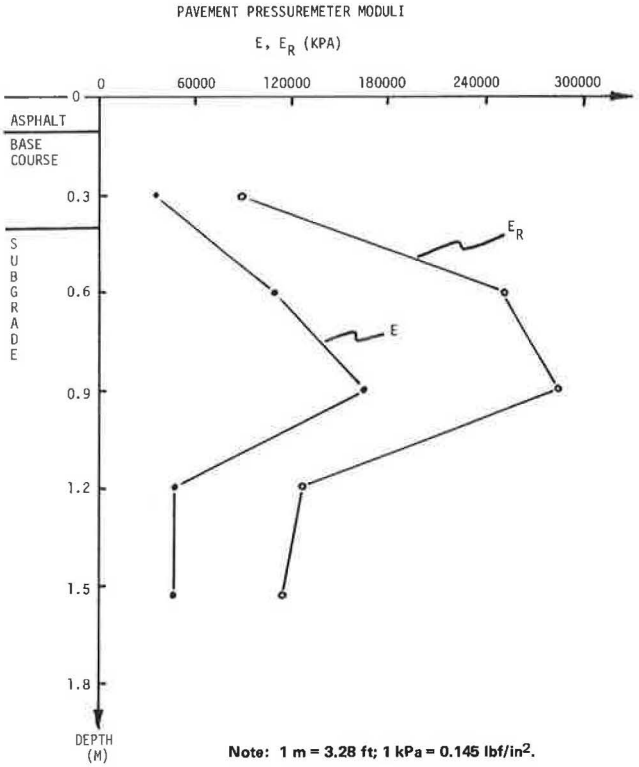

Note: 1 m = 3.28 ft; 1 kPa = 0.145 lbf/in^2.

Table 4. Sarnia Airport: summary of pressuremeter moduli results.

	Pavement Pressuremeter Moduli, E and E_R (MPa)											
	New Airport				Old Airport							
	Hole 1		Hole 2		Hole 3		Hole 4		Hole 5		Hole 6	
Depth (m)	E	E_R	E	E_R	E	E_R	E	E_R	E	E_R	E	E_R
0.25	47.4	114.0	35.4	88.0	17.5	41.2	18.0	65.5	40.2	84.1	21.5	64.2
0.6	27.5	70.0	109.3	251.6	13.9	36.0	16.2	55.8	32.7	78.7	25.6	72.5
0.9	106.9	298.0	163.9	283.8	14.5	41.1	11.3	36.7	13.0	42.0	16.7	55.0
1.2	100.7	224.9	45.9	126.3	4.6	7.3	7.8	19.1	16.6	42.5	11.2	27.4
1.5	64.6	16.6	47.7	110.0	4.1	12.5	8.7	2.1	13.7	34.0	10.4	17.4
1.8					8.4	19.4	9.9	21.4			16.9	33.8

Note: 1 m = 3.28 ft; 1 MPa = 145.037 lbf/in^2.

Table 5. Equivalent pressuremeter moduli.

Item	Ottawa International						Sarnia Airport				
	New Airport		Old Airport								
	Hole 1	Hole 2	Hole 3	Hole 4	Hole 5	Hole 6	Hole 3	Hole 5	Hole 6	Hole 7	Hole 15
E_{EP} (MPa)	76.5	83.9	15.4	18.0	31.0	24.7	5.1	17.8	12.2	24.1	24.5
E_{REP} (MPa)	160.2	167.1	38.2	51.6	69.9	70.5					
E_{ES} (MPa)									5.7		
E_{RES} (MPa)	105.4				54.3						

Note: 1 MPa = 145.037 lbf/in^2.

Figure 7. Correlation between plate and pressuremeter: E_{ep} versus S_p.

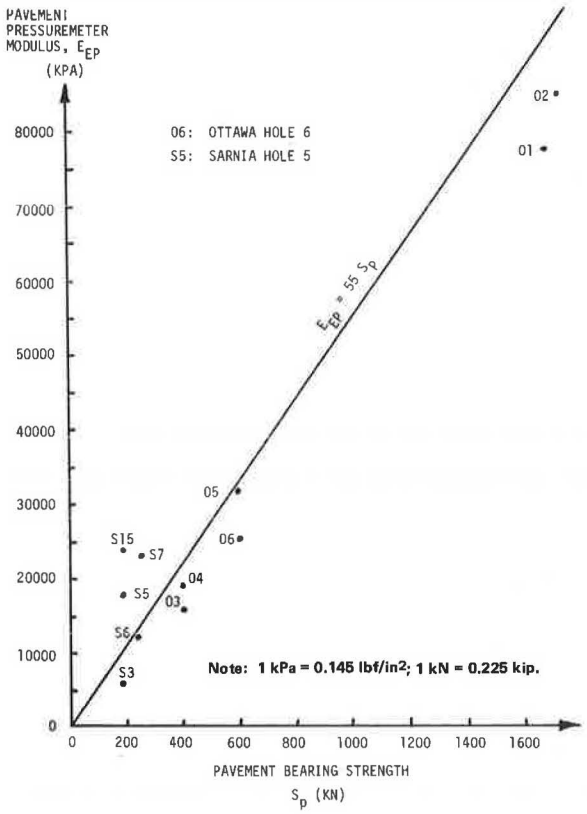

Figure 8. Correlation between plate and pressuremeter: E_{rep} versus S_p.

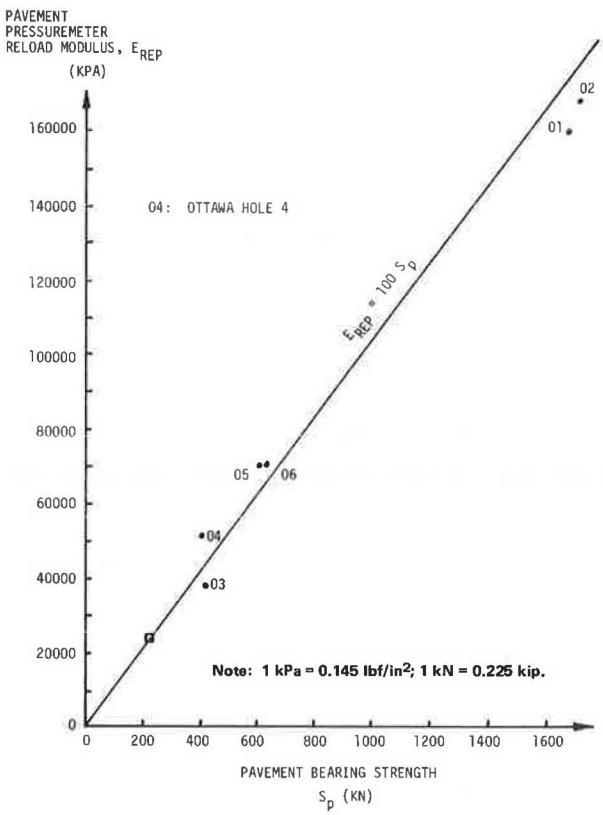

4. The subgrade equivalent pressuremeter reload modulus (E_{res}), the modulus of a fictitious homogeneous soil that is equivalent to the layered subgrade that have pressuremeter reload moduli (E_r) as layer moduli.

In the case of E_{ep} and E_{rep}, which involve the surface layer of the pavement, a deformation modulus for the asphalt concrete had to be assumed since the probe of the pressuremeter is too long to enable the modulus of the asphalt concrete to be measured. A value of 1.5 million kPa was considered to be reasonable for the asphalt modulus in all cases. The theory required a value of Poisson's ratio for each layer. Since neither the pressuremeter nor the plate test measure Poisson's ratio, a value of 0.33 was simply assumed for all cases. This value is a reasonable average for soils and, in addition, variations in Poisson's ratio usually have a relatively small influence on the magnitude of settlement (6, p. 160; 7).

The moduli E_{ep} and E_{rep} are obtained for the load S_p; E_{es} and E_{res} for the load S_s. A summary of all the equivalent moduli that were calculated for the different test locations at Sarnia and Ottawa International Airports is given in Table 5.

Correlations

Figure 7 presents a plot of E_{ep} versus S_p, and Figure 8 presents a plot of E_{rep} versus S_p. In both cases it seems reasonable to represent the test results by straight lines, as shown, where

$$E_{ep} = 55\ S_p \quad (7)$$

with E_{ep} in kilopascals and S_p in kilonewtons, and

$$E_{rep} = 100\ S_p \quad (8)$$

Figure 9. Design chart for flexible airport pavement by using pavement pressuremeter.

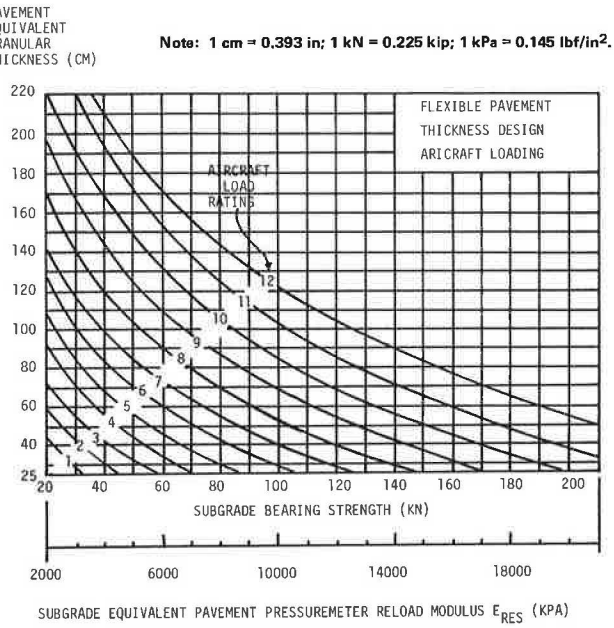

Referring to Figure 7, the scatter in results is appreciable for low values of E_{ep} and S_p (Sarnia Airport). This large scatter may occur because the soil is fine grained and would be disturbed somewhat when the boreholes are made. The large scatter may also be because the plate test and pressuremeter test results were not as reliable in Sarnia as in Ottawa. In Sarnia there were calibration problems with the jack that was used for the plate tests, and the operators for the pressuremeter tests were inexperienced.

The scatter in values is small in Figure 8. One reason for the limited amount of scatter is that there are no points shown for Sarnia Airport because the reload modulus (E_r) was not measured. An average value of E_r for Sarnia can be estimated as follows: E_r was measured in one test in Sarnia, and for that test the ratio E_r/E was 1.4; given that the average E_{ep} value for Sarnia is 16 700 kPa, then an estimate of the average E_{rep} is 16 700 x 1.4 = 23 380 kPa. The corresponding average S_p value is 220 kN. This point is represented by a square on Figure 8.

Figures 7 and 8 tend to prove that there is a simple correlation between McLeod plate test results and pavement pressuremeter test results. It seems reasonable to assume, therefore, that the empirical design rules for flexible airport pavements based on the McLeod plate test can be employed equally successfully by using the pressuremeter test.

CHART DESIGN

Engineers are familiar with the chart approach to pavement design, so little needs to be said here concerning the method. For the purpose of demonstration only, the empirical chart method employed by Transport Canada is used in this section because we are most familiar with this procedure.

Canadian Design

The design of new flexible airport pavements is carried out in accordance with Transport Canada manual AK-68-12 (8):

1. The subgrade of the airport site is classified according to the Unified Soil Classification System; the subgrade bearing strength (S_s) is estimated from the subgrade classification;
2. The design plane that will be landing at the airport site is classified according to its aircraft load rating (ALR); the ALR is a number that ranges from 1 to 12; for example, the ALR is 12 for a Boeing 747 or a Concorde, but it is 1 for very small planes;
3. Once S_s and the ALR are known, Figure 9 is used to find the equivalent granular thickness (t) of the pavement; t takes into consideration the equivalency factors for various components of the pavement;
4. The pavement is then designed to have the minimum required thickness of asphalt, the minimum required thickness of base course, and the remaining portion of t in subbase; these minimum requirements depend on the maximum tire pressure;
5. Once the pavement is built, a number of McLeod plate tests are carried out; the tests generate pavement bearing strength parameters (S_p); and
6. At any one plate test location, a new S_s value is deduced from the S_p value by using Equation 5; the S_s values are multiplied by a reduction factor, if necessary, to account for a loss in strength during the thawing of frozen ground in the spring of the year; the lower quartile adjusted S_s value is determined and is considered to be the applicable in situ S_s value; comparison of this S_s value with the design S_s value from step 1 provides the engineer with a check on the design.

In Canada, the evaluation of existing pavements is carried out as follows:

1. A number of McLeod plate tests are performed on the pavement, which gives rise to a number of S_p values; the corresponding S_s values are obtained by using Equation 5.
2. As is done during the design of new pavements, the S_s values are multiplied by a spring reduction factor, if necessary. The lower quartile adjusted S_s value is determined and is considered to be the applicable in situ S_s value.
3. The ALR of the design plane is obtained, and, by using the thickness design chart of Figure 9, the required value of t is determined.

If the existing t is greater than the required t, the pavement is satisfactory. If the opposite is true, the pavement needs to be strengthened, and the thickness of the necessary overlay is deduced from the difference between the required and existing t-values.

Pavement Pressuremeter Design

The design chart of Figure 9 is based on S_s values that are either assumed (initial design) or calculated from plate-bearing tests. A similar chart can be produced based on pressuremeter modulus values by making use of the plate-pressuremeter correlation equations that were deduced from the research program outlined in this paper. E_{rep} is considered to be a more reliable parameter than E_{ep} for this purpose because E_{rep} is less influenced by disturbance to the soil than is E_{ep} and the fit between E_{rep} and S_p is better than that between E_{ep} and S_p. Equation 8 is a relation between S_p and E_{rep}, and it seems reasonable to assume that the same relation holds between S_s and E_{res}. On Figure 9 an E_{res} axis has been added that allows flexible airport pavements to be designed on the basis of pressuremeter moduli.

The following procedure can be followed to design new airfield flexible pavements on the basis of pressuremeter test results.

1. Pavement pressuremeter tests should be performed in the subgrade at regular intervals along the proposed runway. This represents a considerable advance over the existing method because the actual deformation properties of the subgrade are measured rather than chosen based on a soil classification. The test holes should be spaced about 100 m (300 ft) apart, and at each hole location a test should be performed every 0.3 m (1 ft) of depth down to 1.5 m (5 ft).
2. The modulus (E_r) should be calculated for each test, and an E_r profile obtained for each location.
3. The subgrade equivalent pressuremeter reload modulus (E_{res}) should be calculated for each test-hole location. In order to do this, a fictitious, but reasonable, subgrade bearing strength (S_s) has to be chosen to calculate s by using multilayer elastic theory. An S_s value of 100 kN (~20 000 lb) is recommended. Because of the superposition law of linear elasticity, the value of S_s has no influence on the E_{res} value, which is calculated. If the required computer program is not available, an approximate value of E_{res} can be obtained by using the following formula:

$$1/E_{res} = (1/100)\,[(22.1/E_1) + (33.5/E_2) + (24.6/E_3) + (14.8/E_4) + (5/E_5)] \quad (9)$$

where E_1 is the reload modulus obtained at the shallowest depth in the subgrade. E_2, E_3, E_4, and E_5 are the reload moduli obtained at a depth of 1 ft below, respectively, E_1, E_2, E_3, and E_4. This formula was obtained by assuming a single average vertical strain distribution below the plate (2). Incidently, correlation between pressuremeter and plate results by using this approach presents much less scatter than in Figure 7.
4. The E_{res} values are multiplied by the applicable spring reduction factor, and the lower quartile factored E_{res} value is determined. The lower quartile E_{res} is considered to be the design in situ E_{res} value.
5. ALR of the design plane is obtained. The in situ E_{res} and the chart of Figure 9 are used to determine the required equivalent granular thickness (t_1).
6. If base-course material is available from different borrow pits, it may be desirable to prepare pavement test sections with the different base-course materials and to test them with the pressuremeter.

For the evaluation and design of overlays for existing pavements, the following procedure should be followed:

1. Pavement pressuremeter tests should be performed at regular intervals along the runway. At each hole location, a test is performed immediately below the asphalt layer, and subsequent tests are performed at 0.3-m (1-ft) intervals down to a depth of about 1.8 m (6 ft). The test holes should be about 100 m (300 ft) apart.
2. The modulus (E_r) should be calculated for each test, and an E_r profile obtained for each location.
3. Only the results of tests in the subgrade should be considered for use with the design chart (Figure 9), but the tests in the base and subbase are of considerable value because they allow the engineer to assess directly the competence of thin layers in the make-up of the pavement. The subgrade equivalent pressuremeter reload modulus (E_{res}) for each test-hole location should be calculated from the subgrade pressuremeter tests by following step 3 of the new pavement design procedure.
4. Follow step 4 of the new pavement design procedure.
5. Follow step 5 of the new pavement design procedure.
6. This required thickness (t_1) is compared with the equivalent granular thickness of the existing pavement (t_2). An overlay is necessary if t_1 is greater than t_2; the overlay thickness is

$$t\,(\text{overlay}) = (t_1 - t_2)/\text{equivalency factor} \quad (10)$$

The above design procedure points out two advantages of the pressuremeter test over the plate test. The first advantage is that pressuremeter tests can be carried out in situ before the pavement is designed and built in areas where it would be impractical to carry out plate tests. Real deformation values are then available for design rather than estimated values. The second advantage is that, even with the pavement in place, the subgrade modulus is measured directly by the pressuremeter, whereas with the McLeod procedure the subgrade bearing strength (S_s) is estimated from the pavement bearing strength (S_p) by means of Equation 5.

MULTILAYER ELASTIC DESIGN

The alternative to the empirical chart route to pavement design and evaluation is the use of elastic theory.

Existing Procedures

In the multilayer elastic design, the pavement-subgrade system is considered to be a multilayer elastic continuum. Each layer is characterized by a modulus of elasticity and a Poisson's ratio. The strains generated in the multilayer elastic continuum by the load from the design aircraft are calculated by using a computer program. Two strains are considered to be critical: the maximum horizontal tensile strain (ε_H) at the lower face of the asphalt layer and the maximum vertical compressive strain (ε_V) at the top of the subgrade. The design asphalt and pavement thicknesses are the thicknesses that are required to ensure that the magnitudes of ε_H and ε_V are within acceptable limits, called the limiting strain criteria.

The multilayer elastic theory approach to pavement design is coming into greater use. The evaluation of the moduli of deformation for the various pavement layers has not kept pace with the rapid advance in theory and computational capabilities. A number of ways exist to estimate the necessary moduli, including a correlation between California bearing ratio (CBR) and deformation modulus and triaxial tests on prepared samples, but none of the ways are direct in the sense of measuring actual in situ deformation properties. In this regard, the pavement pressuremeter test represents a real improvement because of its ability to measure deformation moduli in situ.

Pavement Pressuremeter Procedure

For both Sarnia and Ottawa International Airports, the strains ε_H and ε_V were calculated by assuming the pavements to be loaded with the respective design plane: the Convair 440 for Sarnia Airport, the DC-8-63 for the new section of Ottawa Airport, and the DC-3 for the older section of Ottawa Airport. The Poisson's ratio for all layers

was assumed to be 0.33 (7). An asphalt modulus of 1.5 million kPa (≈200 000 lbf/in²) was assumed to be a reasonable value. The base course, subbase, and subgrade were divided into layers that have boundaries at the midpoint between two consecutive pressuremeter tests. The pressuremeter reload moduli (E_r) were considered to be the applicable moduli of elasticity of each layer. Since E_r was not measured at Sarnia Airport, an estimate of the E_r value of each layer was obtained by averaging the E values of holes 5, 6, 7, and 15 and then simply doubling the resulting E values. For Ottawa International Airport, the E_r values for each layer were obtained by averaging the E_r values of holes 1 and 2 for the newer section and of holes 3, 4, 5, and 6 for the older section. This selection process led to one profile of elastic constants being made available for each of the three pavements.

The computer program bitumen-structures-analysis-in-roads (BISAR) (7) was used to calculate ε_H, ε_V, and the maximum pavement deflection (s) under the load of one leg of the design airplane. The results are shown in the table below (1 mm = 0.039 in):

	Ottawa International		
Item	New Airport	Old Airport	Sarnia Airport
Design plane	DC 8-63	DC-3	Convair 440
Asphalt strain, H	0.001 66	0.000 81	0.000 44
Subgrade strain, V	0.003 04	0.003 1	0.003 03
Settlement, s (mm)	3.9	3.1	2.2

A reasonable estimate of the activity at the two airports is 5000 landings and takeoffs of the design plane per year. Given this level of activity and the properties of most asphalts, the limiting strain in the asphalt can be assessed at 0.0011 (7). A limiting subgrade strain can also be assigned depending on the level of activity at the airport (9). For cases being considered here, the limiting subgrade strain would be of the order of 0.002. These limiting strain criteria mean that if the asphalt strain (ε_H) is 0.0011 of less and if the subgrade strain (ε_V) is 0.002 or less, under the static load of the design plane, the pavement will perform satisfactorily for at least 5000 passes of the design plane.

If we compare the calculated strains (see table above) with the limiting strains, we can see that (a) the calculated strains are not far from the limiting strains and (b) the calculated strains for the subgrade are somewhat higher than the subgrade limiting strain. This comparison would imply that the future performance of the pavements is questionable. Given that the pavement at Sarnia Airport had just been overlaid at the time of testing and that the pavements of Ottawa International Airport are in excellent condition, the future performance of the pavements does not really seem to be questionable. A more logical conclusion is that the use of the pressuremeter modulus (E_r) in multilayer elastic design is not compatible with the use of the established limiting strain criteria. In this instance, E_r values are too small, which results in calculated strains that are too large.

Even though the E_r values are measured during a reload cycle, they are measured over an average of 4 percent volumetric strain. Continuing research on the subject shows that much higher E_r values are obtained at lower strain levels and that even an initial tangent modulus can be obtained with the pavement pressuremeter. The choice then is between (a) continuing to use E_r values measured over 4 percent strain and establishment of more-appropriate limiting strain criteria by direct calibration with pavement performance or (b) keeping the established strain criterion and selection of E_r values at a more appropriate (smaller) strain level. The second solution is favored and will be the subject of further discussion in another article.

ADVANTAGES AND DISADVANTAGES OF THE PAVEMENT PRESSUREMETER METHOD

Disadvantages of the pavement pressuremeter method include that the test requires a 35-mm (1.38-in) diameter hole through the pavement. This does not seem to be a major drawback because a hole of this size can be backfilled and patched easily. The pressuremeter loads the soil laterally, not vertically as does a wheel. This criticism is not as serious as it may appear because (a) pressuremeter tests have been carried out in both vertical and horizontal boreholes in a wide range of soils, and the results show that the horizontal and vertical moduli are within a few percent of each other (1) and (b) support for the wheel of a truck or a plane does not come only from vertical soil reaction but from horizontal soil reaction as well. The pavement pressuremeter cannot measure, as yet, a modulus E_r in the thin asphalt layer.

Some of the advantages of the pavement pressuremeter method are that the apparatus is relatively inexpensive and is available commercially. It is portable and a test is relatively quick. The quality of a test can be evaluated from the shape of the pressure-volume curve; the engineer can therefore develop a level of confidence in the results. The average magnitude of the six moduli measured at each station allows an assessment to be made of the overall pavement stiffness, although the profile of moduli indicates the variation of pavement stiffness with depth and can be used, for example, to single out a weak layer. The test can be used not only for the evaluation of existing pavements and the design of overlays but also for the design and control of new pavements. The pressuremeter moduli are sound input parameters for the multilayer elastic theory.

Other potential uses of the pavement pressuremeter include the selection for strength of base-course materials, the determination of equivalency factors, the determination of subgrade reaction value for the design of rigid pavements, the control of compaction, and the determination of the plastic properties of each layer by repeating the inflation-deflation of the probe a number of times.

CONCLUSIONS

A new pressuremeter and test method have been described that show promise for pavement design. The equipment is compact, sturdy, and can be easily carried by two people. The test procedure is simple, the test is of short duration, and the results are reproducible.

Each test yields a modulus of deformation for the soil, and a moduli profile is obtained at each test station. A total of 93 pavement pressuremeter tests and 11 McLeod plate tests were run in parallel at two airports in Canada. The McLeod plate test is the test that is used by Transport Canada for the design of flexible airport pavements. The pavement pressuremeter was shown to have definite potential for the design of airport pavements by showing that a correlation exists between pavement pressuremeter test results and McLeod plate test results. This correlation was used to generate a design procedure based on the pavement pressuremeter and a simple chart (Figure 9). This chart was obtained by replacing the McLeod plate parameters by an equivalent

pressuremeter parameter in the well-established Transport Canada design chart (Figure 9).

The multilayer elastic design method makes a more thorough use of the moduli profile obtained with the pavement pressuremeter than does the chart design procedure. The multilayer elastic design is therefore recommended. In the examples quoted in the text the calculated strains were probably larger than they should be. The overestimation of strain was attributed to the fact that the pressuremeter modulus is measured at strain levels that are larger than the strains developed by the wheel load. Recently a means of obtaining pressuremeter moduli at much lower volumetric strains has been devised, and the method will be the subject of another article.

ACKNOWLEDGMENT

This research was funded by Transport Canada and we are grateful for the support and encouragement given by L. Hunter, G. Argue, and J. Bertok of Transport Canada throughout the project. The National Research Council of Canada provided a scholarship to Briaud that enabled him to carry out the work as part of a doctoral program at the University of Ottawa, where Shields was a professor of civil engineering.

REFERENCES

1. F. Baguelin, J.F. Jezequel, and D.H. Shields. The Pressuremeter and Foundation Engineering. Transtech Publication, Rockport, MA, 1978.
2. J.L. Briaud. The Pressuremeter: Application to Pavement Design. Univ. of Ottawa, Ontario, Canada, Ph.D. thesis, 1979.
3. J.L. Briaud and D.H. Shields. A Special Pressuremeter and Pressuremeter Test for Pavement Evaluation and Design. Geotechnical Testing Journal, Vol. 2, No. 3, 1979, pp. 143-151.
4. S. Serota and G. Lowther. A New and Simple Penetration Pressuremeter. Ground Engineering, Vol. 9, No. 1, London, England, 1976, pp. 29-31.
5. N.W. McLeod. Airport Runway Evaluation in Canada. Internal Rept., Transport Canada, Ottawa, Ontario, Canada, Aug. 1947.
6. T.W. Lambe and R.V. Whitman. Soil Mechanics. Wiley, New York, 1969.
7. A.E.M. Claessen, J.M. Edwards, P. Sommer, and P. Uge. Asphalt Pavement Design: The Shell Method. Proc., 4th International Conference on the Structural Design of Asphalt Pavements, Vol. 1, Univ. of Michigan, Ann Arbor, 1977, pp. 39-74.
8. Pavement Design and Rehabilitation. Transport Canada, Ottawa, Ontario, Canada, Manual AK-68-12, 1976.
9. W. Barker, W. Brabston, and Y. Chou. A General System for the Structural Design of Flexible Pavements. Proc., 4th International Conference on the Structural Design of Asphalt Pavements, Vol. 1, Univ. of Michigan, Ann Arbor, 1977, pp. 209-248.

Publication of this paper sponsored by Committee on Strength and Deformation Characteristics of Pavement Sections.

Load Equivalency Factors of Triaxle Loading for Flexible Pavements

M.C. WANG AND R.P. ANDERSON

This paper presents the load equivalency factors of triaxle loading for flexible pavements. Two different approaches were used to determine load equivalency factors—American Association of State Highway Officials' (AASHO) empirical and mechanistic approaches. AASHO's empirical approach was used first to determine the load equivalency factor of 338-kN (76-kip) triaxle loading. For this approach, experimental pavements were subjected to approximately 55 000 repetitions of 338-kN triaxle loading. The load equivalency factor determined was 2.60 for the range of structural numbers studied and for a terminal serviceability index of about 2.0. The mechanistic approach was used in order to include a broad range of triaxle loading intensity. For this approach, the maximum vertical compressive strain on the top of the subgrade was analyzed by using the bitumen-structures-analysis-in-roads (BISAR) computer program. The maximum subgrade compressive strains were related with load equivalency factors in logarithmic coordinates for single- and tandem-axle loadings. The relation for triaxle loading was established by first plotting the equivalency factor determined from the AASHO approach against the maximum subgrade strain. Then a line was drawn through this point parallel to the lines of single- and tandem-axle loads. The load equivalency factors of various triaxle loading intensities were then obtained by entering the maximum subgrade strain of each load intensity into the relation.

One of the most important tasks of highway officials and engineers is the maintenance of the deteriorating, existing highway system. The deterioration of the highway network is augmented by the continued growth of traffic and the accompanying increase in vehicle size and gross weight in an attempt to improve the energy savings and economic efficiency of the transportation system. In order to maintain the heavy gross vehicle weight and still stay within legal axle-to-axle load restrictions, the trucking industry has devised the triaxle or triple-axle configuration. The most common adaptation of this new axle arrangement is the rear assemblage of the familiar single-unit, four-axle coal trucks, although five-axle tractor-semitrailer units that have triaxle configurations are becoming more commonplace.

Highway engineers are concerned about the impact of the innovative heavy triaxle vehicles. Unfortunately, results of the American Association of State Highway Officials (AASHO) road test (1) do not include information that would permit an assessment of the structural damage caused by triaxle vehicles. Consequently, incorporation of triaxle loading into design formulas is not possible. Additional work is necessary to determine the relative destructive effect of heavy triaxle configuration and allow for its application to pavement design and rehabilitation schemes.

One method of assessing the destructive effect of triaxle loading is through the use of the concept of load equivalency factor. The load equivalency factor of a given axle loading is defined as the number

of applications of a standard load that is equivalent in destructive effect to one application of the load under consideration; 80-kN (18-kip) single-axle load is normally used as the standard load. This paper presents the methods of evaluation and the results of load equivalency factors of triaxle loading for flexible pavements.

EVALUATION METHODS

The concept of load equivalency factor is from the AASHO road test (1). The criterion used in the AASHO road test for determination of load equivalency factor is serviceability. At the AASHO road test, equivalency factors were determined for two standard axle configurations: the single axle and the tandem axle, with single-axle load magnitudes up to 178 kN (40 kip) and tandem-axle loads up to 213 kN (48 kip). Since extrapolation from results of earlier tests is not reasonable, establishment of equivalencies for axle configurations not considered in these tests necessitates performance data collected under controlled environments.

Because prototype pavement studies that involve new axle-load configurations are time consuming and costly, analytical methods that use mechanistic approaches to the equivalency determination have received the most attention recently. Among the more noteworthy studies are those of Deacon (2); Treybig and Von Quintus (3); Hicks, Layton, and Glover (4); Terrel and Rimsritong (5); and Kingham (6). These analytical methods use two different modes of pavement distress (fatigue cracking and rutting) rather than pavement serviceability as the criteria for determining equivalency factors. In the analysis, the fatigue mode of distress was related with the maximum tensile strain at the bottom of the stabilized layer; rutting was related with the maximum compressive strain at the top of the subgrade. In their analysis, Treybig and Von Quintus (3) also developed a method by which the maximum compressive strain on the top of the subgrade could possibly be used to extrapolate the load equivalency factors determined at the AASHO road test. This method is based on the assumption that the relation between the maximum compressive strains on the top of the subgrade and the load equivalency factors is unique regardless of the type of axle configurations.

The mechanistic approach either considers only one distress mode at a time or requires assumptions that are not verifiable at this time. These inherent limitations make it very difficult to use the mechanistic approach alone to generate load equivalency factors that are compatible with those developed at the AASHO road test. Therefore, the empirical approach by using pavement performance data is necessary for determination of equivalency factors for triaxle loading. Current economic conditions, however, dictate that the conduct of a full-scale load test similar in scale to the AASHO road test for developing equivalency factors for a spectrum of triaxle loading is infeasible. Therefore, for this research, both empirical and mechanistic approaches were adopted. Specifically, the empirical approach was used to determine the equivalency factor of 338-kN (76-kip) triaxle loading, whereas the mechanistic approach was employed to include a broader range of load intensity for the triple-axle configuration. The 338-kN load intensity was selected on the basis of weigh station data collected in Pennsylvania.

LOADING CONDITION

Loading condition is one of the most important variables that affects the generated load equivalency factors. Conditions that should be considered are load magnitude, axle-load distributions, axle spacing, tire types, tire pressures, and tire spacings.

Magnitude of Load

To obtain a range of the triaxle load that operates on Pennsylvania highways, records from weigh stations were acquired through the Pennsylvania Department of Transportation. According to these data, the triaxle weights varied between 107 and 291 kN (24 and 65.5 kip) with a mean of 80 ±5.8 kN (55 ±1.3 kip). Note, however, that these data were collected at selected weigh stations throughout the state. The difficulty in obtaining an accurate picture of the loads that are actually being hauled, especially in the coalbelt areas, has long been acknowledged. On the basis of this observation, together with recognition of the increasing demand of heavier axle loads, a load range considerably higher than that indicated by the weigh station summaries was adopted in this study. Loads selected were 200, 245, 289, 334, and 378 kN (45, 55, 65, 75, and 85 kip). This range is believed to be sufficiently comprehensive to draw accurate conclusions about the damaging effect of the triaxle configuration.

In addition to the five triaxle loads and the standard 80-kN (18-kip) single-axle load, three other single-axle loads--27, 53, and 107 kN (6, 12, and 24 kip)--and four tandem-axle loads--80, 116, 151, and 187 kN (18, 26, 34, and 42 kip)--were investigated to compare the generated equivalency factors and the equivalency factors developed at the AASHO road test.

Axle Load Distribution

In all previous work involving calculation of triaxle equivalencies [e.g., Treybig and Von Quintus (3), Hicks and others (4), and Terrel and Rimsritong (5)] no mention is made of what axle-by-axle weight distribution was used in the analysis. Therefore, in these studies we must assume that for triaxles this weight is equally distributed among the three axles in the configuration. Although this assumption appears reasonable for tandem axles, it may not be in the case of triaxles. Note that the tandem axle is a fixed configuration, whereas triaxles typically have two fixed axles and one lift axle. Indeed, a majority of triaxles are essentially modified tandem axles with either a lift axle ahead of or behind the tandem. On triaxle dump trucks, this axle is usually ahead of the tandem, whereas on concrete mixers and specialized vehicles it is not uncommon for the lift axle to follow the tandem set.

Pressure in the lift axle may be regulated by the operator (lift systems are controlled by pneumatic or hydraulic pressures) so that the load carried by this axle (and also others in the tridem) may vary considerably. Therefore, distribution of the load (axle by axle) in the tridem is a function of the lift-axle air pressure.

The data from the weigh stations were analyzed to determine whether a typical weight distribution existed among axles in the tridem sets. Although the mean weights for each axle in the set resulted in a weight distribution relation of approximately 1/4, 3/8, and 3/8 for the lift axle, second, and third axles, respectively, these proportions did not hold true for the large majority of individual cases. A statistical regression of proportionate weights on gross triaxle weights likewise yielded no typical axle-by-axle weight that could be used in the loading condition for evaluation of triaxle equivalencies for various load magnitudes. Therefore, since no quantifiable relations could be obtained from

field data regarding the distribution of weight among axles of the tridem set, the assumption of equal weight distribution was adopted in this study for triaxles as well as for tandems.

Axle Spacing

A variety of tandem-axle and triple-axle spacings have been used throughout the literature. For instance, Deacon (2) considered tandem-axle spacings of 91.4, 121.9, and 152.4 cm (36, 48, and 60 in). He recommended the 121.9-cm (48-in) spacing for theoretical work with the caution that axle spacing becomes more critical in terms of its effect on pavement response parameters as the modulus of the stabilized layer increases. Treybig and Von Quintus (3) used a tandem-axle spacing of 127 cm (50 in) and a triple-axle spacing of 136 cm (54 in) in their equivalency factor study. (Why these spacings should not be equal was not explained.) Uzan and Wiseman (7) investigated equivalencies for three different axle spacings of 102.9, 121.9, and 141.0 cm (40.5, 48, and 55.5 in). Since a majority of triaxles are essentially modified tandems, a different spacing for the two-axle configurations does not appear to be justified. Therefore, in this study, an axle spacing of 124 cm (49 in) was used for both tandem axles and triple axles.

Tire Types, Air Pressures, and Spacings

A number of methods for selecting contact areas and pressures for loading input have been used. Treybig and Von Quintus (3) divided tire pressures into four groups that encompass all loads. For gross weights from 27 to 245 kN (6000 to 55 000 lbf), tire pressures were assumed to be 517.5 kPa (75 lb/in^2), and for the range from 245 to 400 kN (55 000 to 90 000 lbf), tire pressures of 552 kPa (80 lb/in^2) were assumed. Terrel (5) assumed that the contact radius is half of the tire width, and he varied the tire or contact pressure to account for changes in the magnitude of the wheel load. This approach yields contact pressures as high as 1097 kPa (159 lb/in^2) for 20.3-cm (8-in) wide tires and as low as 152 kPa (22 lb/in^2) for 47.0-cm (18.5-in) wide flotation tires. But, the majority of researchers, including Uzan and Wiseman (7), use a constant contact radius throughout a spectrum of tire load magnitudes and vary the pressure to account for this difference. This method often gives higher-than-normal tire pressures for heavy cargoes.

A more rational approach for simulating tire loads was undertaken here. Since allowable tire load and tire inflation pressure are a function of tire type, the corresponding inputs required in the analysis are also functions of the type of tire selected. According to the 1978 tire guide (8), the most popular heavy truck tire is the 10.00-20 bias-ply tire, and the second most popular heavy truck tire is the 10.00-22 and its radial equivalent, the 11-24.5 tire. On the basis of this information, all axle loads for which the 10.00-20 bias-ply duals are acceptable were assumed to be carried by these types of tires. If axle loads (and consequently tire loads) exceeded the recommended load limits for the 10.00-20 tire size designation, then the next-popular size tire (10.00-22) was assumed to carry the load. In all cases, the tire inflation pressure that corresponded to the minimum-load range recommended for the particular tire load was used. This information can be extracted from the standards for tire load limits at various inflation pressures as set by the Tire and Rim Association (9).

The spacing of dual tires is dependent on the tire size selected to carry the various axle loads. In most of the previous studies on theoretical equivalency factors, including those by Deacon (2) and Treybig and Von Quintus (3), spacing of dual tires was assumed to be a linear multiple of the equivalent contact radius. Deacon selected dual spacings of 2.5, 3.0, and 3.5 times the contact radius of one tire in the dual set. His results show that the maximum principal tensile strains developed on the bottom of the pavement surface layer are significantly affected by dual-tire spacing, whereas the equivalency factors generated by a fatigue cracking criterion were not as affected by such spacing. Since fatigue cracking is but one of the criteria used to develop equivalencies in this study, a similar lack of variance in equivalency factors developed through the other criteria cannot be readily assumed. Furthermore, the selection of a spacing that varies with the contact area (and hence the wheel load and the axle load) adds another variable that could be a source of considerable discrepancy when comparing equivalencies calculated by using different evaluation criteria. Therefore, a constant dual-tire spacing was adopted in this study. The spacing selected for all dual tires considered here is 33 cm (13.0 in). This distance is the minimum recommended by the Tire and Rim Association [adopted by Goodyear (10)] for 28-cm (11.00-in) nominal width tires installed on 20.3-cm (8.0-in) design rims. The minimum spacing recommended for 25.4-cm (10.00-in) nominal width tires is 31.8 cm (12.5 in). The additional 1.3 cm (0.5 in) is assumed to be a reasonable allowance for proper air circulation and dissipation of tire heat as well as avoidance of the sidewall contact caused by the heavier axle loads.

A summary of the adopted loading conditions is presented in Table 1. The results are expressed in terms of calculations performed for bias-ply tires rather than for the less common radial tires. In all cases, axle loads are assumed to be equally distributed among the 4, 8, and 12 tires of the single, tandem, and triple axles, respectively.

On the basis of these loading conditions, a triaxle trailer was fabricated for field testing. Figure 1 shows the vehicle, and Figure 2 illustrates the axle spacing and the axle load distribution. The total load on the triple axle was 338 kN (76 kip) with a distribution of 31.5, 33.7, and 34.7 percent for the first, second, and third axle, respectively. This load intensity was selected to simulate the highest load possible by using the test trailer and the available steel ingots as lading. Also, because of the size and shape of the steel ingots, this load distribution was considered close enough to the equal distribution assumed above.

EXPERIMENTAL PAVEMENTS

The experimental pavements are part of the Pennsylvania Transportation Research Facility, which is a single-lane, oval-shaped, full-scale experimental highway 1.6 km (1 mile) in length. The facility consists of 21 sections that have different compositions, layer thicknesses, and lengths, as shown in Figure 3. These sections had been subjected to axle loads applied by a conventional single-axle tractor pulling a semitrailer and one full single-axle trailer before triaxle loading was applied. The actual axle loads that were applied were converted to equivalent 80-kN (18-kip) single-axle loads (EAL) by using AASHO-derived equivalency factors. The triaxle loading was applied by using the original single-axle tractor pulling the triaxle trailer shown in Figure 1. A total of 55 000 repetitions of 338-kN (76-kip) triaxle loading was applied to the test pavements.

Table 1. Loading conditions used.

Axle Configuration[a]	Total Load (kN)	Wheel Load (kN)	Tire Size	Load Range	Tire Pressure (kPa)	Contact Radius (cm)
Single	26.7	6.7	10.00-20	F	517.1	6.40
	53.4	13.4	10.00-20	F	517.1	9.07
	80.1	20.0	10.00-20	F	517.1	11.10
	106.9	26.7	10.00-22	H	724.0	10.82
Tandem[b]	80.1	10.0	10.00-20	F	517.1	7.85
	115.8	14.5	10.00-20	F	517.1	9.42
	151.4	18.9	10.00-20	F	517.1	10.80
	187.0	23.4	10.00-20	G	620.6	10.95
Triple[b]	200.3	16.7	10.00-20	F	517.1	10.13
	244.9	20.4	10.00-20	F	517.1	11.20
	289.4	24.1	10.00-20	H	724.0	10.29
	333.9	27.8	10.00-22	H	724.0	11.05
	378.4	31.5	11.00-24	H	724.0	11.76

Note: 1 kN = 0.225 kip; 1 kPa = 0.145 lb/in^2; and 1 cm = 0.394 in.

[a]Center-to-center dual-tire spacing = 33 cm (13 in) for all conditions.
[b]Axle spacing = 124 cm (49 in).

Figure 1. Triaxle trailer used for loading.

Figure 2. Sketch of test vehicle.

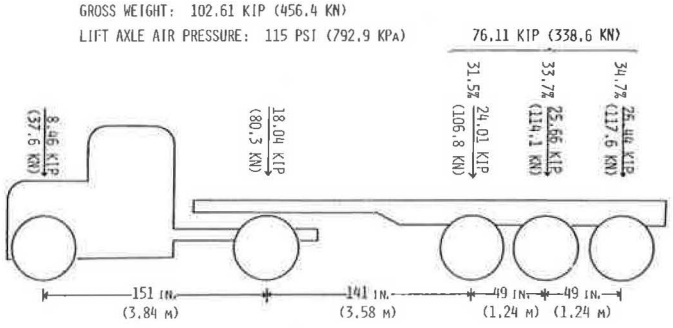

FIELD TESTING

Throughout the axle-loading history, rut depth was measured biweekly every 12.2 m (40 ft) in both wheelpaths. Surface cracking was surveyed and mapped biweekly. Surface roughness was measured in both wheelpaths by using a MacBeth profilograph. The roughness factors obtained from the profilograph data were converted into the present serviceability index (PSI) of the pavement by using the following equations:

$$PSI = 11.33 - 4.06(\log RF) - 0.01\sqrt{C + P} - 0.21\,\overline{RD}^2 \quad (1)$$

$$RF = 63.267 + 0.686\,R \quad (2)$$

where

PSI = present serviceability index,
RF = Mays meter roughness factor,
C = area of cracking (m^2/1000 m^2),
P = area of patching (m^2/1000 m^2),
$\overline{RD}$ = rut depth (cm), and
R = profilograph reading (cm/km).

In addition, surface deflections, profile of the pavement temperature, distribution of the subgrade moisture, and weather data were collected. Detailed information on field testing is available elsewhere (11,12).

LOAD EQUIVALENCY FACTORS

As stated before, the load equivalency factors of triaxle loading were determined by using both the AASHO empirical approach and the mechanistic approach. The AASHO approach was used to compute the equivalency factor of 338-kN (76-kip) triaxle loading only, whereas the mechanistic approach was used to consider a spectrum of triaxle loading of various intensities.

AASHO Empirical Approach

Of the 21 test pavements at the research facility, only 12 pavements were not overlaid, surface treated, or reconstructed, and they produced PSI data for both 80-kN (18-kip) single-axle loading and 338-kN (76-kip) triaxle loading. The 55 000 repetitions of 338-kN triaxle loading, however, were not sufficient to induce a noticeable decrease in PSI for 7 of the 12 pavements. Consequently, only 5 pavements (sections 8, B, E, F, and G) provided PSI data useful for computing the load equivalency factor of 338-kN triaxle loading. Figures 4 and 5 illustrate the PSI data of section 8 for 80-kN EAL and 338-kN triaxle loading, respectively. Data for other sections are documented elsewhere (13). From these PSI data, the loading equivalency factor can be computed as follows:

$$E_{f_{76}} = (N_{18}/N_{76}) - C_f \quad (3)$$

where

$E_{f_{76}}$ = load equivalency factor for 338-kN (76-kip) triaxle loading,
N_{18} = number of 80-kN (18-kip) single equivalent axle loading required to cause a PSI drop of ΔPSI,
N_{76} = number of 338-kN (76-kip) triple-axle loading required to cause ΔPSI, and
C_f = correction factor equal to the sum of the load equivalency factors of the test vehicle's steering and drive axles.

Figure 3. Plan and profile of experimental pavements.

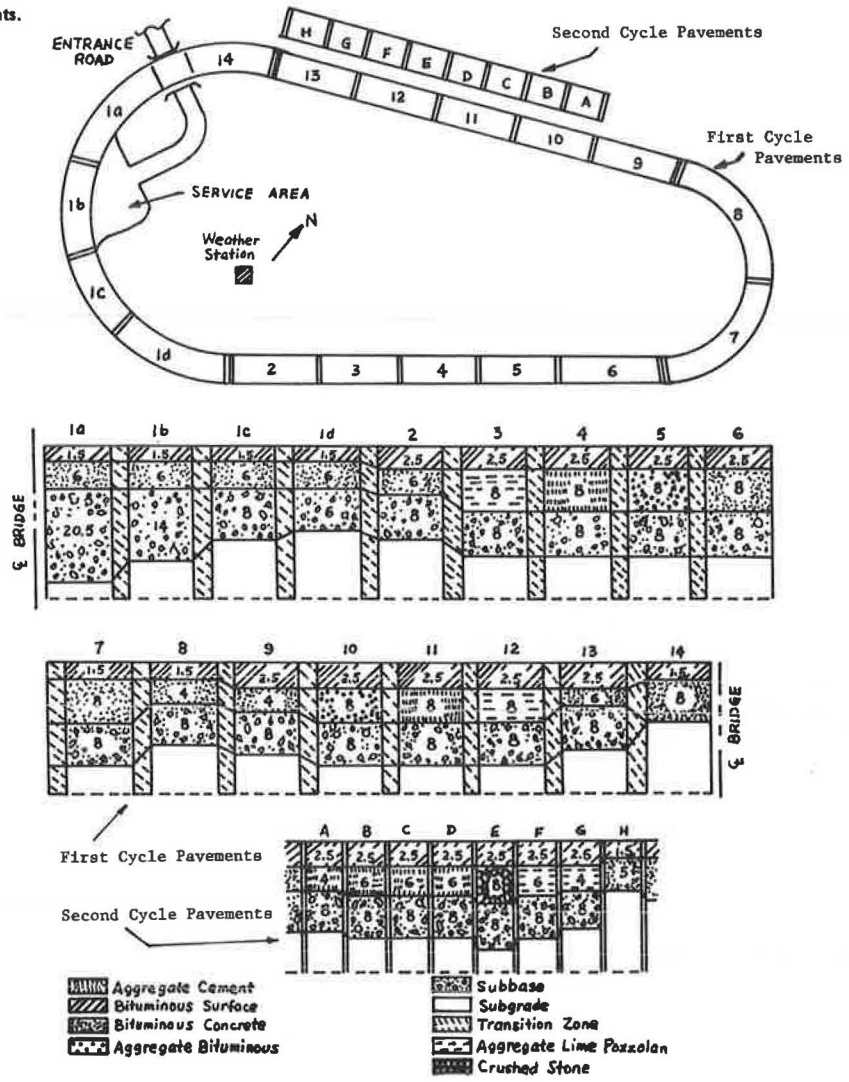

Figure 4. Performance curves for 80-kN EAL, section 8.

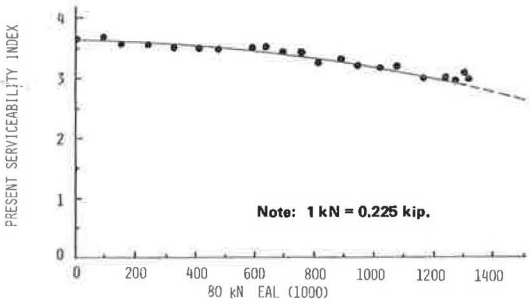

Figure 5. Performance curve for 338-kN triaxle loading, section 8.

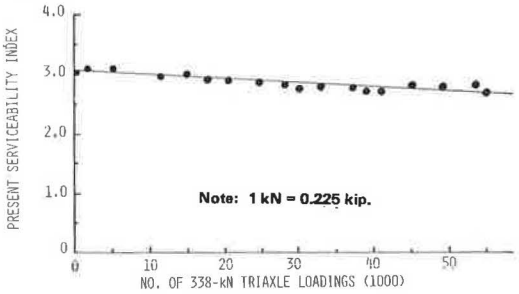

Figure 6. Rationale for calculation of load equivalency factor from pavement performance data.

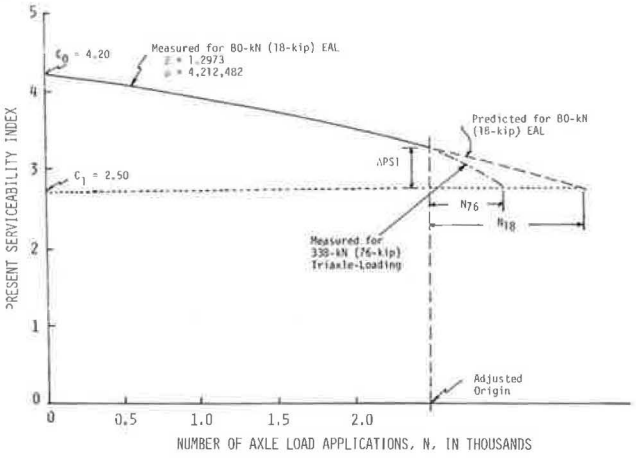

The rationale for this calculation is illustrated in Figure 6. The loading intensities on the test vehicle's steering and drive axles were 37.6 kN (8.46 kip) and 80.3 kN (18.04 kip), respectively, as shown in Figure 2. The load equivalency factors for these two axle loads were 0.04 and 1.00, respec-

tively. Therefore, the correction factor (C_f) equals 1.04.

The predicted PSI curve for 80-kN EALs shown in Figure 6 was obtained by fitting the data points to the AASHO equation in which the serviceability loss is a power function of axle load applications. This power function may be expressed in terms of β and ρ, defined under Equation 4, below.

$$G_t = \beta(\log W_t - \log \rho) \quad (4)$$

where

G_t = a function (the logarithm) of the ratio of loss in serviceability at time t to the potential loss taken to a point where p_t = 1.5,
β = a function of design and load variables that influence the shape of the serviceability curve,
W_t = axle load applications at the end of time t,
ρ = a function of design and load variables that denotes the expected number of axle load applications to a serviceability index of 1.5, and
p_t = serviceability at the end of time t.

Figure 5 shows that, in the approximately 55 000 applications of 338-kN triaxle loading, PSI values of all five test pavements decreased almost linearly with the number of axle load applications. Therefore, a linear extrapolation was used, when necessary, in the computation of load equivalency factors. To avoid extrapolating too far from the range of the available data, a PSI drop of 0.50 was used to compute load equivalency factors. For this PSI drop, the terminal serviceability index values on which the computation was based differed among sections: They were 2.45, 2.30, 1.83, 2.25, and 2.00, for sections 8, B, E, F, and G, respectively. Results of the computation are presented in terms of structural number in Figure 7. The data points fluctuate, and no apparent trend on the variation of load equivalency factors with structural number is seen. For the range of structural numbers studied, the load equivalency factor for 338-kN triaxle loading equals approximately 2.60.

Mechanistic Approach

The mechanistic approach was used to extend the preceding results to a broad range of triaxle loading intensity. According to Treybig and Von Quintus (3), the equivalency factors of triaxle loading may be determined by using the relation between the maximum vertical compressive strain on the top of the subgrade and the equivalency factors of single-axle loading, since the equivalency factors of tandem-axle loading that were determined by using this relation were close to the AASHO equivalency factors. Note that this relationship was developed for flexible pavements similar to some of the pavements at the AASHO road test and that no statistical tests were presented. In all cases, the pavements modeled in the computer program (ELSYM 5) consisted of granular (nonstabilized) base courses. Therefore, new relations for flexible pavements that contain stabilized base courses should be established, and statistical tests should be performed to assess the dependability of the established relationships.

Initially, both single- and tandem-axle loadings were input as the loading conditions to compute the maximum vertical compressive strains on the top of the subgrade. The computations were made by using the bitumen-structures-analysis-in-roads (BISAR) computer program (14) and the material properties are presented in Table 2. Details on the determination of material properties are reported elsewhere (15). AASHO equivalency factors for these loads were then calculated for a terminal serviceability index (p_t) of 2.0. For each pavement section analyzed, logarithmic transformations of both the maximum vertical compressive subgrade strain and the calculated AASHO load equivalency factor (E.F.) for each axle load configuration were obtained. A least-squares-regression analysis of log (ε_V) versus log (E.F.) was then performed by using MINITAB II (16).

Plots of both the single- and the tandem-axle load equivalency factor relations for section 1C are given in Figure 8 as an example. According to the results of the analysis, the two log (ε_V) versus log (E.F.) relations may be parallel but are not necessarily colinear. From a statistical standpoint, this discrepancy makes it impossible to predict triaxle equivalencies because a similar relationship for triples cannot be defined. This conclusion may not hold true if error about the inputted AASHO equivalencies is considered. Recall that the equivalencies used in these relations were not measured but rather calculated by using a regression function that was derived from an analysis of AASHO road test sections. Indeed, since subgrade compressive strains were determined directly from elastic layer theory, neither ordinate nor abscissa in the log (ε_V) versus log (E.F.) relations in these analyses has error. This lack of error and the existence of a functional relation between the logarithmic transforms of load and the mechanistic pavement strain account for the exact correlation between Y and X in these relations. Nevertheless, in lieu of additional information, the analyses show that the relations for load equivalency factors are

Figure 7. Load equivalency factor of 338-kN triaxle loading.

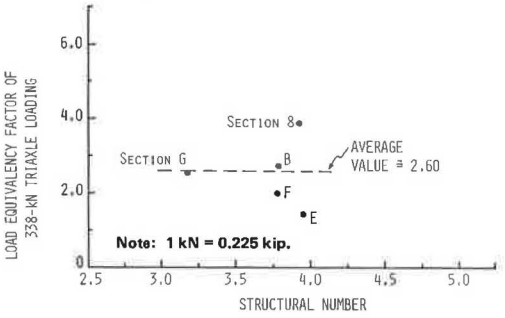

Table 2. Elastic constants of pavement materials.

Layer Description	Elastic Modulus (MPa)	Poisson's Ratio
Surface course		
Asphalt concrete, Spring	966	0.40
Asphalt concrete, Summer	186	0.40
Base course		
Bituminous concrete (BCBC), Spring		
Top sublayer	2 207	0.35
Bottom sublayer	3 034	0.35
BCBC, Summer		
Top sublayer	138	0.35
Bottom sublayer	262	0.35
Aggregate-lime-pozzolan (ALP), Spring	16 552	0.15
Limestone aggregate cement (LAC), Spring	24 828	0.20
Granular subbase, Spring	331	0.40
Subgrade, Spring	55	0.45

Notes: 1 MPa = 145 lbf/in^2.
Evaluations are for initial pavement conditions.

different for single axles and tandem axles, and, therefore, one cannot predict triaxle equivalencies from the relations of single or tandem axles.

It is possible, however, to establish the relation between the maximum vertical subgrade strains and the load equivalency factors for triaxle loading by using the trend of the relations for single- and tandem-axle loadings together with the load equivalency factor (2.60) of 338-kN (76-kip) triaxle loading. This is accomplished by first plotting the load equivalency factor of 2.60 against the maximum subgrade strain for 338-kN triaxle loading, and then drawing a straight line through this point parallel to the lines for single- and tandem-axle loads. Relations are established for pavement sections B, E, 4, and 6 and are presented in Figures 9 and 10. For section 6, the analysis was made for three seasons so that the possible seasonal effect, if any, on load equivalency factors could be observed.

From this newly established relation, the load equivalency factors for various intensities of triaxle loading can be obtained by entering into this line the maximum vertical subgrade strain corresponding to each loading intensity. Results of the computation are tabulated in Table 3. Note that, on the basis of the semiempirical approach, the load equivalency factors did not vary with seasons, as Figure 10 illustrates. This is consistent with AASHO's results. Furthermore, the slight difference in load equivalency factors of triaxle loading between sections, as shown in Table 3, was primarily due to error involved in reading numbers from Figures 9 and 10. Rigorously speaking, this discrepancy should not exist because the equivalency factor (2.60) of 338-kN triaxle loading is assumed to be constant with respect to structural number within the range of conditions studied.

Figure 8. Relation between maximum subgrade compressive strain and AASHO load equivalency factors.

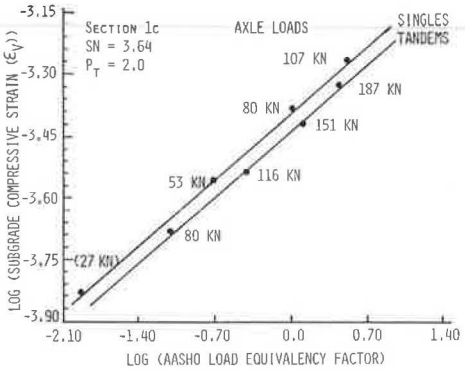

Note: 1 kN = 0.225 kip.

Figure 9. Subgrade compressive strain versus load equivalency factor for sections 4, B, and E.

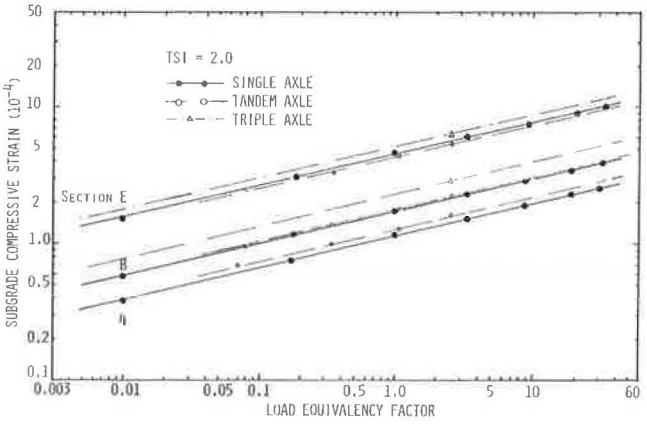

Figure 10. Subgrade compressive strain versus load equivalency factor for section 6.

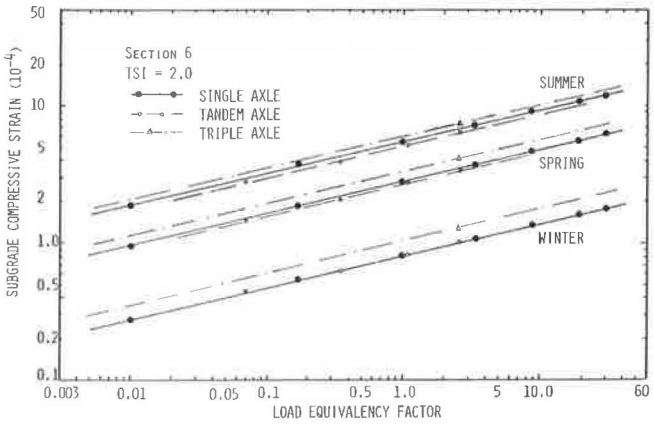

SUMMARY AND CONCLUSIONS

The load equivalency factors of triaxle loading were evaluated by using both the AASHO empirical approach and the mechanistic approach. Specifically, the AASHO approach was adopted to determine the equivalency factors of 338-kN triaxle loading, and the mechanistic approach was used to include a broad range of triaxle load intensities.

To generate the required performance curves for the AASHO approach, the experimental pavements were subjected to approximately 55 000 repetitions of 338-kN triaxle loading. Based on the results obtained from the experimental pavements, the load equivalency factor of 338-kN triaxle loading was approximately 2.60 for the range of structural numbers investigated and for a terminal serviceability index of about 2.0.

For the mechanistic approach, the relations between load equivalency factors and the maximum vertical strain on the top of the subgrade were established for single- and tandem-axle loadings. These relations, in logarithmic coordinates, were straight lines parallel to each other. The load equivalency factor of 338-kip triaxle loading and its corresponding maximum subgrade strain were entered into the figure, and a straight line parallel to the lines for single- and tandem-axle loadings was drawn. The load equivalency factors of various triaxle loading intensities were then obtained by entering the maximum subgrade compressive strain of each loading intensity into the relation. The computed results are tabulated in Table 3.

ACKNOWLEDGMENT

The study presented here is a part of the research project sponsored by the Pennsylvania Department of Transportation in cooperation with the Federal Highway Administration. This support is gratefully acknowledged. The field data reported were collected and reduced with the assistance of W.P. Kilareski, S.A. Kutz, B.A. Anani, and J. Karundeng. This paper represents our views and does not necessarily reflect those of the Pennsylvania Department

Table 3. Load equivalency factors and maximum vertical compressive strain on top of the subgrade.

	Section B, SN = 3.78		Section E, SN = 2.86		Section 4, SN = 5.26		Section 6, SN = 4.94			
Loading (kN)	E_f	$\epsilon_V(10^{-4})$	E_f	$\epsilon_V(10^{-4})$	E_f	$\epsilon_V(10^{-4})$	E_f	Spring	Summer	Winter
Single axle[a]										
27	0.01	0.592	0.01	1.57	0.01	0.392	0.01	0.956	1.89	0.275
53	0.18	1.18	0.19	3.13	0.17	0.784	0.17	1.90	3.75	0.548
80	1.00	1.76	1.00	4.63	1.00	1.17	1.00	2.83	5.44	0.817
107	3.35	2.35	3.45	6.18	3.43	1.55	3.40	3.76	7.38	1.09
133	8.77	2.93	9.32	7.68	8.84	1.94	8.72	4.69	9.18	1.36
160	19.33	3.50	21.37	9.12	19.25	2.32	19.01	5.59	10.9	1.62
178	31.61	3.88	34.71	10.1	30.34	2.58	30.03	6.21	12.1	1.80
Tandem axle										
80[a]	0.08	0.964	0.08	2.53	0.07	0.695	0.07	1.46	2.78	0.450
116[a]	0.35	1.39	0.36	3.36	0.35	0.998	0.35	2.10	3.96	0.630
151[a]	1.08	1.81	1.08	4.38	1.08	1.30	1.08	2.73	5.16	0.824
187[a]	2.62	2.24	2.65	5.39	2.64	1.61	2.64	3.38	6.36	1.02
222[b]	5.2	2.65	5.6	6.41	6.0	1.92	5.80	4.01	7.56	1.21
267[b]	11.1	3.18	12.0	7.65	12.6	2.30	12.60	4.80	9.02	1.45
Triple axle[b]										
67	0.0028	0.577	0.0025	1.30	0.0030	0.444	0.0026	0.833	1.53	0.258
111	0.024	0.962	0.022	2.16	0.024	0.739	0.024	1.38	2.52	0.430
156	0.101	1.35	0.10	3.02	0.11	1.04	0.10	1.93	3.52	0.601
200	0.30	1.73	0.29	3.86	0.30	1.33	0.29	2.48	4.49	0.771
245	0.70	2.11	0.67	4.69	0.70	1.62	0.70	3.18	5.45	0.939
289	1.44	2.50	1.30	5.56	1.40	1.92	1.40	3.57	6.47	1.11
334	2.50	2.87	2.50	6.39	2.50	2.22	2.50	4.10	7.43	1.28
338	2.60	2.91	2.60	6.45	2.60	2.25	2.60	4.15	7.53	1.30
378	4.30	3.25	4.20	7.20	4.60	2.51	4.40	4.64	8.37	1.44
423	7.00	3.63	6.60	8.03	6.70	2.80	7.00	5.18	9.33	1.61
467	10.4	4.01	10.0	8.82	11.0	3.09	10.7	5.70	10.2	1.78
512	15.0	4.38	15.0	9.63	16.5	3.39	16.0	6.23	11.2	1.96

Note: 1 kN = 0.225 kip.

[a] Load equivalency factors were obtained from AASHO road test.
[b] Load equivalency factors were from Figures 8 and 9, except for 338-kN (76-kip) triaxle loading, which was estimated by using the AASHO empirical approach.

of Transportation or the Federal Highway Administration.

REFERENCES

1. The AASHO Road Test: Report 5--Pavement Research. HRB, Special Rept. 61E, 1962.
2. J.A. Deacon. Load Equivalency in Flexible Pavements. Proc., Assoc. of Asphalt Paving Technologists, Los Angeles, Vol. 38, Feb. 1969, pp. 466-491.
3. H.J. Treybig and H.L. Von Quintus. Equivalency Factor Analysis and Prediction for Triple Axles. Presented at the 56th Annual Meeting, TRB, 1977.
4. R.G. Hicks, R.D. Layton, and S. Glover. Evaluation of Increased Truck Size and Weight on Pavement Life and Design Thickness. TRB, Transportation Research Record 671, 1978, pp. 46-53.
5. R.L. Terrel and S. Rimsritong. Pavement Response and Equivalencies for Various Truck Axle and Tire Configurations. TRB, Transportation Research Record 602, 1976, pp. 33-38.
6. R.I. Kingham. Fatigue Criteria Developed from AASHO Road Test Data. Proc., 3rd International Conference on the Structural Design of Asphalt Pavements, London, Vol. 1, 1972, pp. 656-669.
7. J. Uzan and G. Wiseman. Allowable Load on Multiple-Axle Trucks. Paper Presented at 58th Annual Meeting, TRB, Jan. 1979.
8. 1978 Tire Guide. Tire Information Center, Commack, NY, Vol. 21, 1978.
9. 1977 Tire and Rim Association Yearbook. Tire and Rim Assoc., Akron, OH, 1977.
10. Radial Truck Tire Service Manual--Over-the-Road and Special Service Unisteel Tires. Goodyear Tire and Rubber Company, Akron, OH, 1975.
11. E.S. Lindow, W.P. Kilareski, G.Q. Bass, and T.D. Larson. Construction, Instrumentation, and Operation. Pennsylvania Transportation Institute, Pennsylvania State Univ., University Park, Vol. 2, Interim Rept. PTI 7505, Feb. 1973.
12. W.P. Kilareski, S.A. Kutz, and G. Cumberledge. Modification, Construction, and Instrumentation of an Experimental Highway. Pennsylvania Transportation Institute, Pennsylvania State Univ., University Park, Interim Rept. PTI 7607, April 1976.
13. M.C. Wang and R.F. Anderson. Load Equivalency Factors for Triaxle Loading. Pennsylvania Transportation Institute, Pennsylvania State Univ., University Park, Final Rept. PTI 7922, Nov. 1979.
14. D.L. DeJong, M.G.F. Peutz, and A.R. Korswagen. Computer Program BISAR. Koninklijke-Shell-Laboratorium, Amsterdam, External Rept., 1973.
15. M.C. Wang and T.D. Larson. Performance Evaluation for Bituminous-Concrete Pavements at Pennsylvania State Test Track. TRB, Transportation Research Record 632, 1977, pp. 21-27.
16. T.A. Ryan, Jr., B.L. Joiner, and B.F. Ryan. Minitab II Reference Manual. Pennsylvania State Univ., University Park, March 1978.

Publication of this paper sponsored by Committee on Flexible Pavement Design.

Constitutive Equation for Permanent Strain of Sand Subjected to Cyclic Loading

RODNEY W. LENTZ AND GILBERT Y. BALADI

Numerous rational methods for flexible pavement design and rehabilitation have been proposed to overcome some of the deficiencies of current empirical methods. Most of these rational methods predict permanent deformation in subgrade materials so that a pavement structure may be selected that will limit permanent deformation under the application of traffic loads. Thus, procedures for characterizing permanent deformation of subgrade materials are required in each of these methods. This paper presents a constitutive equation for predicting accumulated permanent strain of sand subgrade material after any number of repetitions of load. The parameters needed as input to the equation are obtained from a static triaxial test. To develop the equation, duplicate samples were tested by using both static triaxial apparatus and a closed-loop electrohydraulically actuated triaxial system. The dynamic test results were normalized with respect to parameters obtained from the corresponding static triaxial test. The difference in the normalized cyclic principal stress showed a unique relationship to the normalized accumulated permanent strain. This relationship was found to be independent of moisture content, density, and confining pressure. Based on these findings, a constitutive equation for permanent strain was developed.

Most design agencies base their procedures for pavement design on empirical design nomographs coupled with empirical subgrade strength parameters, individual experience, and local environmental conditions. The trend toward ever-increasing axle loads on highway and airport pavements has revealed serious shortcomings of empirical design methods for flexible pavements. These methods lack the ability to predict the amount of deformation anticipated after a given number of load applications. When pavement load exceeds the range for which performance data are available, empirical methods fail. Since soil is known to behave in a nonlinear fashion, performance under higher axle loads cannot be extrapolated from performance at lower load levels.

Numerous rational methods for flexible pavement design and rehabilitation have been proposed to overcome this deficiency. These are usually quasi-elastic (elastic theory to predict stresses coupled with permanent strains determined by repeated load laboratory tests) (1). Some methods also use visco-elastic theory together with laboratory testing (2,3). To be useful, these methods must have the capability of predicting cumulative permanent deformations in subgrade materials so that a pavement structure may be selected that will limit permanent deformation under traffic loading to an acceptable level. This requires the development of an adequate constitutive equation for prediction of permanent strain (3,4). Further, the method used to evaluate the constants in the constitutive equation should be simple, economical, and not require new and complicated expensive equipment or testing procedure. A constitutive equation that meets these criteria is presented in this paper.

BACKGROUND

Parameters that affect the accumulation of permanent strain in cohesionless material have been reported to be number of load repetitions, stress history, confining pressure, stress level, and density (1,3,5-12). A review of these effects is given by Lentz (10).

The effect of number of load repetitions on permanent strain has been reported by several investigators to be a straight-line relationship on a semilogarithmic plot Cyclic stress versus permanent strain curves have been shown to be analogous to static stress-strain curves (6,10-12) and describable by using hyperbolic functions developed for static test results (13,14). The results of cyclic triaxial tests can be normalized by using parameters obtained from static triaxial tests performed on duplicate samples (12). The difference in normalized principal stress showed a unique relationship to the normalized accumulated permanent strain. This relationship was found to be independent of moisture content, density, and confining pressure.

Testing Procedure and Equipment

The material used in the testing program was uniform, medium sand typical of that found in the northern half of Michigan. Duplicate triaxial samples were tested by using both static triaxial apparatus and a closed-loop electrohydraulically actuated triaxial system.

Three levels of confining pressure (σ_3 = 5, 25, 50 lb/in^2) and two levels of density were used (γ = 99 percent AASHTO T-99 and 99 percent AASHTO T-180). For each combination of these variables, several levels of cyclic principal stress difference (σ_d) were used. Because stress history has a large influence on permanent strain, a new sample was required for each combination of variables. Details of the testing procedure are described elsewhere (10).

Test Results

It has been shown elsewhere (10-12) that the data for each sample could be approximated by a straight line on a plot of permanent strain versus logarithm of number of load cycles. Least-squares technique was used to pass a best fit straight line through each set of data. The equation of the line is of the form

$$\epsilon_p = a + b \ln N \quad (1)$$

where

ϵ_p = accumulated permanent strain,
N = number of load repetitions, and
a and b = regression constants from least-squares best fit.

The constant a represents the permanent strain that occurs during the first cycle of load. The constant b represents the rate of change in permanent strain with increasing number of load repetitions. The values of a and b are, of course, different for each sample, depending on density, confining pressure, and level of cyclic principal stress difference.

DISCUSSION OF RESULTS

The principal objective of this research project was to obtain a constitutive relationship that will predict the amount of permanent strain under any number of load applications at any specified stress level. This relationship should account for sample variables (e.g., density or moisture content) and

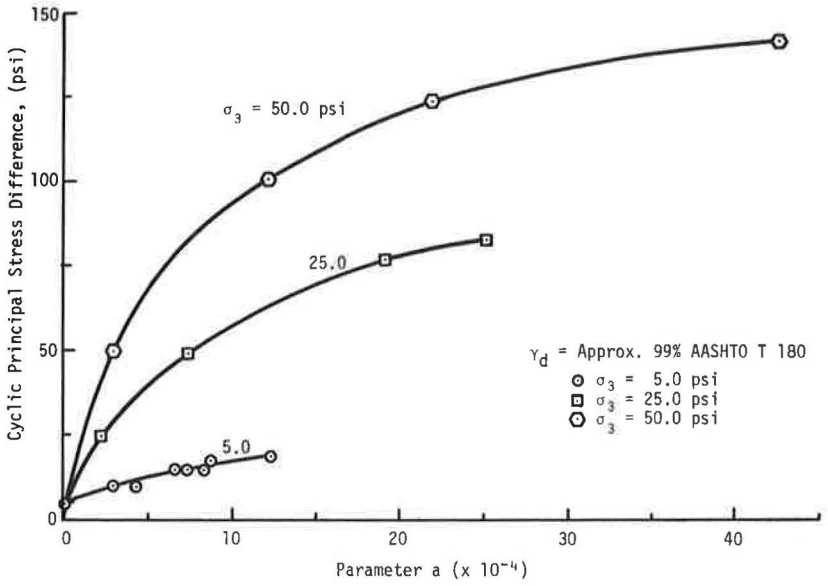

Figure 1. Relationship between cyclic principal stress difference and permanent strain during first load cycle.

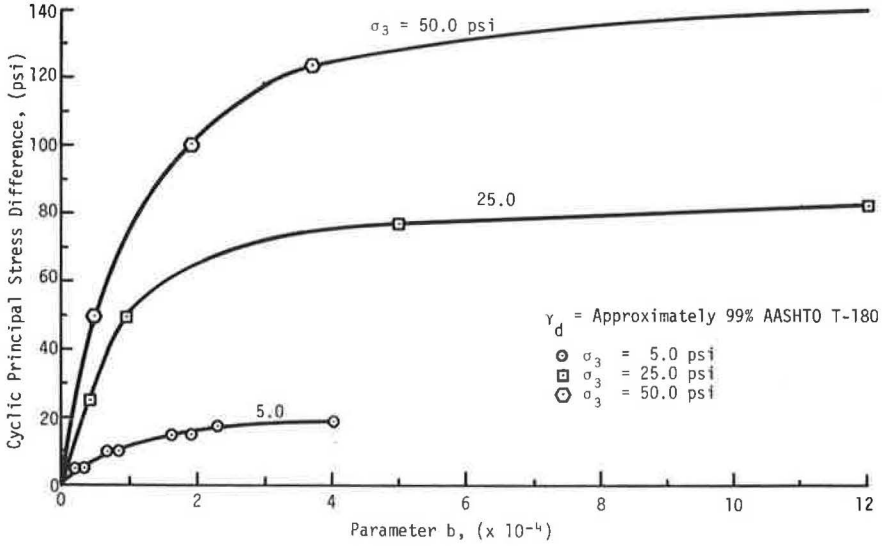

Figure 2. Relationship between cyclic principal stress difference and rate of change of permanent strain during cyclic loading.

confining pressure as well as cyclic principal stress difference and number of load applications.

Equation 1 expresses the cumulative permanent strain as a function of the number of load repetitions. Parameters a and b of the equation were thought to represent characteristics of the sample behavior under the particular testing conditions. Thus, it was convenient to develop the constitutive relationship by starting from Equation 1. Recall that the value of parameter a represents the permanent strain due to the first-load application. The value of parameter b indicates the rate at which permanent strain accumulates with increasing number of load repetitions. Therefore, if parameters a and b are expressed as functions of the sample variables, the testing conditions may provide the desired constitutive relationship.

It was shown (12) that the static stress-strain results of a sample of sand can be used to predict the cumulative permanent strain of an identical sample tested under cyclic loading conditions. Changes in material or testing conditions are reflected by changes in static stress-strain behavior and in parameters a and b. Thus, normalization of the cyclic stress and strain with respect to static stress and strain will eliminate or reduce the effect of these variables. Note that the static stress-strain data should be obtained from a sample identical in every respect to the dynamically tested specimens. This required one static test for each combination of density, water content, and confining pressure used in the dynamic testing program.

Figures 1 and 2 show plots of cyclic principal stress difference versus parameters a and b, respectively, for three different confining pressures. The values of cyclic principal stress difference plotted in Figure 1 were normalized by dividing by the peak static strength (S_d) from the corresponding static triaxial test. The values of parameter a were likewise normalized by dividing by the static strain that corresponds to a stress equal to 95 percent of S_d. The procedure for determining this normalizing strain ($\varepsilon_{0.95S_d}$) has been described elsewhere (12). After the above normalizing procedure was applied, the data from Figure 1 were replotted in Figure 3. Examination of this figure indicates that the data from all tests collapsed together to form a single curve. By inspection, it was found that this curve could be represented by the following function:

$$a/\epsilon_{0.95S_d} = \ln(1 - \sigma_d/S_d)^{-0.15} \quad (2)$$

where

a = regression parameter from Equation 1,
$\epsilon_{0.95S_d}$ = static strain at 95 percent of static strength,
σ_d = cyclic principal stress difference, and
S_d = static strength.

This can be rewritten to give

$$a = \epsilon_{0.95S_d} \ln(1 - \sigma_d/S_d)^{-0.15} \quad (3)$$

Figure 3. Relationship between normalized cyclic principal stress difference and normalized parameter a.

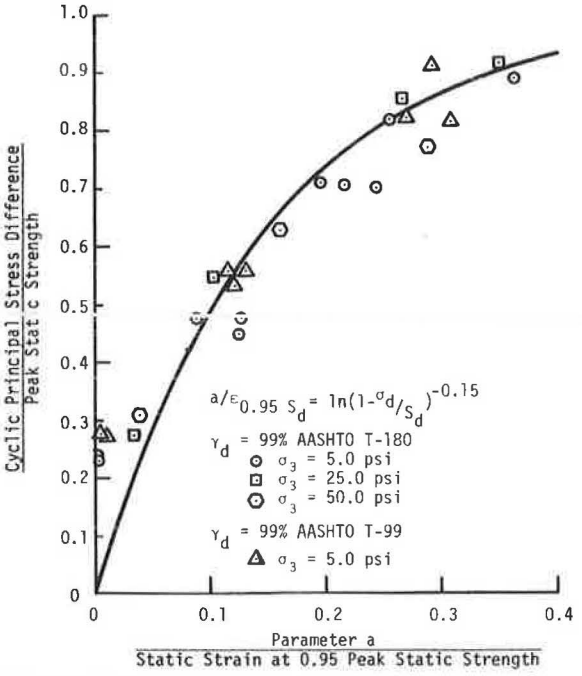

A plot of normalized principal stress difference versus parameter b of Equation 1 is shown in Figure 4. Study of the figure shows that the effect of sample density vanishes, but each value of confining pressure yielded a distinctly separate curve. Note that the shapes of these curves are similar to static stress-strain curves.

Hyperbolic functions can be used to approximate static stress-strain curves (13,14). The applicability of hyperbolic function to describe the relationship between cumulative permanent strain and cyclic stress at a specific number of load applications has been demonstrated for unstabilized base material (6) and for fine-grained subgrade soil (15). Since the curves in Figure 4 appear similar in shape to static stress-strain curves, it seems reasonable to extend the use of the hyperbolic relationship to describe them. The hyperbolic relationship used by others (15) to describe cyclic principal stress difference versus permanent strain is of the form

$$\sigma_d = \epsilon_p/(n + m\epsilon_p) \quad (4)$$

where

n and m = regression constants,
ϵ_p = cumulative permanent strain, and
σ_d = cyclic principal stress difference.

Modification of Equation 4 so that it applies to the relationship between normalized cyclic principal stress versus parameter b (shown in Figure 4) yields the following:

$$\sigma_d/S_d = b/(n + mb) \quad (5)$$

This can be rewritten in linear form to give

$$b/(\sigma_d/S_d) = n + mb \quad (6)$$

Least-squares technique was used to obtain the best-fit straight lines represented by Equation 6 for the data at each confining pressure. The values of n and m that were determined are shown in Figure 4 along with plots of the resulting hyperbolic

Figure 4. Relationship between normalized cyclic principal stress difference and parameter b.

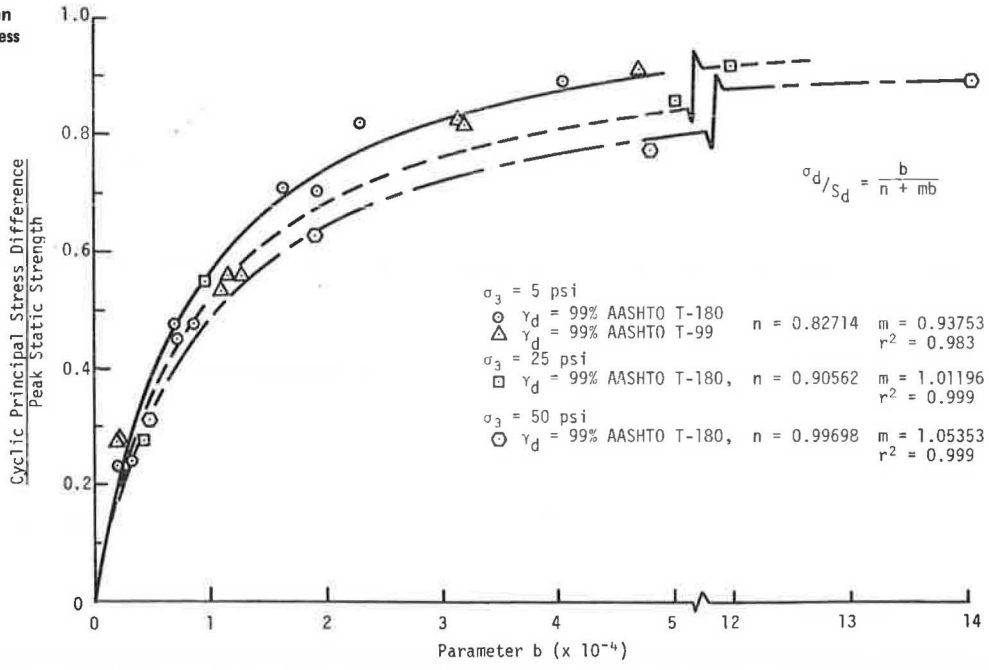

Figure 5. Relationship between confining pressure and regression constants n and m.

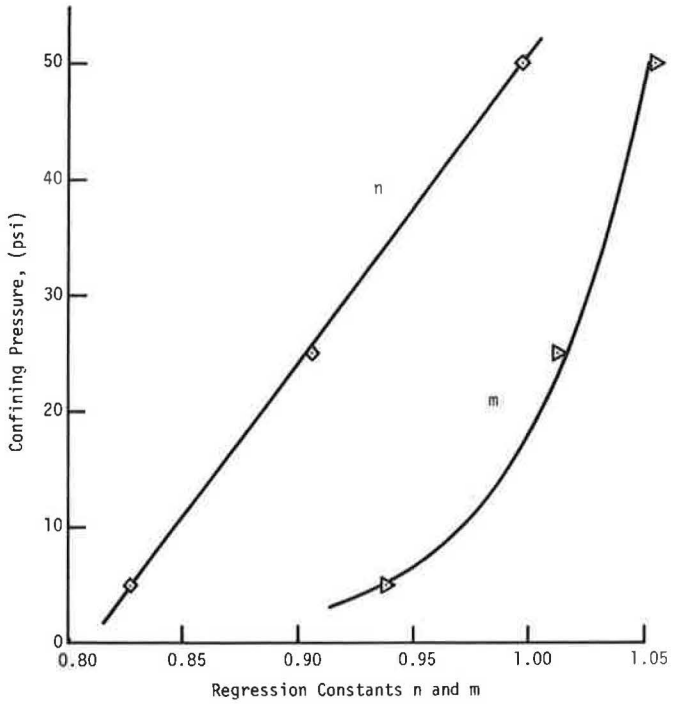

Figure 6. Comparison of measured and calculated permanent strain at N = 10 000.

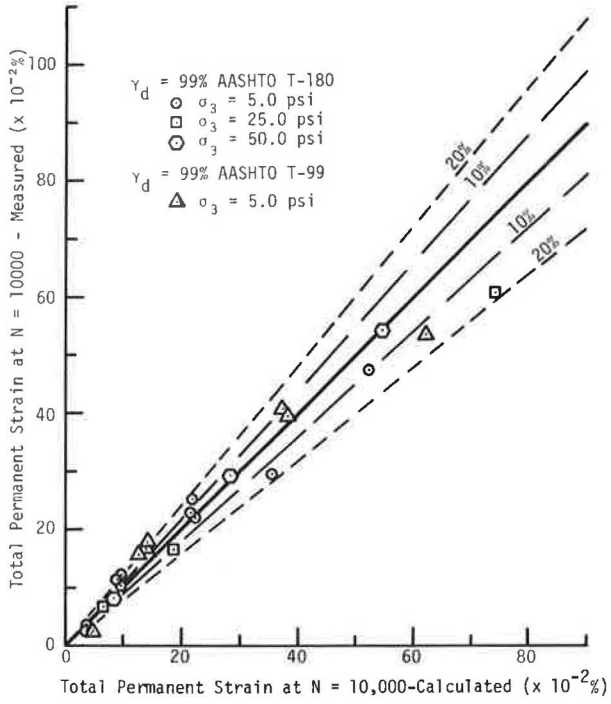

curves and coefficients of correlation. Inspection of the figure indicates that the hyperbolic relationship fits the data rather well. Rearrangement of Equation 6 and solving for b yields

$$b = (\sigma_d/S_d)n/[1 - m(\sigma_d/S_d)] \quad (7)$$

Note that the coefficients n and m in Equation 7 have different values for each confining pressure. Thus, to complete the constitutive equation, n and m should be expressed as functions of confining pressure. The values of n and m were plotted against the confining pressure in Figure 5. Examination of the figure indicated that n can be related to confining pressure by a linear function. The relationship for m was found to be logarithmic. Equations 8 and 9 were obtained by using least-square fitting technique to represent these functional relationships:

$$n = (0.809\,399 + 0.003\,769\sigma_3) \times 10^{-4} \quad (8)$$

$$m = 0.856\,355 + 0.049\,650 \ln \sigma_3 \quad (9)$$

where σ_3 is the confining pressure in pounds per square inch.

The completed constitutive equation can be obtained by substituting the expressions for parameters a (Equation 3) and b (Equation 7) into Equation 1. These substitutions yield

$$\epsilon_p = \epsilon_{0.95S_d} \ln(1 - \sigma_d/S_d)^{-0.15} + (\sigma_d/S_d)n/[1 - m(\sigma_d/S_d)] \ln N \quad (10)$$

where n and m are given by Equations 8 and 9, respectively.

To check the reliability of Equation 10, values of accumulated permanent strain at the end of 10 000 cycles were calculated by using Equation 10. These calculated values were plotted in Figure 6 versus permanent strain measured during the cyclic triaxial testing program. Note that the points plotted in Figure 6 represent samples tested at three different confining pressures and two different densities. Perfect correspondence between calculated and measured permanent strain would result in the plots of all points being along a 45° diagonal line. This diagonal line, along with lines that indicate a deviation of ±10 percent and ±20 percent from it are also shown in the figure. Inspection of Figure 6 shows that most of the data points fall close to the 45° line. This indicates a good correspondence between measured and calculated values. Note, however, that the data used to derive the constitutive equation are from the same samples used for the measured permanent strain plotted in Figure 6. Thus, the figure indicates how well the equation fits the data it was derived from rather than its predictive capability.

To examine the predictive capability of Equation 10, three additional samples were prepared at a density of 99 percent of AASHTO T-99. One of these samples was tested in a static triaxial test to obtain the parameters (S_d and $\epsilon_{0.95S_d}$) that are needed in Equation 10. These values were used to calculate the cumulative permanent strains for the other two samples at two different stress levels. These calculated values were then compared with measured permanent strain. This comparison yielded results similar to those presented in Figure 6. Note that the only parameters needed in Equation 10 can be obtained from a static triaxial test conducted at the expected density and confining pressure.

CONCLUSION

This paper has presented a constitutive equation that will predict the amount of permanent strain that will occur under any number of load applications at any specified stress level. The equation accounts for sample and test variables and requires only the results of a static triaxial test. The development of this equation was based on results from a single sand subgrade material. Hence, addi-

tional research is needed to extend the usefulness of the equation to a wider range of subgrade materials. Once additional research has verified or modified these findings, use of this constitutive equation for predicting permanent strain should result in significant saving of laboratory time and equipment because only static triaxial test results are required for its use. Also, rational methods of pavement design, which require characterization of permanent strain behavior, will be more likely to gain quick acceptance by practicing engineers if they have available such a simple means of predicting permanent strain.

REFERENCES

1. E.J. Yoder and M.W. Witczak. Principles of Pavement Design, 2nd ed. Wiley, New York, 1975.
2. W.J. Kenis. Predictive Design Procedure--A Design Method for Flexible Pavements Using the VESYS Structural Subsystem. Proc., 4th International Conference on Structural Design of Asphalt Pavements, Ann Arbor, MI, Vol. I, 1977, pp. 101-130.
3. W.L. Huffered and J.S. Lai. Analysis of N-Layered Viscoelastic Pavement Systems. FHWA, 1977, 220 pp. NTIS: PB 282578.
4. P.S. Pell and S.F. Brown. The Characteristics of Materials for the Design of Flexible Pavement Structures. Proc., 3rd International Conference on Structural Design of Asphalt Pavements, London, England, 1972. pp. 326-342.
5. J.R. Morgan. The Response of Granular Materials to Repeated Loading. Proc., 3rd Conference of the Australian Road Research Board, Sydney, Vol. 3, Pt. 2, 1966, pp. 1178-1191.
6. R.D. Barksdale. Laboratory Evaluation of Rutting in Base Course Materials. Proc., 3rd International Conference on Structural Design of Asphalt Pavements, London, England, 1972, pp. 161-174.
7. Y.T. Chou. Engineering Behavior of Pavement Materials: State of the Art. U.S. Army Engineers Waterways Experiment Station, Vicksburg, MS, Tech. Rept. S-77-9, 1977,
8. I.V. Kalcheff and R.G. Hicks. A Test Procedure for Determining the Resilient Properties of Granular Materials. Journal of Testing and Evaluation, Vol. 1, No. 6, 1973, pp. 472-479.
9. S.F. Brown. Repeated Load Testing of a Granular Material. Journal of the Geotechnical Engineering Division, Proc., ASCE, Vol. 100, No. GT7, July 1974, pp. 825-841.
10. R.W. Lentz. Permanent Deformation of Cohesionless Subgrade Material Under Cyclic Loading. Department of Civil Engineering, Michigan State Univ., East Lansing, Ph.D. dissertation, 1979.
11. R.W. Lentz and G.Y. Baladi. Simplified Procedure to Characterize Permanent Strain in Sand Subjected to Cyclic Loading. Proc., International Symposium on Soils Under Cyclic and Transient Loading, Swansea, United Kingdom, 1980, pp. 89-95.
12. R.W. Lentz and G.Y. Baladi. Prediction of Permanent Strain of Sand Subjected to Cyclic Loading. TRB, Transportation Research Record 749, 1980, pp. 54-58.
13. J.M. Duncan and C.Y. Chang. Nonlinear Analysis of Stress and Strain in Soils. Journal of Soil Mechanics and Foundations Division, Proc., ASCE, Vol. 96, SM5, Sept., 1970, pp. 1629-1653.
14. R.L. Kondner and J.S. Zelasko. A Hyperbolic Stress-Strain Formulation for Sands. Proc., 2nd International Pan American Conference of Soil Mechanics and Foundation Engineering, Sao Paulo, Brazil, Vol. 1, 1963, pp. 289-324.
15. C.L. Monismith, N. Ogawa, and C.R. Freeme. Permanent Deformation Characteristics of Subgrade Soils Due to Repeated Loading. TRB, Transportation Research Record 537, 1975, pp. 1-17.

Publication of this paper sponsored by Committee on Strength and Deformation Characteristics of Pavement Sections.

Abridgment

Evaluation of In Situ Elastic Moduli from Road-Rater Deflection Basin

M.C. WANG AND B.A. ANANI

This paper presents a computer method for evaluating the in situ modulus of pavement layers from road-rater deflection basins. The method that is developed on the basis of the results of a theoretical analysis uses the bitumen-structures-analysis-in-roads (BISAR) computer program and the procedure of successive approximation. The method was used to evaluate the in situ modulus of experimental pavements at the Pennsylvania Transportation Research Facility. The computed modulus values were analyzed statistically to determine the factors that most significantly influence the in situ modulus of each pavement layer. Results indicate that, for the bituminous concrete surface and base materials, the sum of pavement surface temperature and the average five-day air temperature prior to the deflection measurements is the most significant among the factors analyzed. For the subbase material, no single influential factor is identified as significant. The subgrade modulus is influenced most by the subgrade water content, as expected.

One major difficulty in response analysis of pavement structure is to determine the elastic moduli of pavement constituent layers. Two methods are currently available for modulus determination. One method is by means of laboratory testing on specimens either compacted in the laboratory or extracted from the pavement structure; the other method is by nondestructive testing on the pavement surface. Because of its relative ease in data collection in addition to the advantage of nondestruction to the pavement structure, the method of using surface-deflection basins to determine elastic modulus is preferred. Further, of the various instruments available for surface-deflection measurement, the road rater has received increased use due to its relatively high degree of mobility. For these reasons, this paper presents a method for evaluating the in situ elastic modulus from road-rater surface-deflection basins.

Table 1. Variation of surface deflection with layer modulus.

Moduli	Surface Deflections [x 10^{-7} in (lb/in^2)]			
	$\partial\delta_1$	$\partial\delta_2$	$\partial\delta_3$	$\partial\delta_4$
∂E_1	0.009 00	0.000 23	0.000 08	0.000 00
∂E_2	0.019 67	0.004 67	0.000 10	0.000 00
∂E_3	0.006 10	0.004 20	0.001 80	0.000 01
∂E_4	0.510 00	0.470 00	0.410 00	0.326 00

Note: Variations are derived by dividing the surface deflections by the moduli.

THEORETICAL CONSIDERATIONS

The majority of available solutions for evaluating elastic modulus from surface-deflection basins has been limited to two-layer pavement systems (1,2). For three-layer systems, assumptions have been made so that essentially only two modular ratios are unknown (3). Because explicit equations of surface deflection as a function of elastic modulus are available only for a maximum of three elastic layers (4), Burmister's approach (5) is used to formulate such equations for flexible pavements that contain surface, base, subbase, and subgrade.

In the formulation, the pavement is idealized as an elastic system composed of three elastic layers that overlay the elastic half space, and the traffic loading is represented by a uniform circular loading. With this axisymmetrical loading condition, the surface deflection can be determined from the equilibrium and compatibility equations. The general expression contains Airy's stress function (ϕ), which is defined as follows:

$$\phi = J_o(mr)(A_i e^{mz} - B_i e^{-mz} + C_i Z e^{mz} - D_i Z e^{-mz}) \quad (1)$$

where m is a parameter and J_o (mr) is a Bessel function of the first kind of order zero. A_i, B_i, C_i, and D_i are constants that must be chosen to satisfy the boundary conditions and the biharmonic equation $\nabla^4 \phi = 0$. The subscript i refers to the number of layers under consideration; r and z are radial and vertical coordinates.

Equation 1 indicates that there are four unknowns for each layer and, therefore, a total of 16 unknowns for a four-layer system. However, since the stresses and displacements are very small when Z approaches infinity, 2 unknowns equal zero, and the total number of unknowns becomes 14. These 14 unknowns may be solved from 14 equations that can be derived from the following boundary conditions:

1. At the top of the surface layer, the shearing stress equals zero;
2. At the top of the surface layer within the loaded area, the normal stress equals the applied pressure; and
3. At interlayer contacts, a welded bond is assumed (with this assumption, the vertical and radial displacements and vertical and shear stresses above and below the interface must be equal; thus, there are 4 equations at each interface and 12 equations altogether for the three interfaces in a four-layer system).

Details on the formulation of these equations are given by Anani (6). Anani also developed a computer program based on the method of Gaussian elimination to solve the 14 unknowns.

The general equation for the pavement surface deflection at distance r from the loading center is shown below:

$$\delta_{st}(r) = (-1.5\ qa/E_1)\int_o^\infty J_o(mr)(A_1 m^2 e^{-m} - B_1 m e^{m} - C_1 e^{-m} + D_1 e^{m})dm \quad (2)$$

In this equation, A_1, B_1, C_1, and D_1 are functions of elastic moduli and layer thicknesses. The complete functions are given elsewhere (6). As shown, the equation of surface deflection involves nonlinear terms of modulus values.

According to Equation 2, the surface deflections at different radial distances are unique. Therefore, for a four-layer system where the surface deflections at four radial distances are known, the modulus value of each individual layer can be determined theoretically. Because of the extreme complexity of the equation, however, direct solution is not possible at this time. For this reason, instead of seeking direct solutions, these equations are used to investigate the effect of changing the modulus value of one layer on the surface deflections.

SENSITIVITY ANALYSIS

Within the practical range of modulus values, the modulus of each pavement layer is assumed. To determine the rate of change of the deflection at a point [δ(r)] with respect to E_i of one layer, the modulus value is increased and also decreased by the same amount, which is approximately 0.1 percent of the original modulus value. Let E_i' and E_i'' denote the two new modulus values and δ'(r) and δ''(r) denote the corresponding surface deflections when the modulus values of other layers remain unchanged, then the rate of change of surface deflection with respect to the change in layer modulus equals

$$\partial\delta(r)/\partial E_i = [\delta''(r) - \delta'(r)]/(E_i'' - E_i') \quad (3)$$

The analysis is made for a flexible pavement that has layer thicknesses of 1.5, 8, and 8 in for the surface, base, and subbase courses, respectively. The modulus values used are 300 000, 500 000, 45 000, and 30 000 lbf/in^2, and the Poissons' ratios are 0.35, 0.35, 0.40, and 0.45 for the surface, base, subbase, and subgrade materials, respectively. Surface deflections are computed at four locations: 0, 1, 2, and 3 ft from the center of a circular load. A uniform pressure of 13.0 lbf/in^2 is used. These distances and pressures correspond to the conditions used in the road-rater deflection measurement.

Table 1 summarizes the results of analysis. As indicated, the rate of change of subgrade modulus has the most-pronounced effect on the deflection basin. The effect of change of surface and base moduli on the surface deflection appears to be noticeable only at distances 0 and 1 ft from the loading center. The deflection at the furthermost point (3 ft from the loading center) seems to be affected solely by the change in the subgrade modulus. According to these results of analysis, the surface-deflection basin can be expressed as a function of elastic modulus as follows:

$$\delta_1 = f_1(E_1, E_2, E_3, E_4) \quad (4)$$

$$\delta_2 = f_2(E_1, E_2, E_3, E_4) \quad (5)$$

$$\delta_3 \simeq f_3(E_3, E_4) \quad (6)$$

$$\delta_4 \simeq f_4(E_4) \quad (7)$$

The last two approximate expressions provide a reasonable degree of accuracy for the range of conditions analyzed. Thus, according to Equation 7, there is only one value of E_4 associated with a deflection value δ_4. Once E_4 is obtained, the unique value of E_3 can be determined from Equation

Table 2. Results of modulus evaluation for section 2.

E_1 (lb/in^2)	E_2 (lb/in^2)	E_3 (lb/in^2)	E_4 (lb/in^2)	RRD1 (10^{-6} in)	RRD2 (10^{-6} in)	RRD3 (10^{-6} in)	RRD4 (10^{-6} in)	EAL	ST (°F)	AT (°F)	MC (%)
693 418	860 132	45 803	41 340	324	231	206	143	7 560	61	43	18.1
320 190	486 364	47 350	32 150	608	416	238	117	569 510	109	73	18.8
330 513	584 769	42 165	32 163	542	382	226	138	642 812	110	80	18.8
392 574	792 560	36 861	34 390	472	345	214	117	733 739	80	75	19.4
890 135	1 205 347	47 485	43 175	354	265	198	122	810 241	33	45	17.9
860 337	913 111	32 758	20 470	331	272	202	151	914 134	48	41	20.2
840 947	810 543	36 250	17 831	393	313	223	163	1 031 520	54	37	21.4
390 349	547 584	31 676	28 964	531	336	221	156	1 082 450	89	64	19.1
943 650	870 569	39 596	25 640	455	365	262	196	1 259 840	47	35	19.7
830 930	792 681	40 855	24 765	416	358	231	162	1 366 250	54	37	21.0
717 537	825 756	43 564	25 973	397	332	220	170	1 423 750	40	54	20.7
494 637	603 568	49 137	22 623	425	343	211	179	1 487 650	85	60	19.2
946 567	1 103 765	36 784	22 259	568	409	295	177	1 700 660	34	45	20.0
538 027	798 098	41 422	33 623	531	413	337	220	1 749 950	43	54	21.0
354 930	556 960	34 450	35 360	517	377	227	118	1 959 520	93	76	18.8

6. The determination of unique values of E_1 and E_2 is not as simple because both δ_1 and δ_2 can vary with both moduli. In this study, in order to ensure that the solution for E_1 and E_2 is reasonable, a ratio of E_1/E_2 of 0.7 is used; this ratio is determined from laboratory resilient-modulus testing on core samples.

METHOD OF EVALUATION

The method developed requires the use of the bitumen-structures-analysis-in-roads (BISAR) computer program and the procedure of successive approximation. As the first step in this method, a set of initial values of the modulus is assumed. By using the BISAR computer program, the deflection values δ_1, δ_2, δ_3, and δ_4, which correspond to the assumed modulus values, are calculated. These calculated deflections are compared with the deflections obtained from the four geophones of a road rater, designated here as RRD1, RRD2, RRD3, and RRD4, and the assumed modulus values are corrected.

The correction begins from the subgrade modulus (E_4). To ensure a gradual convergence and also to avoid a drastic correction that might greatly influence the other modulus values, only one-half of the discrepancy is adjusted. Thus, the newly assumed value of E_4 is

$$E_{4_{new}} = E_{4_{old}} \times [(RRD4 + \delta 4)/2]/RRD4 \quad (8)$$

With this new E_4 value and the previously assumed modulus values for other layers, a new set of δ values are calculated. By using the newly computed values of δ, a procedure similar to that described above is followed to adjust the subbase modulus (E_3). The new E_3 value is computed from the previous value by using the following equation:

$$E_{3_{new}} = E_{3_{old}} \times [(RRD3 + \delta 3)/2]/RRD3 \quad (9)$$

Then, the deflection values are computed for the new E_3 and previous E_1, E_2, and E_4 values. By using these computed deflection values, the base-course modulus (E_2) is adjusted as follows:

$$E_{2_{new}} = E_{2_{old}} \times [(RRD2 + \delta 2)/2]/RRD2 \quad (10)$$

After the new set of deflections is calculated, the surface modulus (E_1) is corrected by using the equation below:

$$E_{1_{new}} = E_{1_{old}} \times [(RRD1 + \delta 1)/2]/RRD1 \quad (11)$$

Thus, one complete iteration has been made where new modulus values have been generated. The second iteration begins from the correction of the subgrade E_4 by following the same procedure. This iteration process is repeated until the differences between the calculated and measured deflections for all four sensors (geophones) are within the specified tolerance. A 5.0 percent error is considered allowable for δ_1; however, a 1.0 percent error is the maximum allowed for the other deflections. This difference in the allowable limits is necessary because more iterations are needed to converge on δ_1 than on others. In general, it takes only about 4 iterations for δ_4 and as many as 20 iterations for δ_1 to converge the computed deflections to the measured deflections.

Note that since there are only four geophone readings in a road-rater deflection basin, the procedure is valid only for a maximum of four-layer systems. However, the procedure can be easily adapted for elastic systems that have greater numbers of layers if more sensor readings for a deflection basin are available.

IN SITU MODULUS

The in situ modulus values of experimental pavement at the Pennsylvania Transportation Research Facility are evaluated by using the preceding procedure; the results of modulus evaluation for section 2 are summarized in Table 2. Included with the modulus values are road-rater deflections, surface temperatures (ST), five-day average air temperatures prior to deflection measurements (AT), subgrade moisture contents (MC), and the equivalent 18-kip single-axle loads (EAL). This pavement section has a 2.5-in dense-graded, hot-mixed bituminous concrete surface, 6-in bituminous concrete base, 8-in crushed limestone subbase, and silty clay subgrade. The deflection basins are obtained by using a model-400 road rater operated at 25 H_Z vibration frequency. The pavement section is 220 ft long and the sites of deflection measurements are marked on the pavement surface 25 ft apart. The deflection readings are averaged for the test section for each particular date.

The modulus data for other test pavements are documented in a research report (7). Also included in the report are the results of statistical analyses for the variation of the modulus values with various influential factors, such as air and pavement temperatures, subgrade moisture, EAL, layer thickness, and others. Results of the analyses indicate that both the surface modulus and the base modulus are most influenced by the total temperature, which is the sum of the pavement surface temperature and the average five-day air temperature. As expected, both modulus values decrease

with an increase in total temperature. The subgrade modulus is only affected by the subgrade moisture content; the higher the water content, the lower the subgrade modulus. For the subbase modulus, no single factor can be considered as significant, namely, the subbase modulus remains almost constant throughout the test facility and the testing period.

SUMMARY

Based on the results of a theoretical analysis, a method for evaluating the in situ moduli of pavement constituent layers from road-rater deflection basins was developed. By using this method, the moduli of pavement layers at the Pennsylvania Transportation Research Facility were evaluated.

ACKNOWLEDGMENT

This study is a part of the research project entitled A Study of Flexible Pavement Base Courses and Overlay Design, sponsored by the Pennsylvania Department of Transportation in cooperation with the Federal Highway Administration. Their support is gratefully acknowledged. W.P. Kilareski, R.P. Anderson, and J. Karundeng assisted in collecting and reducing field data. The contents of this paper reflect our views and do not necessarily reflect the official views of the Pennsylvania Department of Transportation or the Federal Highway Administration.

REFERENCES

1. F.H. Scrivner, C.H. Michalak, W.M. Moore, and H.Y. Fang. Calculation of the Elastic Moduli of a Two-Layer Pavement System from Measured Surface Deflections. HRB, Highway Research Record 431, 1973, pp. 12-24.
2. G. Swift. Graphical Technique for Determining the Elastic Moduli of a Two-Layered Structure from Measured Surface Deflections. HRB, Highway Research Record 431, 1973, pp. 50-54.
3. R.A. Jimenez. Pavement-Layer Modular Ratios from Dynaflect Deflections. TRB, Transportation Research Record 671, 1978, pp. 23-28.
4. F. Moavenzadeh and J.E. Ashton. Analysis of Stresses and Displacements in a Three-Layer Viscoelastic System. Department of Civil Engineering, Massachusetts Institute of Technology, Cambridge, Research Rept. R67-31, 1967.
5. D.M. Burmister. The General Theory of Stresses and Displacements in Layered Soil Systems I. Journal of Applied Physics, Vol. 16, 1945.
6. B.A. Anani. An Evaluation of In-Situ Elastic Moduli from Surface Deflection Basins of Multilayer Flexible Pavements. Department of Civil Engineering, Pennsylvania State Univ., University Park, Ph.D. dissertation, Nov. 1979.
7. B.A. Anani and M.C. Wang. An Evaluation of In-Situ Elastic Moduli. Pennsylvania Transportation Institute, Pennsylvania State Univ., University Park, Rept. PTI 7923, Nov. 1979.

Publication of this paper sponsored by Committee on Strength and Deformation Characteristics of Pavement Sections.

Fabric Use in Low-Deformation Transportation Support Systems

M. R. THOMPSON AND L. RAAD

The feasibility of using fabrics in the construction or rehabilitation of conventional transportation support systems such as secondary roads or track beds was considered. Structural improvement concepts were analyzed. Several theoretical behavior models (ILLI-PAVE, LSTRN3, BISAR, and a simplified confinement model) were used in the structural analyses of soil-fabric-aggregate (SFA) systems. Structural improvement effects, as evidenced by ILLI-PAVE, calculated vertical stress distributions, and vertical deflections in a conventional SFA system are not achieved, thus previous experimental data are confirmed. However, BISAR structural analyses of a typical SFA system indicated the beneficial effects of no slippage conditions at the aggregate-subgrade interface. A simplified confinement model indicated that, if significant permanent deformation is developed in an SFA system, a substantial percentage increase in confinement can be developed. Proposed SFA behavior mechanisms indicated that a stage construction sequence for low-traffic-volume roads and track systems provided for use of the full potential (separation and structural improvement) of fabrics in SFA systems.

Laboratory studies and field performance data have shown that soil-fabric-aggregate (SFA) systems are effective for soft soil (large rut-depth development) applications. Equivalent performance (SFA - conventional aggregate layer construction) can be achieved with a reduced aggregate thickness if a fabric is installed at the soil-aggregate interface.

The success of SFA systems for soft soil applications has led to the development of increasing interest in the potential of fabric use in conventional transportation support systems (e.g., railroads, highway pavements, and airfield pavements). The major difference between conventional transportation support and SFA systems constructed over soft soils is the magnitude of tolerable levels of rut development and surface deflection. Permissible levels of rutting and resilient deflection for conventional transportation support systems are on the order of 1.5 and 0.500 in (38 and 12.7 mm), respectively. Rut depths on the order of 3-5 in (76-127 mm) and resilient deflections in excess of 1 in (25.4 mm) are commonly incurred in SFA systems on soft soils.

The influence of fabric on the structural behavior and performance of low-deformation (SFA) systems is not well established. The purpose of this paper is to investigate potential mechanisms of improvement and thereby determine the feasibility of using fabrics in the construction or rehabilitation of conventional transportation support systems such as primary and secondary roads and trackbeds.

EFFECTS OF STRUCTURAL IMPROVEMENT

Fabrics are thin and exhibit resistance to applied

tensile forces but little resistance to compressive forces. To simulate this structural behavior, the fabric should be treated as an element that can carry tension but no compression.

Fabric stiffness is defined as the force required to produce a unit displacement. If the given fabric is replaced by a transformed section of the same stiffness, the modulus of the transformed section is given by

$$E_E = E_F T_F / T_E \quad (1)$$

where E_F and T_F are the modulus and thickness of original fabric and E_E and T_E are the modulus and thickness of the transformed section. The transformed section concept was used (1) to demonstrate how the responses of a soil-fabric system are affected if the original fabric is replaced by an equivalent transformed section. An elastic-based finite-element computer model (LSTRN 3) (2) that incorporates truss type elements (elements can carry tension but not compression) was used. Results of analysis indicate that lateral strains in the fabric, vertical subgrade stresses and strains, and surface deflections are not affected if the transformed section has a thickness that does not exceed 12 times the thickness of the original fabric.

The transformed section concept was used in available nonlinear finite element (ILLI-PAVE) and linear elastic (BISAR) programs to analyze SFA systems.

Resilient Behavior Considerations

The potential effect of a fabric layer on a SFA system was considered by using ILLI-PAVE (a stress-dependent finite-element model developed at the University of Illinois). A typical low-traffic-volume road section [8 in (203 mm) of crushed stone] and a very soft subgrade were assumed. The very soft subgrade condition accents any beneficial effects of the fabric (increased fabric tensile forces are developed at high deflections). ILLI-PAVE assumes full friction (no slip) at all material interfaces. Fabric properties [modulus = 30 lb/1 percent (0.13 kN/1 percent), Poisson's ratio = 0.2] were used. Subgrade and granular resilient properties are shown in Figure 1. Subgrade shear strength (cohesion) was 3 lbf/in² (20.7 kPa). A ϕ angle of 40° was assumed for the granular material. Pavement loading was a 9-kip (40-kN) wheel load and 80 lbf/in² (551 kPa) tire pressure.

Results of analysis show that there is no fabric effect on vertical stress distribution, failure zones in the granular base, and deflection pattern (Figure 2) in the pavement section.

Previous experimental studies (3-6) and data from this study have demonstrated that the resilient behavior of SFA systems is not significantly influenced by the presence of a fabric. The ILLI-PAVE data confirm that finding. Note that the surface deflection of the pavement was only 0.070 in (1.78 mm). Such a small deflection is not sufficient to mobilize the fabric tensile reinforcement effect.

Slippage Considerations

The BISAR elastic layered program can accommodate slippage between layers. The crushed stone-fabric section was analyzed for no slippage and complete slippage. Comparative deflection data for the two conditions are shown in Figure 3.

Slippage at the interface between the granular base and subgrade increases the resilient deformations of the pavement, which would hasten its rate of deterioration. Use of fabric at the interface should reduce the slippage effect and therefore improve performance. Reduction of resilient deflections is most pronounced in the subgrade and could be as much as 30 percent.

Figure 1. Resilient properties of subgrade and granular materials.

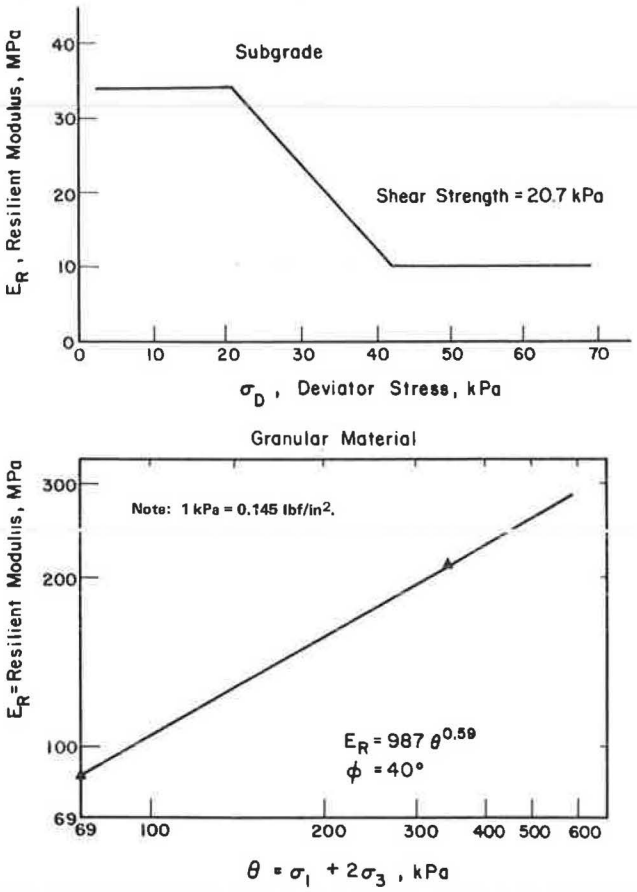

Figure 2. Fabric effect on vertical deflections (ILLI-PAVE model).

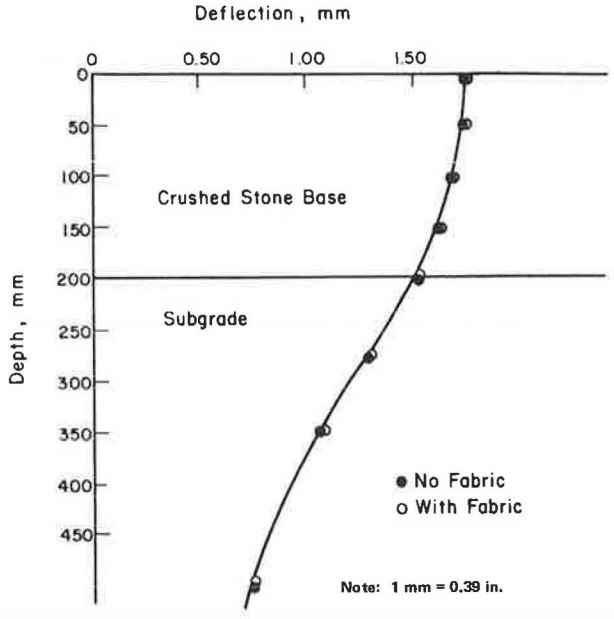

Figure 3. Effect of slippage on vertical deformations (BISAR model).

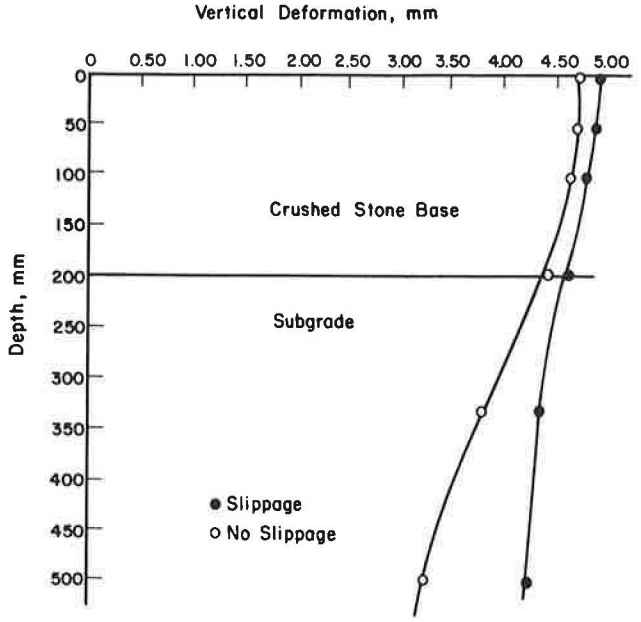

Figure 4. Increased confinement-effect model.

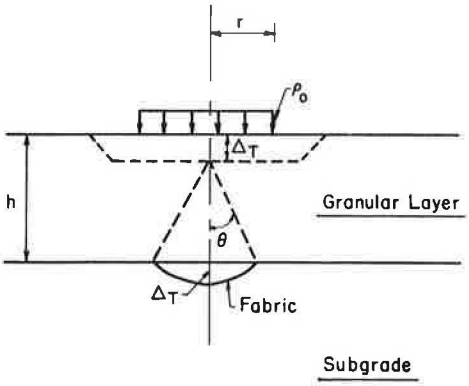

Δ_T = Total Deformation = $\Delta_p + \Delta_r$
Δ_p = Permanent Deformation
Δ_r = Resilient Deformation

Increased Confinement Considerations

As the SFA system deforms, increased lateral confining pressures develop due to the horizontal component of the normal stresses at the fabric-subgrade interface. If the fabric-subgrade interface is level, no horizontal component of the normal stress is mobilized.

Assume that the aggregate layer is incompressible and the deformed shape of the fabric is approximated by a circular arc, as shown in Figure 4. If we ignore the confining effect of shear stresses and tensile stresses in the fabric (they act in opposite directions), the following can be demonstrated:

$$\Delta\sigma/\sigma = [P_o(r)/K_s K_o h\,(h + r)]\,(1 + \alpha) \quad (2)$$

where

$$\alpha = \Delta_p/\Delta_r \quad (3)$$

P_o = applied surface pressure;
r = radius of loaded area;

Figure 5. Increase in confinement for SFA systems.

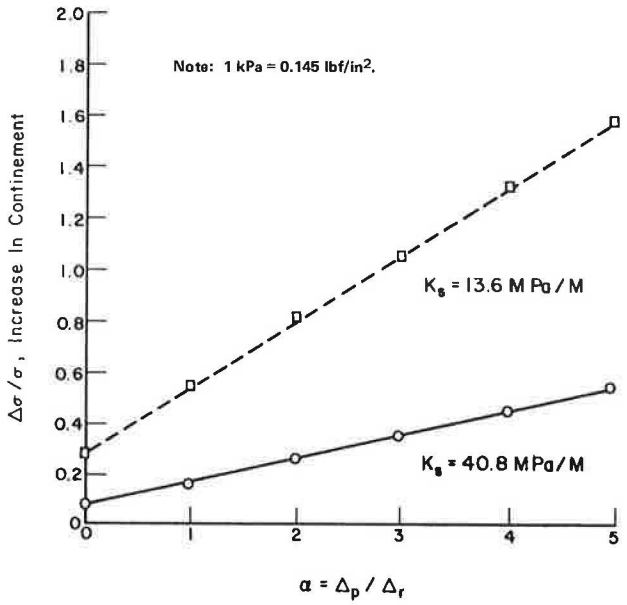

K_S = modulus of subgrade reaction;
k_o = coefficient of earth pressure at rest;
h = thickness of granular layer;
$\Delta\sigma/\sigma$ = increase in confinement at interface due to deformation of fabric, expressed in terms of original confinement (σ) before fabric deforms;
Δ_p = permanent deformation; and
Δ_r = resilient deformation.

For example, for K_S = 50 (lbf/in²)/in (13.5 MPa/m), h = 6 in (152 mm), r = 6 in (152 mm), P_o = 80 lbf/in² (551 kPa), and K_o = 0.5. Then, $\Delta\sigma/\sigma = 0.27\,(1 + \alpha)$.

For K_S = 150 (lbf/in²)/in (40.7 MPa/m). Then $\Delta\alpha/\sigma = 0.09\,(1 + \alpha)$.

$\Delta\sigma/\sigma$ relations represented by the last two calculations are shown in Figure 5. Note that $\Delta\sigma/\sigma$ improvements on the order of 80 percent are realized for soft subgrade conditions and α values (Δ_p/Δ_r) of approximately two. It is apparent that the increased confinement effects are accentuated for the soft subgrade condition.

Small increases in confining pressure significantly improve the shear strength, stiffness, and permanent deformation behavior of granular materials. The improved characteristics of the granular material should contribute to better SFA system performance.

PERFORMANCE CONSIDERATIONS

Although no significant improvement is achieved for low-deformation SFA systems, larger deformations [greater than 0.5 in (12 mm)] due to weakened subgrade conditions or load repetitions could mobilize the tensile reinforcement in the fabric and reduce the subgrade stresses (7). Moreover, the development of larger deformations could increase the confinement of the base, as described earlier in this paper. Such behavior mechanisms in terms of increased tensile reinforcement and base confinement indicate the validity of a stage-construction concept for SFA systems. The concept can be used for low-traffic-volume roads and track systems. The SFA system for low-traffic-volume roads is not immediately surfaced.

Following the first period of weak subgrade support and after rut development has stabilized, the SFA system surface is graded (with or without the addition of aggregate) and smoothness is restored. The SFA system is then surfaced (probably with a surface treatment). If necessary, the SFA system could be surfaced initially and then resurfaced following the period of development of rut depth.

A similar approach is possible for applications of track systems. Following initial development of permanent deformation in the ballast-subgrade system, the track could be resurfaced, thus a desirable level of track geometry could be restored. Subsequent development of permanent deformation would be minimized because of the structural improvement affected by the fabric.

The construction procedure in stages permits the use of the full potential of the fabric (separation and structural improvement). Note that to maximize structural improvement effects it is necessary to develop significant permanent deformation in the fabric.

SUMMARY

Structural improvement effects, as evidenced by ILLI-PAVE-calculated vertical stress distributions and vertical deflections in a conventional SFA system, are not achieved for the small permanent deformations typically experienced, thus previous experimental data are confirmed. BISAR structural analyses of a typical SFA system indicated the beneficial effects of no-slippage conditions at the aggregate-subgrade interface (it is postulated that fabric will decrease slippage at the interface).

A simplified confinement model indicated that, if significant permanent deformation is developed in an SFA system, a substantial percentage increase in confinement can be developed. This effect is most pronounced for soft subgrade conditions.

Fabric can be used beneficially in the construction or rehabilitation of the transportation support system in many situations. The most-promising applications are unsurfaced aggregate layers (low-traffic-volume roads and track systems). We postulate that a construction procedure in stages (surface treatment of an aggregate road following the initial period of reduced subgrade support) would be feasible for low-traffic-volume roads. The concept of construction in stages also can be applied to track system problems.

ACKNOWLEDGMENT

This study was conducted by the Department of Civil Engineering, University of Illinois, at Urbana-Champaign under the sponsorship of the Celanese Fibers Marketing Company.

REFERENCES

1. M.R. Thompson and L. Raad. Fabric Utilization in Transportation Support Systems. Univ. of Illinois, Urbana-Champaign, Rept. UILU-ENG-79-2021, Dec. 1979.
2. E.L. Wilson. LSTRN3, A Computer Program for Finite Element Analysis of Plane Structures. Univ. of California, Berkeley, Jan. 1967.
3. J. Hales, J. Dowland, and E.J. Barenberg. Interim Report: Evaluation of Fabric Membrane in Pavement Systems. Univ. of Illinois, Urbana-Champaign, 1975.
4. O. Anderson. The Use of Plastic Fabrics for Pavement Protection During Frost Break. International Conference on the Use of Fabrics in Geotechnics, Paris, Vol. 1, April 20-21, 1977.
5. O. Anderson and S. Freden. The Influence of a Plastic Fabric Upon the Pavement at Frost Break. Frost I Jord, Norwegian Committee on Permafrost, Oslo, Norway, July 1977.
6. S.F. Brown, B.V. Brodrick, and J.W. Pappin. Permanent Deformation of Flexible Pavements. European Research Office, U.S. Army, London, Final Tech. Rept., June 1980.
7. T.C. Kinney. Fabric-Induced Changes in High Deformation Soil-Fabric-Aggregate Systems. Univ. of Illinois, Urbana-Champaign, Ph.D. dissertation, June 1978.

Publication of this paper sponsored by Committee on Strength and Deformation Characteristics of Pavement Sections.

New Interpretation of Plate-Bearing Tests

R. BUTTERFIELD AND M. GEORGIADIS

A new procedure for interpreting plate-bearing tests is proposed that allows the complete nonlinear pressure versus displacement curve to be described in terms of stiffness parameters that are quite independent of the plate size. The nonlinear model incorporates shear springs in between the usual Winkler compression springs and requires conventional plate tests on plates of two different sizes in order to determine the two stiffness contributions. The predictive capacity of the procedure has been demonstrated by tests on both London clay and Kaolin with square plates that span an 8:1 size range as well as in situ tests from the literature. Examples are also included to illustrate its application to the analysis of soil-supported, very flexible elastic beams.

The conventional plate-bearing test, in which a rigid plate (area A) is pushed vertically into the ground at a constant rate, is a convenient way to generate information on the stiffness and load capacity of such a system. The load (Q) (or pressure, $q = Q/A$) versus displacement (w) curves obtained are usually of the form shown in Figure 1, which depicts the mean results of a series of circular plate tests on a remolded London clay bed ($\bar{w}_L$ = 65 percent; $\bar{w}_p$ = 23 percent; $\bar{w}$ = 25 ± 1 percent; and $c_u \simeq 97$ kN/m²). Each of the curves shown is, in fact, a very close, best-fit representation of the experimental results by using the empirical equation for a plate of diameter D.

$$q/q_u = Q/Q_u = 1 - \exp[-(K_o - K_f)(w/D)] + K_f(w/D) \quad (1)$$

where

$K_o = k_o D/q_u$,
$K_f = k_f D/q_u$,

Figure 1. Pressure-displacement curves for rigid plates.

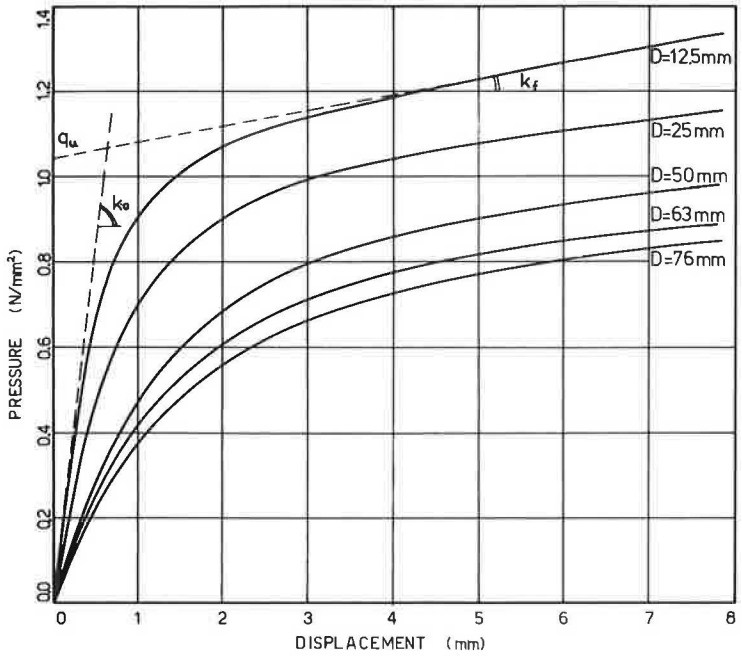

Table 1. Diameter-dependent stiffness parameters for a remolded London clay.

Item	Parameter				
	D = 12.5 mm	D = 25 mm	D = 50 mm	D = 63.5 mm	D = 76 mm
q_u (N/mm²)	1.03	0.94	0.83	0.78	0.75
k_o (N/mm³)	1.95	1.15	0.65	0.56	0.48
k_f (N/mm³)	0.04	0.026	0.018	0.014	0.012
K_o	23.7	30.6	39.2	45.6	48.6
K_f	0.49	0.69	1.08	1.14	1.22

k_o = initial stiffness,
k_f = final stiffness, and
q_u = pressure axis intercept.

The key parameters k_o, k_f, and q_u are all defined as shown in Figure 1. We have used Equation 1 in previous papers (1,2), although neither the values of q_u, k_o, and k_f nor Q_u, K_o, and K_f, which generate each best-fit curve, are constant and, as is well known, q_u, k_o, and k_f all decrease with increasing size of bearing plate (Table 1). In all the tests being discussed, the loads varied slowly enough for dynamic effects to be negligible and sufficiently rapidly for soil consolidation not to be the underlying cause of the dependence on the plate size.

That the coefficient of subgrade reaction (k_o = Q/Aw), which represents the initial, approximately linear, part of the loading curves, decreases with increasing plate size was first noted by Engesser (3). He suggested, in relation to beams (of breadth B) on elastic foundations, that an empirical equation should be used, of the form

$$k = a + (b/B) \quad (2)$$

Equation 2 is actually a compromise between the k = constant (Winkler) model and the result for a linear elastic half space [$k \propto 1/B$]. A similar empirical equation was proposed by Housel (4) for the interpretation of plate-bearing tests on cohesive soils. He introduced the concept of an edge shear contribution around the plate perimeter (P) and assumed the plate pressure (q) to consist of a base reaction component (α) and a peripheral component [$\beta(P/A)$]

$$q = \alpha + \beta(P/A) \quad (3)$$

The objective of most plate tests is to provide data that can be used to predict the response of larger footings, pavements, beams, and rafts. Although analyses can be developed to include the nonlinear behavior implicit in Equation 1 (5), the crucial problem still remains that, inevitably, the diameter of the plate used to establish the curves (Figure 1) radically affects the results obtained. As an illustration of this point, Figure 2 (1) shows the predicted load-displacement response at the midpoint of a centrally loaded elastic beam (500x63.5x3.9 mm) based on the Figure 1 plate-test data and Equation 1. The heavy line is the experimental result obtained, which shows that the correct plate size to use was D = 125 mm--about twice the breadth of the beam. This is, of course, not known a priori and is unlikely to be a useful general rule. Indeed, Georgiadis (5) found that the best-fit plate size varied with both beam breadth and thickness.

This paper presents an extension of Engesser's idea, which follows naturally from a generalization of the Winkler spring model, due to Pasternak (6), in which the simple compression springs are each interconnected by a shear spring. The Winkler stiffness (k) is thereby augmented by a shear spring (stiffness = g). We shall extend this model to include a complete nonlinear response, as in Figure 1, and show how unique, plate-diameter-independent stiffnesses can be obtained quite simply that remove, for example, the ambiguities of Figure 2.

ANALYSIS OF PLATE-BEARING TESTS

The extended Pasternak model is illustrated in Figure 3 and incorporates nonlinear shear spring coupling [stiffness $g(w_o)$] between each nonlinear compression spring [stiffness $k(w)$]. The shear springs are entirely equivalent to adding a foundation resistance proportional to the curvature of the

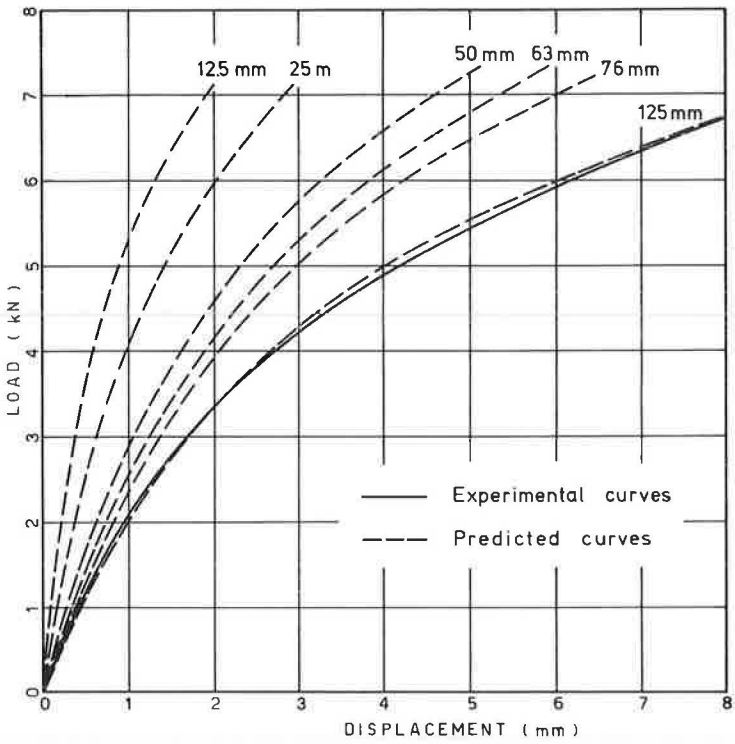

Figure 2. Center point load-displacement curves for a soil-supported flexible beam.

soil surface, which leads to a pressure-displacement relationship for the ground given by Kerr (7),

$$q = kw - g(d^2w/dx^2) \quad (4)$$

where we have written, for convenience, k = k(w) and g = g(w_o), both of which are nonlinear functions of displacement but quite independent of plate size.

By analyzing plate test results we found that g influences the displacement much less than does k and, therefore, since shear deformation is also maximum adjacent to the plate, we have adopted the assumption indicated above that g = g(wo) (i.e., that g varies with plate displacement but is otherwise constant throughout the supporting soil).

For an unloaded surface region q = 0 and, therefore, if we write p(w) ≡ kw, we have

$$p(w) = g(d^2w/dx^2) \quad (5)$$

Figure 3. Idealized foundation model.

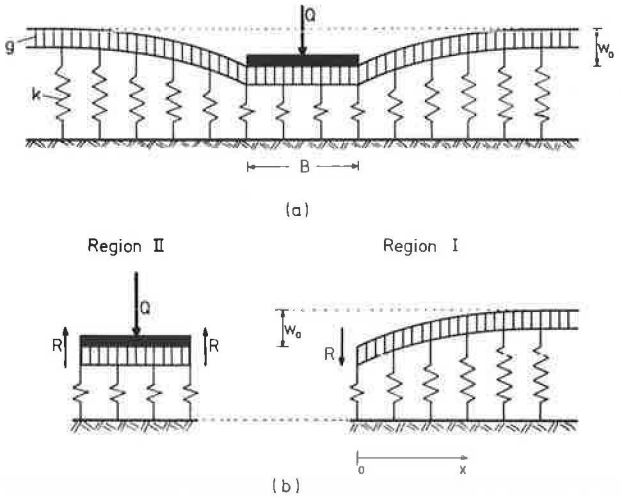

Because g is only a function of wo, it is easily established by integrating Equation 5,

$$dw/dx = \sqrt{(2/g) \int p(w) \cdot dw} \quad (6)$$

Since many practical applications of plate tests relate to rectilinear beams and foundation slabs, we consider that this provides a justification for studying square plates rather than circular ones.

Figure 3 shows a rigid square plate (B x B) supporting a total load (Q). There are four regions (such as I) surrounding it, each of which, if they deform independently, contributes a reaction R to the plate calculable from Equations 5 and 6 as

$$R = B \int_o^\infty p(w)\,dx = Bg^{0.5} \int_o^{w_o} [p(w) \cdot dw / \sqrt{2 \int p(w)\,dw}] \quad (7)$$

The soil reaction immediately under the plate (region II) is (from Equation 4) simply $kw_o \equiv p(w_o)$, hence

$$q = Q/B^2 = p(w_o) + (4g^{0.5}/B) \int_o^{w_o} [p(w) \cdot dw / \sqrt{2 \int p(w)dw}] \quad (8)$$

In the development of this equation we have ignored the effect of the four regions immediately outside the corners of the plate. Calculations of the lateral extent of the deformed soil surface, when plates are displaced up to 10 percent of their breadth, suggest that errors due to this will be very small even for 50 mm plates. Experiments bear this out and the effect will be even less for larger plates.

Although at first sight Equation 8 looks rather formidable, comparison with Equation 3 will show that they have a similar form (a term dependent on B and one that is not). Suppose, therefore, that we have results from two plate tests (side lengths B_1 and B_2) then, if we start from the unloaded state, we can rewrite Equation 8 for each plate as

$$q_1 = \alpha + \beta/B_1 \quad (9a)$$

and

$$q_2 = \alpha + \beta/B_2 \quad (9b)$$

In these equations q_1 and q_2 are the pressures that displace each plate by w_o and, since g, k, and p are functions of w_o only, α and β are identical in each of them. The simultaneous solving of the equations provides $\alpha(w_o) = p(w_o)$ and $\beta(w_o)$. If p and β are known, we can approximate the integrals in Equation 7 numerically and thereby evaluate $g(w_o)$. By repeating this procedure at successive pairs of points along the load-displacement curves we can generate a complete set of p(w) and $g(w_o)$ values. For example, the full lines in Figures 4a and 4b are the results of two plate tests (B = 100 and 50 mm) on the London clay bed mentioned previously. Pairs of points were interpreted as explained above, which resulted in the p versus w and g versus w_o curves shown in Figure 5. The first of these (Figure 5a) is of the same general form as those of Figure 1 and can be fitted very closely, by an equation similar to Equation 1.

$$p(w) = p_u\{1 - \exp[-(\kappa_o - \kappa_f)w/p_u] + \kappa_f(w/p_u)\} \quad (10)$$

with p_u, κ_o, and κ_f defined in Figure 5a, all of which are now independent of plate size. The form of g versus w_o also suggests a three-parameter exponential decay equation and

$$g(w_o) = (g_o - g_f)\exp(-\lambda w_o) + g_f \quad (11)$$

provides a close fit; g_o and g_f are defined in Figure 5b and at $w_o = 0$, $(dg/dw_o) = -\lambda(g_o - g_f)$.

Figure 4. Square plate tests on London clay.

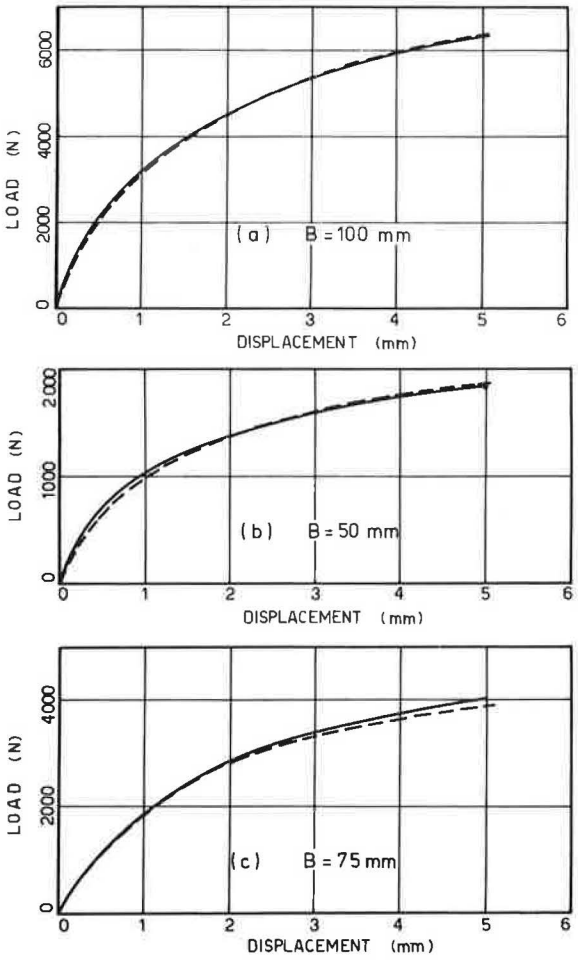

PREDICTION OF PLATE TEST RESULTS

We can now substitute Equation 10 into Equation 8, integrate the denominator, and arrive at the following equation that will predict the pressure-displacement curve for a plate of any breadth,

$$q = p + (2/B)\sqrt{(2g/p_u)}\int_0^{w_o} \left\{pdw\ \sqrt{w - [p/(\kappa_o - \kappa_f)] + [\kappa_f w/(\kappa_o - \kappa_f)] + (\kappa_f w^2/2p_u)}\right\} \quad (12)$$

The integration proceeds numerically, step by step, and generates for, say, B = 75 mm, the dashed curve shown in Figure 4c. A 75-mm plate test produced the full line that agrees very closely with the predicted result.

However, it is much more usual to need to extrapolate test results to larger plates than to interpolate between them as above. Therefore, a series of square plate tests that cover a much greater range of sizes B = 12.5-100 mm were performed on a much softer bed of Kaolin clay ($\bar{w}_L$ = 56 percent; $\bar{w}_p$ = 23 percent; $\bar{w}$ = 34 ± 1 percent; and $c_u \simeq$ 21 kN/m²). The results from the smaller plates (B = 12.5, 25 mm), Figures 6a and 6b, were used to calculate the (p - w) and (g - w_o) curves shown in Figure 7.

An interpolated prediction (B = 18 mm) is compared with a test result in Figure 6c and an extrapolated one (B = 100 mm) in Figure 6d. In all cases

Figure 5. Foundation reaction and shear stiffness curves for plates on London clay.

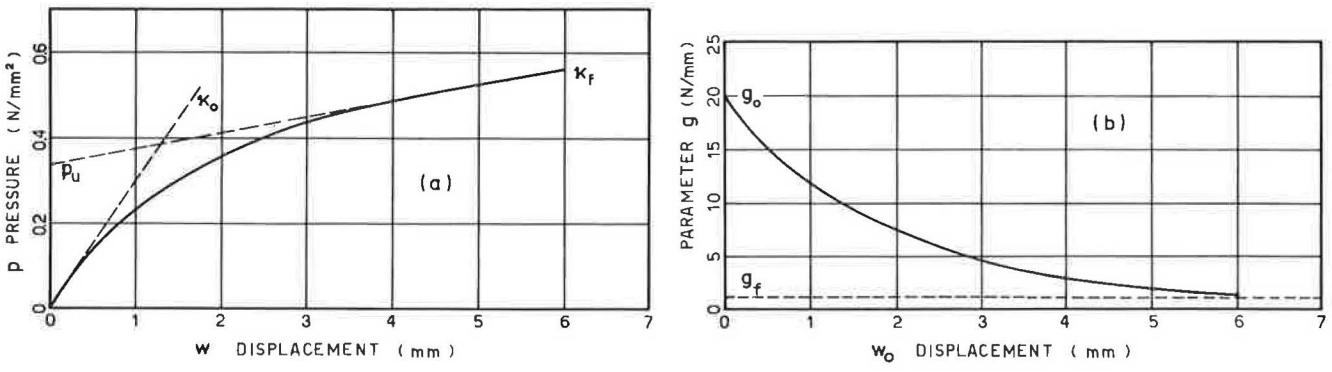

Figure 6. Square plate tests on Kaolin.

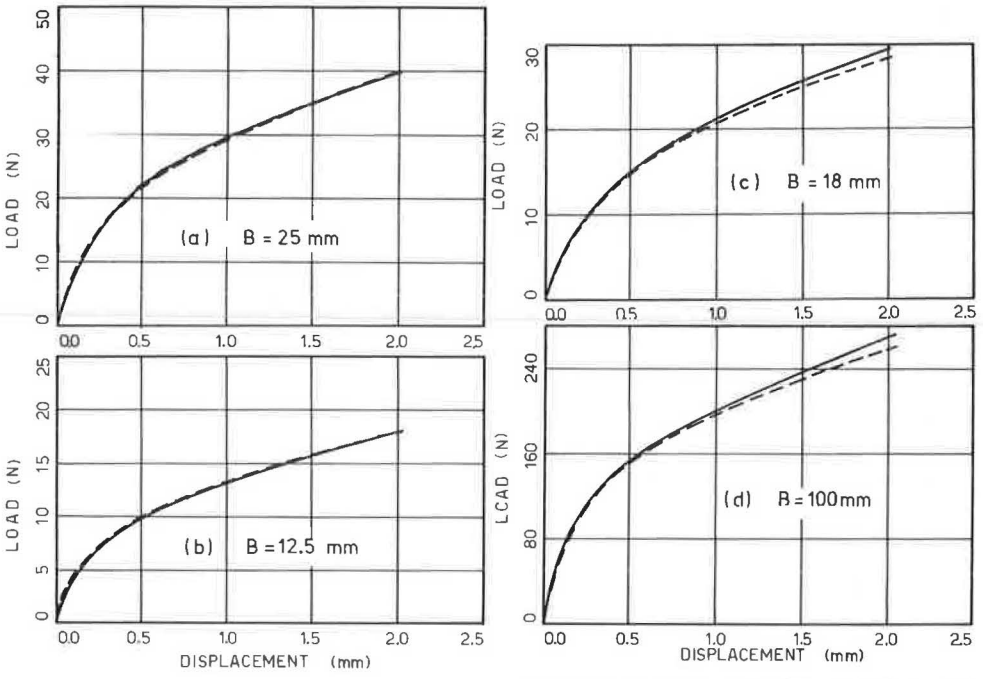

Figure 7. Foundation reaction and shear stiffness curves for plates on Kaolin.

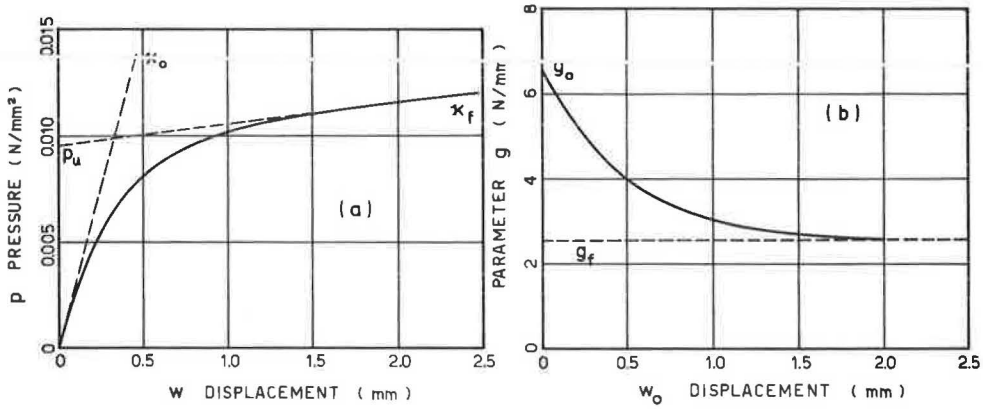

Figure 8. Interpretation of field test data.

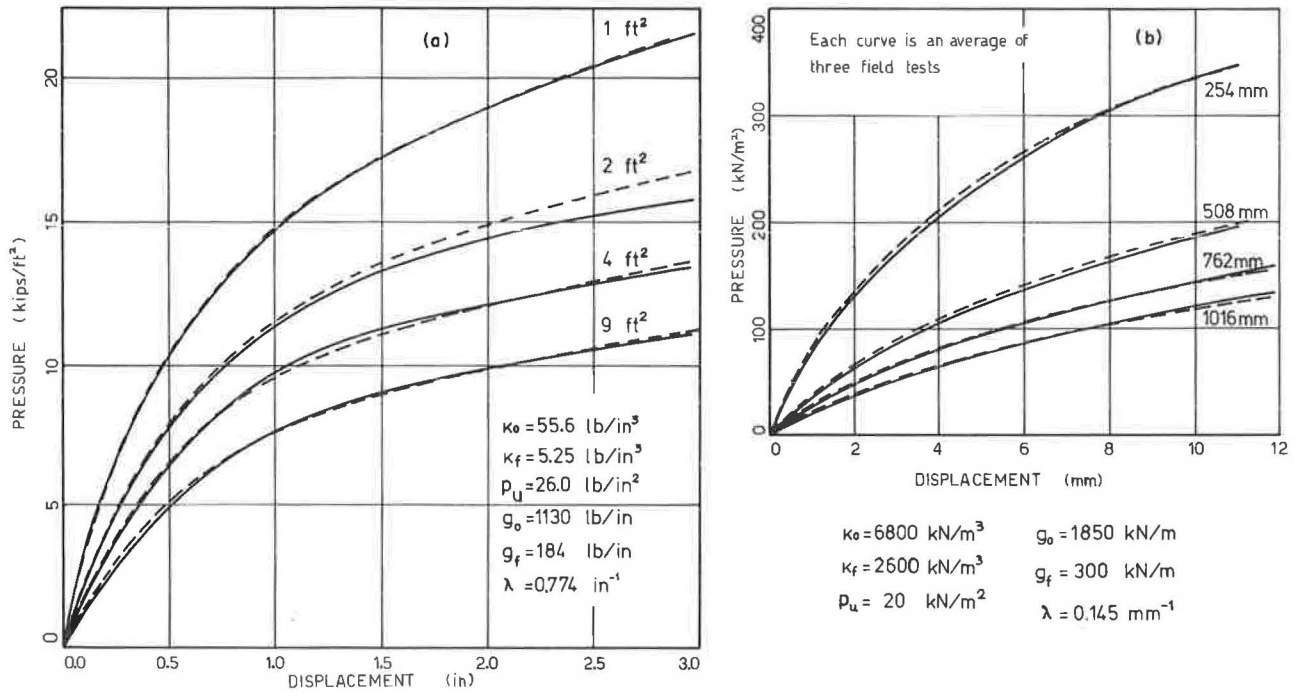

prediction and experiment agree very closely, even over an 8:1 range of plate sizes, which appears to confirm that the new interpretation procedure does establish a valid set of size-independent stiffness parameters.

Further supporting evidence is shown in Figure 8a and 8b, in each of which the full lines refer to experiments and the dashed ones to predicted curves based on two of the tests interpreted as explained previously. The results in Figure 8a are Housel's (4) tests on a plastic yellow clay and those in Figure 8b are due to Osterberg (8) who used Buckshot clay. These tests were not really continued far enough to predict the constant, final stiffness (κ_f) value, although they do show that the fitting technique can be used successfully in spite of this.

INTERPRETATION OF BEAM ON ELASTIC FOUNDATION TESTS

The work stemmed from a study of very flexible, metal, aircraft landing mats, one aspect of which was to predict the static, load-deflection characteristics of any centrally loaded component of the mat from plate-bearing test data.

A nonlinear, transfer-matrix (9) analysis of the problem was developed based on Equation 1 together with a no-tension condition across the soil-plank interface (2,5). Such an analysis can predict the mat response (Figure 2) if one is fortunate enough to guess the correct plate size to use. The new interpretation of plate tests reported here eliminates this problem, as exemplified by Figures 9 and 10, which compare experimental and analytical load-displacement curves at both central and offset points for model mats ($\bar{B}$ = 63.5 mm) of two different thicknesses (t = 3.9 and 5.9 mm) bedded on London clay. The parameters used in the analyses were those obtained from Figure 5 and the computer program was modified to include the edge shear contribution, which arises from g, along the plank boundary.

Mat tests were also performed on the Kaolin clay bed. Figures 11 and 12 show similar comparisons

Figure 9. Comparison between experiment and prediction: flexible beams on London clay (t = 3.9 mm and $\bar{B}$ = 63.5 mm).

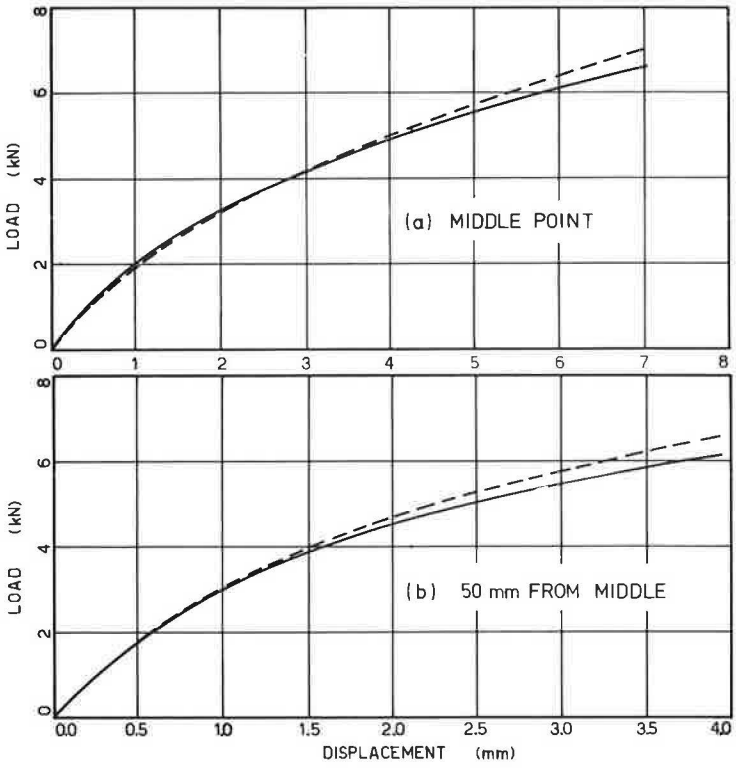

Figure 10. Comparison between experiment and prediction: flexible beams on London clay (t = 5.9 mm and $\bar{B}$ = 63.5 mm).

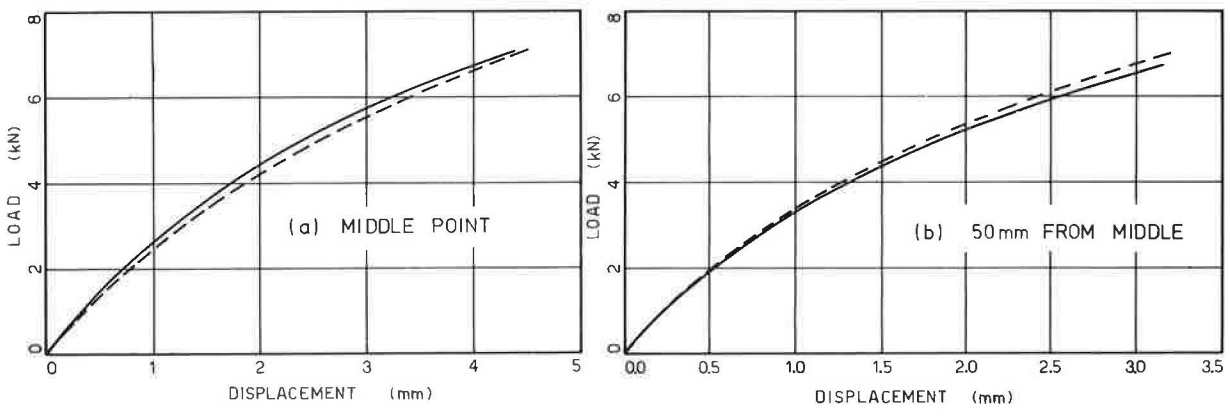

Figure 11. Comparison between experiment and prediction: flexible beams on Kaolin clay ($\bar{B}$ = 30 mm and t = 1.2 mm).

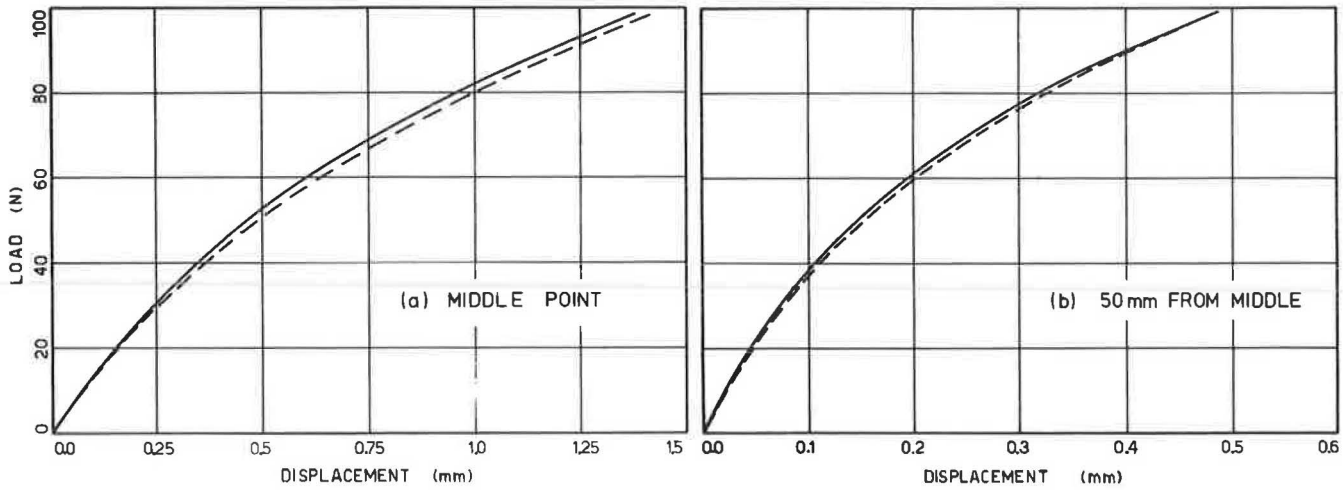

Figure 12. Comparison between experiment and prediction: flexible beams on Kaolin clay ($\bar{B}$ = 40 mm and t = 1.2 mm).

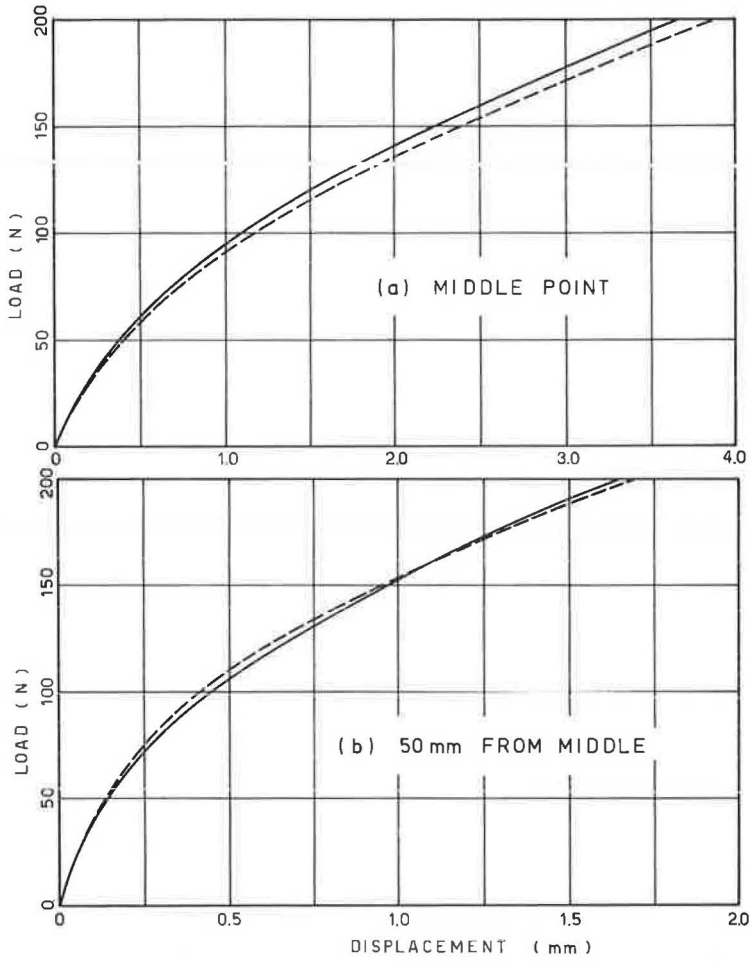

between measurement and prediction (now based on the Figure 7 parameters) for mats of different breadth ($\bar{B}$ = 30, 40 mm). In every case the predictions are remarkably good.

CONCLUDING REMARKS

The salient features of the new, general interpretation of static plate-bearing tests are as follows:

1. An extension of the use of shear-spring coupling is given, originally due to Pasternak (6), between conventional Winkler springs to develop a nonlinear model of the supporting soil;
2. The stiffness parameters introduced can be determined from conventional tests on plates of two different sizes; and
3. These parameters, six in number and summarized in Table 2, are independent of plate size and describe accurately the complete nonlinear load-displacement curve for all plates within at least an 8:1 range of dimensions.

Table 2. Size-independent stiffness parameters.

Item	Parameter	
	London Clay	Kaolin Clay
p_u (N/mm^2)	0.33	0.0095
κ_o (N/mm^3)	0.32	0.031
κ_f (N/mm^3)	0.038	0.001
g_o (N/mm)	20.0	6.6
g_f (N/mm)	1.0	2.6
λ (1/mm)	0.53	2.1

The nonlinear Winkler-spring-plus-shear-spring model has been used successfully in soil-supported flexible beam analyses, following Kerr (7), augmented by an edge shear resistance along the beam length, and also for the prediction of the response of rigid plates and footings to eccentric loads (10) and as an improvement on the conventional p-y analysis of laterally loaded piles (11).

ACKNOWLEDGMENT

We are pleased to acknowledge the support provided by the Military Vehicles and Engineering Establishment, Christchurch, for the work on landing mats and plates.

REFERENCES

1. R. Butterfield and M. Georgiadis. The Response of Model, Flexible Landing Mats to Cyclic Loading. International Symposium on Soils under Cyclic and Transient Loading, Swansea, England, 1979, pp. 697-703.
2. R. Butterfield and M. Georgiadis. Cyclic Plate Bearing Tests. Journal of Terramechanics, Vol. 17, No. 3, 1980, pp. 149-160.
3. F. Engesser. Zur Theorie des Baugraundes. Zentralblatt der Bauverwaltung, Berlin, Germany, 1893.
4. W.S. Housel. A Practical Method of the Selection of Foundations. Univ. of Michigan, Engineering Research Bull., 1929.
5. M. Georgiadis. Flexible Landing Mats on Clay. Univ. of Southampton, Southampton, England, Ph.D. thesis, 1979.
6. P.L. Pasternak. On a New Method of Analysis of an Elastic Foundation by Means of Two Foundation Constants. Gosudarstvennoe Izdatelstvo Literaturi po Stroitelstvo i Arkhitekture, Moscow, 1954.
7. A.D. Kerr. Elastic and Viscoelastic Foundation Models. Journal of Applied Mechanics, ASME, Transactions, Vol. 31, No. 3, 1964, pp. 491-498.
8. T.O. Osterberg. Discussion: Symposium on Load Testing of Bearing Capacity of Soils. ASTM, No. 79, 1948, pp. 128-148.
9. E.G. Pestel and F.A. Leckie. Matrix Methods in Elastomechanics. McGraw-Hill, New York, 1963.
10. R. Butterfield and M. Georgiadis. The Non-Linear Load Displacement Response of Eccentrically Loaded Footings. 3rd International Symposium, Soil Mechanics Foundation Engineering, Dresden, East German Democratic Republic, 1980.
11. R. Butterfield and M. Georgiadis. A Non-Linear Analysis of Laterally Loaded Piles. Division of Soil Mechanics, ASCE (forthcoming).

Publication of this paper sponsored by Committee on Pavement Condition Evaluation.

Nottingham Pavement Test Facility

S.F. BROWN AND B.V. BRODRICK

The Nottingham pavement test facility was developed for the experimental study of pavement structures under wheel loading. A description is given of its mode of operation and capabilities. It is located in a laboratory and allows pavement sections 4.8x2.4 m to be subjected to moving wheel loads up to 15 kN at contact pressures comparable with actual commercial traffic and at speeds up to 16 km/h. Electronic controls allow a lateral distribution of wheel passes while loading may be either unidirectional or bidirectional. Controlled temperature and moisture conditions can be achieved. Each pavement under test is instrumented to measure transient stress and strain. Permanent strains and surface deformations are measured at intervals during loading. Typical tests continue until 100 000 wheel passes have been applied. The main objective of the research for which the facility has been developed is the provision of data for comparison with theoretical predictions of pavement response to load as part of an effort to produce analytically based methods of pavement design.

In developing workable procedures for pavement design based on the use of theoretical concepts, data from controlled, realistic pavement tests play an important part in the validation exercise. Philosophically, we must demonstrate that theoretical models work in a controlled situation so that their use in the more variable real environment can be approached with confidence.

The pavement test facility at Nottingham grew out of an earlier dynamic plate loading and test pit facility (1) through a need to apply rolling wheel loads so that the stresses generated in the structures were representative of those expected in real pavements. The earlier work had demonstrated that linear elastic theory was valid, but the equipment could not provide data for tackling the extension of this to the prediction of pavement performance and, in particular, the development of permanent deformation.

Although some full-scale trials, such as that at Brampton (2), had produced data on rutting that was used for comparison with theoretical predictions, a laboratory-based test facility was considered more helpful in checking the details of computational procedures and for understanding the mechanisms of deformation. This is possible by use of more detailed in situ instrumentation than is generally available with full-scale trials and the exercise of greater control over materials and test conditions. Nonetheless, the full-scale trial still has a valuable role to play in extending theory to practice.

The design of the pavement test facility was, to some extent, dictated by the available space. A test pit 2.4 m on each side by 1.5-m deep was doubled in size to occupy almost the full length of

the laboratory. A linear wheel-loading device was the only practical solution, although rapid reversal of direction and quick acceleration to test speed at either end of the travel were needed. These were made possible by use of a hydraulic motor with suitable servocontrols.

A general view of the facility is given in Figure 1. It moves a loaded wheel in a straight line at a constant speed over a semifull scale pavement structure. Each test pavement contains instrumentation to measure stresses and strains and these, together with surface profile data, provide the necessary information for comparison with theoretical predictions. Wheel speed and load, temperature, direction in which the load is applied, and lateral distribution of the wheel path can all be controlled. The facility is contained in a temperature-controlled room that has insulated walls and a low, false insulated ceiling.

PAVEMENT CONSTRUCTION AND INSTRUMENTATION

Pavements may be constructed by using different materials and thicknesses although, to date, all tests have involved a single silty clay subgrade and structures either of full-depth asphalt or thin asphalt surfacing over a granular base. A roller shutter door adjacent to the facility provides access during construction and excavation of pavements.

The rectangular concrete-lined pit shown in Figure 2 was waterproofed prior to placement and compaction of the subgrade. Provision has not yet been made for control of the level of the water table. Pavement construction is arranged so that the finished surface is level with the laboratory floor. Reference levels along each side are provided by a pair of accurately positioned angle irons, which are used to take measurements of surface deformation.

Figure 3 shows a plan view and section through a typical instrument layout for one of the three-layer structures. The instruments are being installed as the pavement is constructed (3,4).

Transient stresses are measured with Nottingham pressure cells that operate on the strain-gauged diaphragm principle (5). Resilient and permanent strains are measured with Bison strain coils that consist of two, free-floating, carefully aligned, wire-wound discs (6). The spacing between these discs is converted to a voltage related to the strength of their electromagnetic coupling when one coil is energized. Displacement transducers and bonded foil-strain gauges have also been used to supplement the strain coils. Temperatures within the pavement are monitored by using copper constantan thermocouples. An automatic data acquisition system prints out the transient stresses and strains; permanent strains are read manually from the Bison control box and transverse surface profiles are determined with a profilometer (7).

Figure 1. General view of pavement test facility.

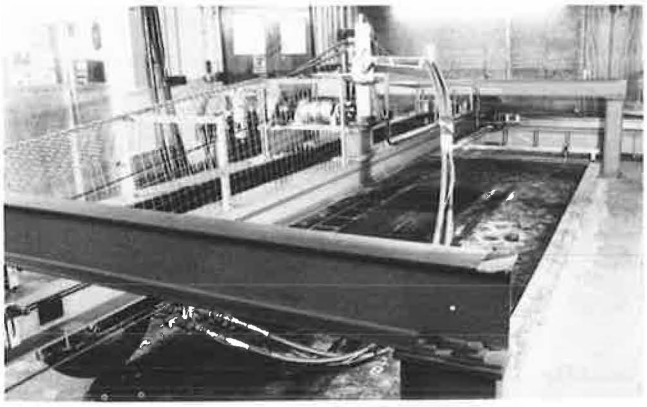

PAVEMENT TEST FACILITY

The facility can be divided into four major components:

1. A moving carriage that supports the loading wheel,
2. A framework to support and guide the carriage,
3. Drive arrangements for longitudinal and transverse movements of the carriage, and
4. Electronic control systems.

Closed-Loop Servocontrol

The load applied by the wheel together with its speed and position are all controlled by using the servohydraulic principle illustrated in Figure 4. A command signal is fed to the amplifier, and this causes a positive drive at the control, or servovalve, that operates an actuator (e.g., a ram or motor). The actuator directly or indirectly drives a transducer that supplies a feedback signal that opposes the command signal at the amplifier input.

Figure 2. Longitudinal section of test pit.

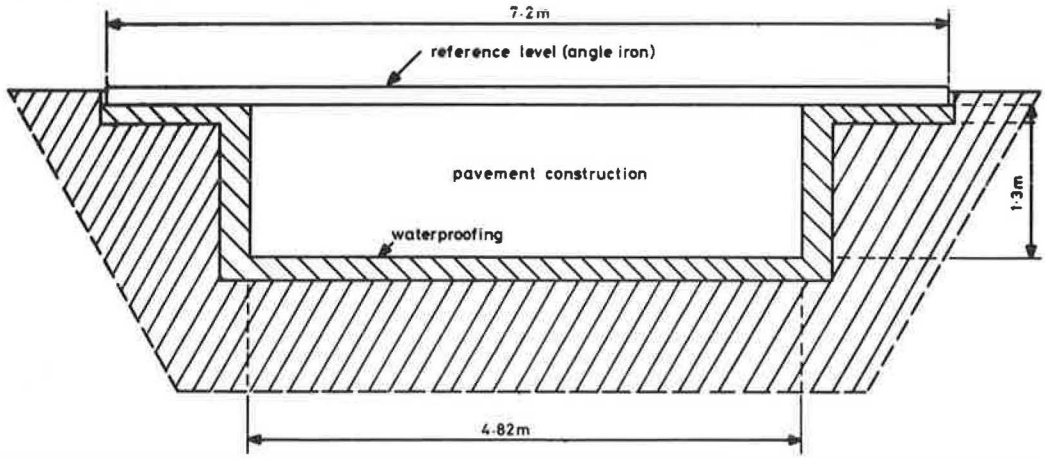

Figure 3. Typical instrumentation layout.

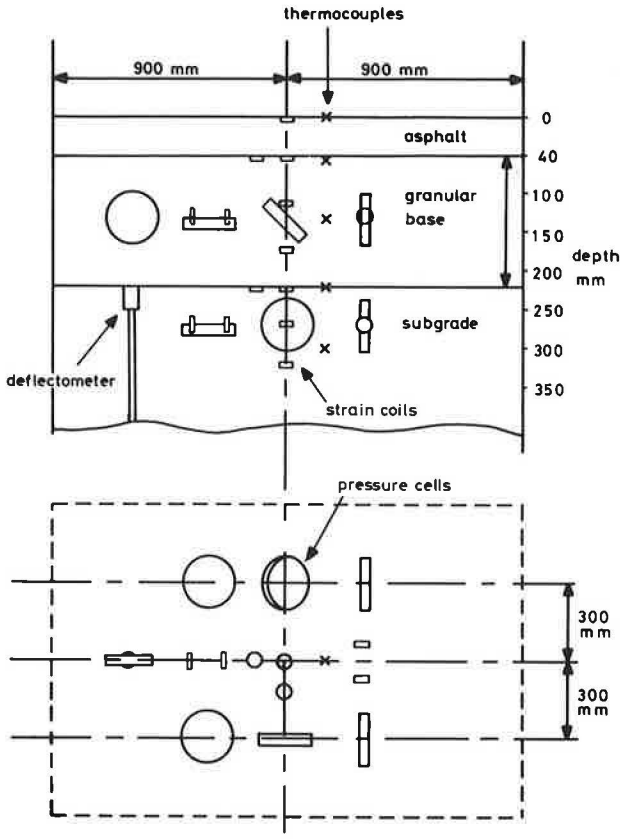

Figure 4. Basic principle for servocontrol with negative feedback.

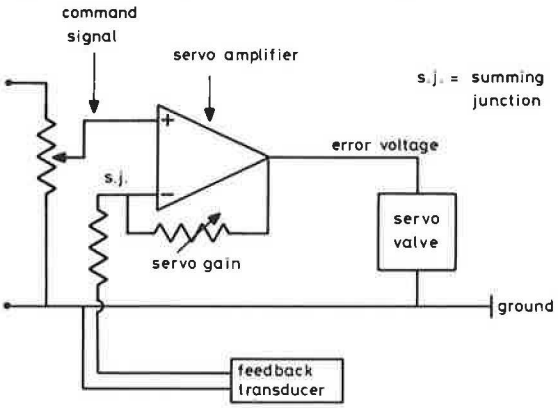

Because the amplifier has a finite gain, the two signals cannot reach equilibrium and an error voltage is produced at the output. A change in the command signal will result in a proportional error voltage that controls the movement of a spool within the valve. This connects pressurized fluid (hydraulic oil) to one of two output ports either fully to the actuator or with some flow diverted to the return line. In the case of the pavement test facility, the actuators for load control are double-acting rams, and wheel speed and direction are derived from a hydraulic motor.

Loading Carriage

The loading carriage has a rigid aluminium chassis with vertical and horizontal bearings mounted on each side that allow it to run along the reaction and guide beams. A servohydraulic loading system is built into the carriage and operates two rams that lever the wheel up or down about a pivot (Figure 5). The feedback is obtained from a strain-gauge bridge on the levers. Holes were drilled near the gauges to increase the strain at this location and hence provide larger electrical output.

The servovalve that controls the rams is served hydraulically by short rigid pipes and is protected by filters on the high and low pressure lines. An accumulator is fitted to absorb surges. The carriage has to be supplied with hydraulic power while it moves over a distance of some 7 m. This is accomplished by using flexible hoses carried by a swinging arm (Figures 1 and 5) that also supports the electrical cables. The hoses are connected to the carriage by quick-release swivel couplings.

Support Framework

The carriage runs between two 8.2-m long, 200x200 mm, I-section beams. Both beams are bolted at each end to bogies that run along rails set at right angles to the beams (see Figure 6). This arrangement allows lateral movement of the beams and carriage but is not heavy enough to resist the upthrust of the carriage when wheel load is applied to the pavement. Two transverse portal frames provide the necessary reaction (Figures 1 and 6), and these are bolted to the floor 1.2 m from each end of the beams. Small wheels are mounted on the beams so that the reaction can continue to be provided during lateral traversing of the wheel under load.

Drive System

Two main drives are necessary to fulfill the testing requirements. The first reciprocates the carriage over the pavement at a constant speed above the area that contains instruments, and the second sets the facility at various transverse positions across the pavement.

Figure 6 illustrates the system used to move the carriage longitudinally. It involves a tensioned wire rope wrapped around a centrally located grooved drum and attached at either end to the carriage via pulleys mounted on the support frame (Figure 6). The drum is driven by a hydraulic motor to which it is connected by a flexible coupling. A remote oil pump supplies pressurized oil to the motor, which is relatively small (compared with an equivalent electric motor) and has a high acceleration capability.

The control system is shown schematically in Figure 7. There is a manual control facility in which the wheel position feedback signal is used to place the wheel at any point along its travel. During testing, an automatic mode is operative and the velocity feedback from a tachogenerator is used to end the acceleration phase and then hold the wheel speed constant until deceleration is initiated by feedback from the position transducer. Reversal of direction is initiated when the velocity output approaches zero.

The wheel position is monitored by the arrangement shown in Figure 8. This involves a linear variable differential transformer (LVDT) displacement transducer attached to a screw thread driven by a pulley that is connected to the moving carriage by a long belt. A tachogenerator is axially coupled to the motor shaft (Figure 5) to provide a velocity feedback that is directly related to the speed of the wheel. The command signal in Figure 7 is trapezoidal and provides acceleration, constant velocity, and deceleration before reversal of direction. This motion is also used to move the swinging arm

Figure 5. Arrangement of wheel-loading system.

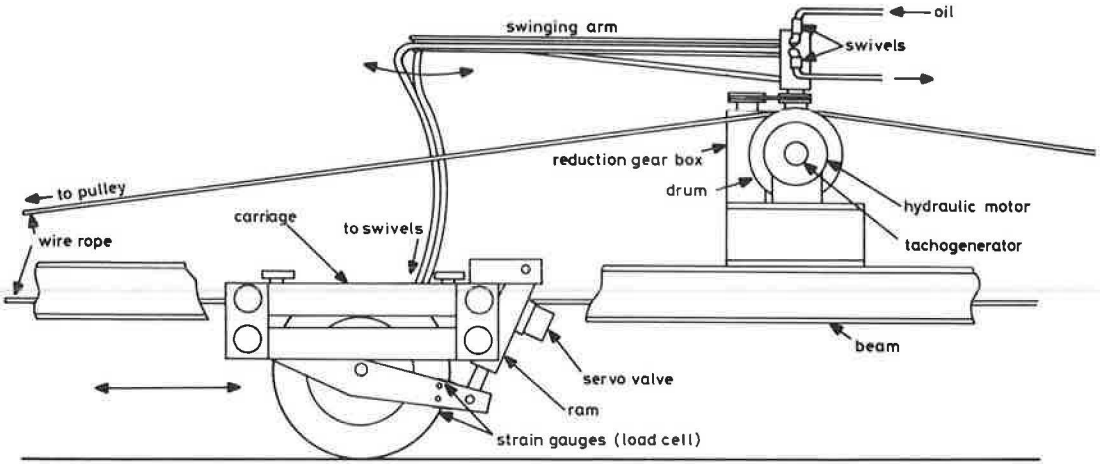

Figure 6. Side view of pavement testing facility.

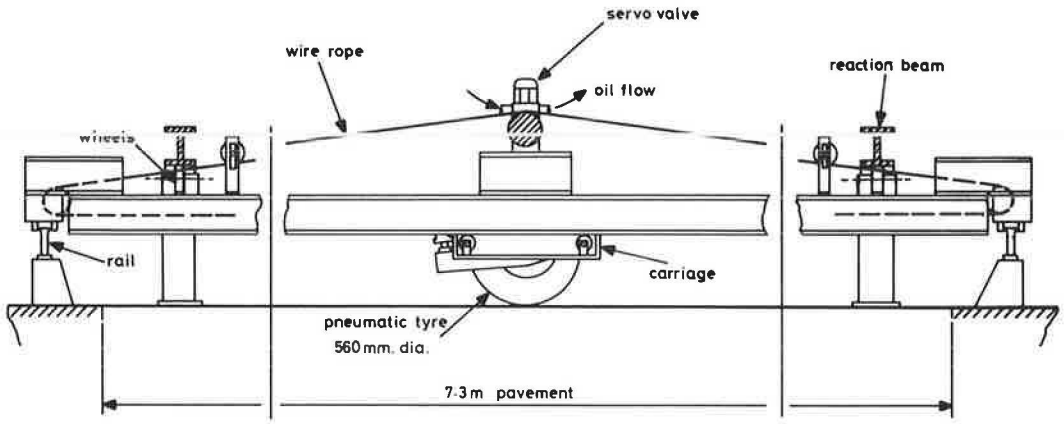

Figure 7. Carriage control system.

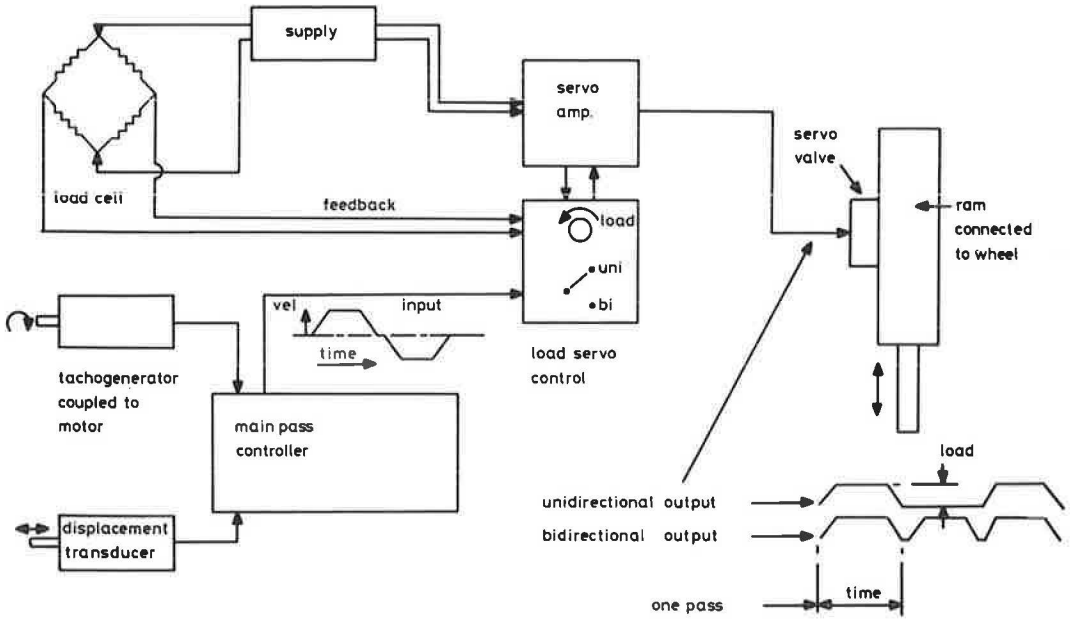

Figure 8. Wheel position feedback transducer.

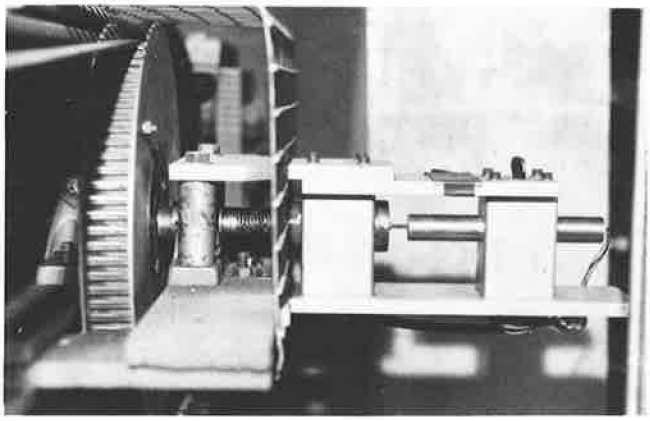

Figure 9. Swinging arm driven by gearbox coupled to grooved drum.

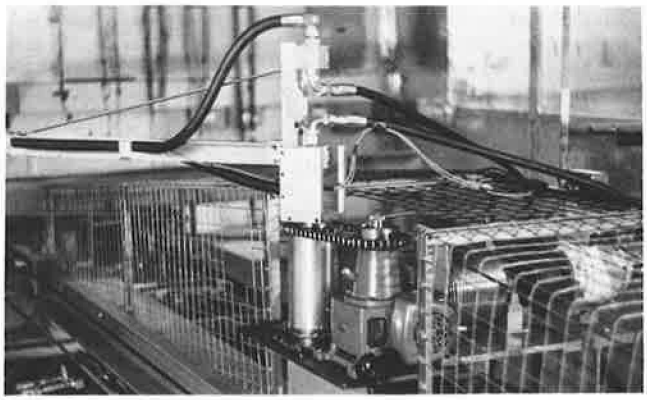

Figure 10. Traversing facility.

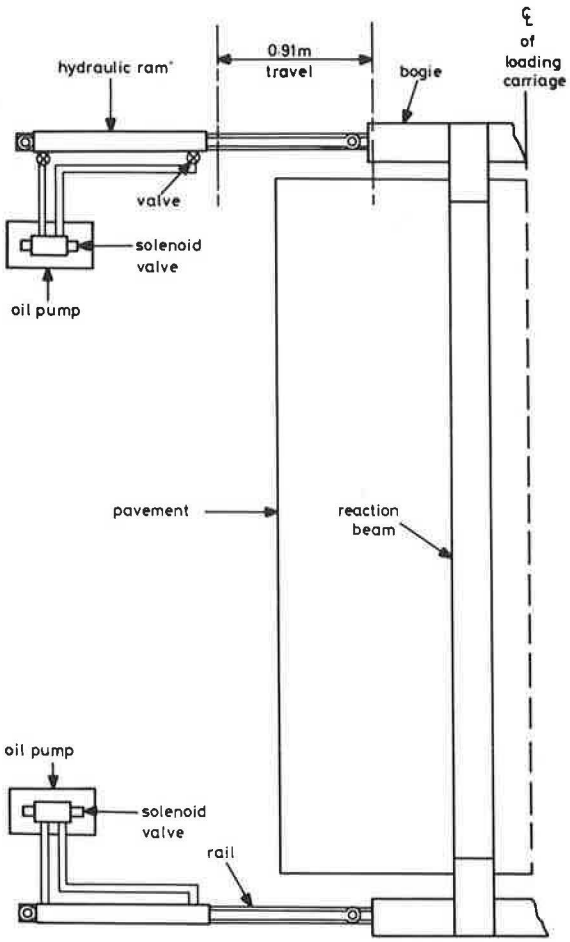

that carries the hoses and cables to the carriage in synchronization with the carriage movement. This is done by a chain drive and geared connection between the pivot for the arm and the grooved drum, as can be seen in Figure 9.

The main beams and carriage can be moved across the pavement by long stroke rams attached to the end bogies (Figure 10). A similar arrangement to the wheel position feedback transducer is used to convert the lateral position of the assembly to a voltage, but in this case a toothed wheel driven by a fixed chain is used to reduce the lateral movement of the facility to a small displacement. An oil pump was provided for each ram to avoid long lengths of connecting pipe. This results in a positive movement of the rams when the oil pumps are switched on and reduces the risk of skewed movement. When the desired position is reached (as indicated by the position transducer), the pumps are switched off. During testing the lateral movement of the test facility is fully automated and is initiated after a set number of load applications have been completed at any one position.

Electronic Control Systems

The wheel speed and load and the lateral traversing program are all controlled electronically. Wheel speed is set on a pass controller, which can be operated in either a manual or automatic mode (Figure 11). Under manual control, a position potentiometer controls the location of the wheel in situations that require static loading or when the wheel is moved to the end of the track during measurements on the pavement surface. A potentiometer is used to set the velocity level for automatic operation.

The command signal for load control follows the velocity profile so that the load increases during acceleration, is held constant when the wheel speed is constant, and then decreases during deceleration. Again, a potentiometer (Figure 11), applied under the automatic operation mode, is used to preset the load. If the load is to be applied while the wheel moves only in one direction (as happens on an actual highway), then a switch on the load servo-control is operated (see Figure 7). This negates the signal for load application in one direction.

A counter on the pass controller is connected to the traverse-control electronic system shown in Figure 11. This unit was designed to control movement of the test facility to preset positions when the count reaches a predetermined number of passes at each of nine positions. These can be selected in any order. The number of passes are dialed into each position by using thumb wheel switches. For the experiments to date, a normal distribution of load applications over a tracking width of 600 mm has been used. Each position ensures a 75-mm overlap of the tire, which has a contact patch of 150 mm width. A complete traverse generally takes 1000 passes. The total number of passes for most tests has been 100 000 and loading has been stopped after 1000, 2000, 5000, 10 000, etc. passes to facilitate permanent strain and surface deformation measurements. Full details of the electronic systems are

Figure 11. Electronic control systems.

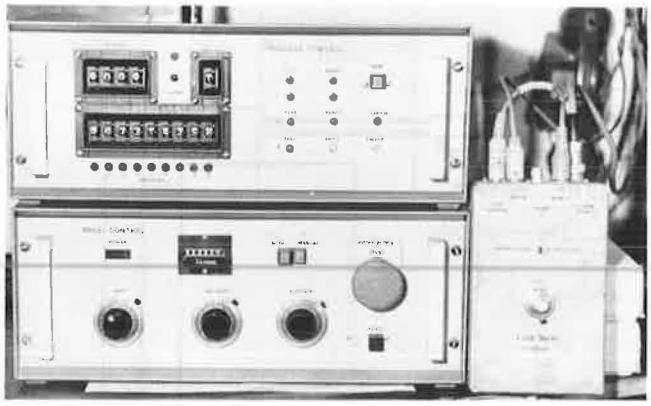

available in the relevant research reports (4,7).

SUMMARY OF SPECIFICATIONS AND PERFORMANCE

In five years, 11 pavements have been tested, and some of these have received two sets of multitrack tests together with single track tests when the traversing facility is not used. Although the maximum number of passes for each multitrack test was limited to 100 000, the test facility has completed more than 1 million passes. During this time, modifications have continually taken place, but Figure 1 shows the test facility in, what will probably be, its final form. Improvements have also been made to the data-acquisition facilities that are now largely automatic (7).

The specification of the facility is shown below:

Facility	Specification
Load range	0-15 kN
Tire pressure	570 kPa
Contact area at 10 kN	0.02 m²
Contact stress at 10 kN	500 kPa
Speed range	0-16 km/h
Length of travel	6.7 m
Length of assembly	8.2 m
Temperature range	20°-25°C

A likely development in the future will provide for an extension to the testing temperature range that is currently restricted to ambient conditions and above.

The pavement test facility has, to date, been used on two projects, the results of which have been reported elsewhere (4,7,8). Although these were primarily concerned with permanent deformation, detailed in situ measurements were also obtained of transient stress and strain for comparison with the theoretical predictions. An investigation was also carried out into the potential of fabric inclusions below granular layers in permanent road construction.

A typical pavement test takes about 10 weeks to complete. Six weeks are needed to construct and instrument the structure and four weeks to perform a test that involves 100 000 passes. To date, operations have been restricted to normal working hours, partly because of the need to interrupt loading for permanent strain and deformation measurements. However, in principle, there is no reason why 24-h operation should not be performed as the equipment has numerous safety devices. The carriage drive system is protected by a wire cage (Figure 1) and the hydraulic pump may be shut down in various ways. These include the operation of a discrepancy detector between the position transducer and the tachogenerator that operates in the event of the cable breaking, an overshoot detector that operates if the carriage velocity is too high near the end of its travel, and limit switches that are tripped if the carriage reaches the end of the support frame or the hose support arm overtravels. In addition, an emergency stop button on the pass controller (Figure 11) may be operated manually.

The Nottingham pavement test facility has been developed at low cost and provides an extremely useful means of carrying out realistic pavement experiments. The scale of the tests is large enough to provide data that can be used to validate theoretical computations of pavement response to load. Once a test is under way, it can be performed by a single operator, although other staff are needed during the construction and excavation phases. It is considered essential that data from tests of this kind are processed rapidly and that the projects involved have a theoretical and materials testing dimension to them.

ACKNOWLEDGMENT

The pavement test facility has been developed in the Department of Civil Engineering at the University of Nottingham. This development has been made possible by financial support from the European Research Office of the U.S. Army; ICI Fibres, Ltd.; and the department itself. We are grateful to R.C. Coates, our head of department, for his support; P.S. Pell, for his advice and encouragement; A. Leyko, who built much of the equipment; and to the staff of the university's electronics workshop for their services. C.A. Bell was involved with some of the early development work.

REFERENCES

1. S.F. Brown and P.S. Pell. An Experimental Investigation of the Stresses, Strains, and Deflections in a Layered Pavement Structure Subjected to Dynamic Loads. Proc., 2nd International Conference on the Structural Design of Asphalt Pavements, Ann Arbor, MI, 1967, pp. 487-504.
2. J. Morris, R.C.G. Haas, P. Reilly, and E. Hignell. Permanent Deformation in Asphalt Pavements Can Be Predicted. Proc., Assn. of Asphalt Paving Technologists, Vol. 43, 1974, pp. 41-76.
3. S.F. Brown and B.V. Brodrick. Stress and Strain Measurements in Flexible Pavements. Proc., Conference on Measurements in Civil Engineering, British Society for Strain Measurement-Institution of Civil Engineers, Newcastle, England, 1977.
4. S.F. Brown, C.A. Bell, and B.V. Brodrick. Permanent Deformation of Flexible Pavements. European Research Office, U.S. Army, Univ. of Nottingham, Nottingham, England, Research Rept., 1974.
5. S.F. Brown. State-of-the-Art Report on Field Instrumentation for Pavement Experiments. TRB, Transportation Research Record 640, 1977, pp. 13-28.
6. E.T. Selig. Soil Strain Measurement for Using Inductance Coil Method. Proc., ASTM Symposium on Performance Criteria and Monitoring for Geotechnical Construction, 1974.
7. S.F. Brown, B.V. Brodrick, and J.W. Pappin. Permanent Deformation of Flexible Pavements. European Research Office, U.S. Army, Final Rept., June 1980.
8. S.F. Brown and C.A. Bell. The Prediction of Permanent Deformation in Asphalt Pavements. Proc., Assn. of Asphalt Paving Technologists, Vol. 48, 1979, pp. 438-474.

Publication of this paper sponsored by Committee on Strength and Deformation Characteristics of Pavement Sections.

Instrumentation for the Nottingham Pavement Test Facility

S.F. BROWN AND B.V. BRODRICK

A description is given of the instrumentation that has been used successfully in the Nottingham pavement test facility to obtain in situ measurements of stress, strain, and permanent deformation in pavements subjected to moving wheel loads. The data from tests of this kind are being used to validate theoretical computations of pavement performance. Diaphragm-type earth pressure cells have been used in asphalt, unbound aggregate, and soils; details are given of installation and calibration techniques. Bison strain coils have proved useful for in situ measurements of both transient and permanent strains. An electronic unit has been developed to linearize the output from these transducers, thus making it easier to use. Electrical foil-strain gauges and post-yield gauges were also used for measurements in asphalt and on fabric inclusions, respectively. An automatic data-acquisition system allows a direct printout to be obtained of peak stresses and strains from the pulses generated by moving wheel loads. A typical layout of instruments is presented, which was designed to obtain maximum information from a short section of pavement.

Data from carefully instrumented pavement test sections are available for the continuing development of analytically based procedures for pavement design. A general review of suitable equipment has been presented by Brown (1). At Nottingham, such installations have been used in a pavement test facility (see our other paper in this Record) and in a few full-scale trials on public roads.

This paper concentrates on the work done with the pavement test facility. We describe the instruments and how they were used to obtain in situ measurements of stress and strain. The materials involved were representative of the three components of a flexible pavement--asphalt, unbound aggregate, and clay.

The instruments that have been used most extensively are the Nottingham pressure cell (2), Bison-strain coils (3), and foil-strain gauges. All these have been calibrated in or on the relevant pavement materials or checked during testing in order to quantify their influence on the local stress and strain fields. This in situ calibration follows the philosophy that the transducer output must be processed to give a measurement that is representative of the stress or strain that would have existed had the transducer not been present. Care with installation is extremely important and, if carried out incorrectly, may result in large errors. Despite the precautions necessary for accuracy, scatter is still inevitable, and the variability in material properties (either inherent or due to compaction) and the complexity of the loading effects all result in the need to take as many replicate measurements as is practical. A data-acquisition system was, therefore, developed to provide direct printout of stress and strain values. This system operates in parallel with an analogue recorder so that the shape of the output pulse can be observed. A linearizer unit was introduced for the strain coil instrument to facilitate easy direct reading of transient signals due to moving wheel loads.

INSTRUMENTS

Only the instruments used in the pavement test facility and site investigations are described. They were chosen because of previous experience in their use and their simplicity of design, which fulfilled the compromise between practicality and ideal characteristics. A stress gauge, for instance, should be robust but have a large diameter-to-thickness ratio, and a strain transducer also needs to be robust but it should not reinforce the pavement material.

Nottingham Pressure Cell

The Nottingham earth-pressure cell (2) consists of a recessed titanium disc that, in effect, is a diaphragm attached rigidly to a guard ring (Figure 1). A four-arm strain-gauge bridge is attached to the diaphragm and physically arranged and connected to reduce cross sensitivity and compensate for temperature. A lid is riveted in place to form a cavity that is partly filled with silicon rubber and a cable entry is sealed into the side of the cell body. The instrument can be either alternating current (AC)- or direct current (DC)-powered and is suitable for transient or short-term stress measurements. Its characteristics have been well documented elsewhere (2,4).

Strain Coils

The development of strain coils for in situ measurements was described by Selig and Grangaard (3) and Selig (5). The technique consists of a pair of wire-wound discs, which can be obtained in various sizes (Figure 2) and installed either in a coaxial or coplanar alignment and are connected to a Bison-soil-strain-gauge instrument. An AC signal is supplied to one coil and an electromagnetic coupling is developed with the other coil. The strength of this coupling is related to the spacing between the coils in a nonlinear way and is converted to a voltage by the Bison instrument. When balanced by means of phase and amplitude potentiometers, a reading is obtained that can be interpreted as the gauge length. Any transient change from this gauge length can be monitored on a suitable recorder and resilient strain can be calculated. Long-term changes in gauge length can be evaluated from a curve that relates coil spacing to amplitude dial reading in order to determine permanent strain values. A calibration and sensitivity control can be used to produce a signal on a recorder of a known strain over the spacing range, which is approximately 1-4 diameters.

Strain Gauges

Strain gauges are simply wire or foil grids on a thin backing that can be attached to any structural component subjected to strains within the range of the gauge. In the pavement field, they are usually limited to use on bituminous materials, particularly in the tensile zone at the bottom of the layer (1). Carrier blocks cut from sections of the asphalt mix may be placed within the layer or a thin sandwich that contains the gauge can also be used. In a situation where high initial strains may be expected during compaction or on fabric inclusions over a soft subgrade, post-yield gauges can be used that remain operational up to a strain of 10 percent.

INSTRUMENT CALIBRATION

The calibration procedures for the pressure cells and strain coils in a subgrade and granular material (maximum particle size 9.5 mm) have been previously described (1,2,4,6) so discussion here is restricted to more recent work in a bituminous material and in a granular material that has a larger maximum particle size. Calibrations of strain gauges have also

Figure 1. Nottingham earth-pressure cell.

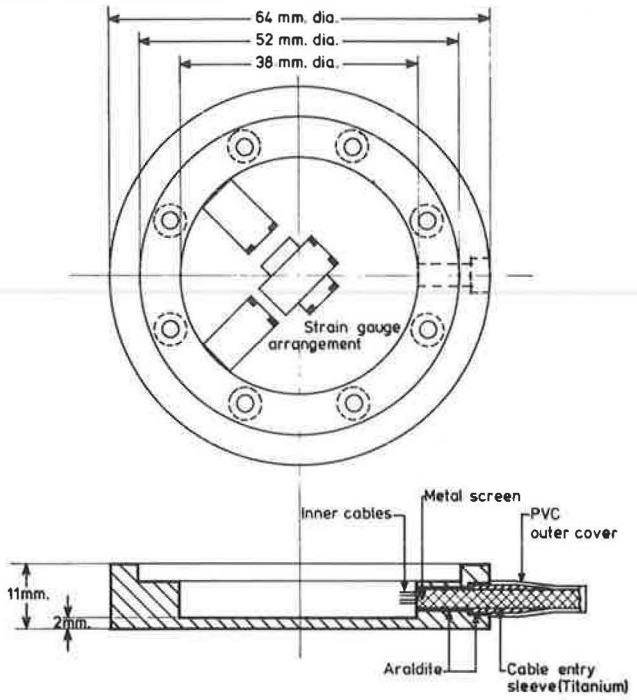

Figure 2. Strain coils.

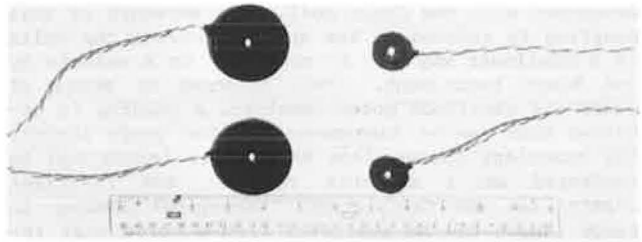

been carried out on a nonwoven fabric. Strain coils have yet to be calibrated in asphalt, but evidence suggests (6,7) that the coils give an accurate representation of the true strains unless a dense or weak pocket develops during installation or some metal is present that will distort the flux linkage between the coils.

Pressure Cell in Crushed Stone

The material involved was a dry, crushed limestone of 40 mm maximum particle size and well graded to the specification for road bases in the United Kingdom (8). The accepted ratio of diaphragm diameter to maximum particle size for pressure cells is 50:1 (9), so clearly the cell shown in Figure 1 was incompatible with this design parameter. To overcome this, fine material was packed over the diaphragm, to protect it from point loading by large particles of aggregate. Thin plastic film held the fines in position, as shown in Figure 3.

A bench calibration, which involves application of fluid pressure directly to the diaphragm (1), and calibrations in several 230-mm diameter triaxial test specimens were then carried out. A cell-registration factor, which is the measured stress divided by a true stress, was thus obtained. The apparatus for in situ calibration is shown in Figure 4, which is the general arrangement for the calibration of both stress and strain transducers. Specimen preparation involved compaction of two layers of aggregate in a mold on a vibrating table prior to installation of the instrument at midheight.

The specimen was load cycled 10 times before testing to improve repeatability and relevance of subsequent results. Increments of vertical load were then applied at various confining stresses and the output of the pressure cell was monitored. The true stress was calculated from the applied load divided by the specimen cross-sectional area. This procedure was repeated after further load cycling was carried out. As the load could only be applied relatively slowly, this exercise was essentially a static calibration, but time effects were unlikely to be significant in dry granular material.

The results shown in Figure 5 indicate cell registrations just below 1.0 at a confining stress of 48 kPa; lower values were obtained with higher confinement. Further load cycling did not have any significant effect at the lower confining stress, but a large hysteresis curve was noted during unloading. These trends were observed for two other specimens, and it was concluded that the prepacked pressure cell could be used successfully in the pavement experiments that involved relatively low confining stresses.

Pressure Cell in Asphalt

The experimental arrangement for pressure cells in asphalt was similar to that in Figure 4, but a continuously graded dense asphaltic material was used. This calibration work was required in connection with a project that involved full-depth asphalt paving (10). Compaction of the asphaltic specimen was by falling hammer. A servohydraulic load test facility was then used to apply static and repeated uniaxial loads to the specimen. Fine material was again placed around the instrument; both a sand asphalt and fines from the asphalt mix were used.

Specimen testing was carried out at various rates of uniaxial loading and a range of temperatures in order to cover a range of mix stiffnesses. A typical set of results is presented in Figure 6, and this also includes the theoretical relationship predicted by Tory and Sparrow (11). Flexibility factor (F) is the ratio of the soil stiffness to cell stiffness and is defined as

$$F = E_s d^3/E_c t^3 \quad (1)$$

where

E_s = Young's modulus of the soil,
E_c = Young's modulus of the cell,
d = diaphragm diameter, and
t = diaphragm thickness.

Higher registrations were obtained compared with the predicted curve when sandsheet was used over the cell, and good agreement can be seen when fines from the actual mix were involved.

In practice, it is best to operate in a stiffness range that gives a cell registration of about 1.0, and on the flat (left-hand) part of the theoretical curve. When practical considerations make this impossible, the theoretical curve may be used. In bituminous mixes and crushed-stone materials, an interface of fine materials is required over the cell diaphragm if the cell dimensions are to be practical, but the material actually used has an influence on the results that needs checking by calibration tests. To obtain good data from these high stiffness applications, it is necessary to know the material stiffness with some accuracy.

Figure 3. Pressure cell prepacked for granular material.

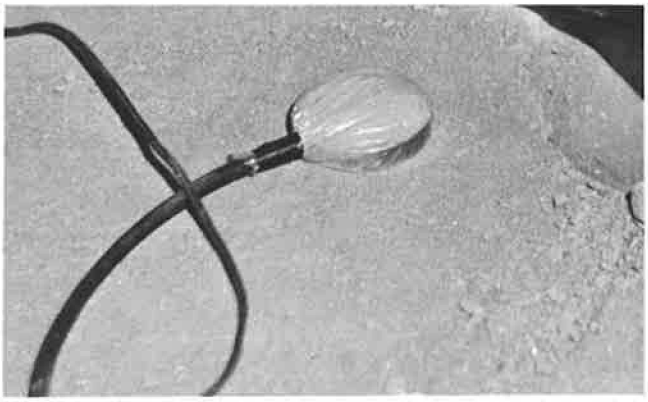

Figure 4. Arrangements for instrumentation calibration.

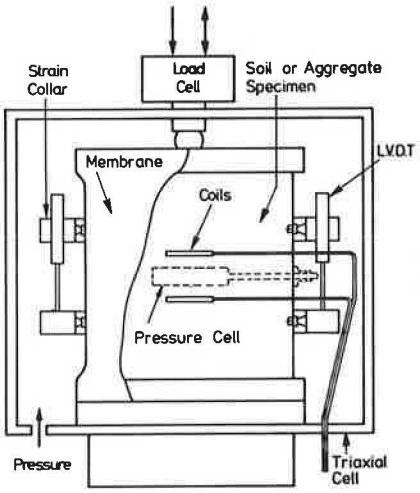

Strain Gauges on Nonwoven Fabric

A series of pavement tests that incorporate fabric between the subgrade and granular layer of a three-layer system (12) required that strains in the fabric due to wheel loading be measured. Coplanar strain coils were used initially and then supplemented with strain gauges. These were 60-mm gauge length post-yield gauges capable of operating up to 10 percent strain and they were attached to the fabric with cyanoacrylate adhesive. Fabric segments were positioned over the gauges for protection and to present the correct surface texture to the adjacent soil. This technique was even more important with strain coils since they would otherwise tend to lock into the soil, and any relative movement between the soil and fabric would not be accurately measured.

Prior to installation, a calibration test was conducted with the gauge on a 200-mm wide strip of fabric, which was clamped between the jaws of a tensile test apparatus (Figure 7). The true or reference strain about the gauge was measured with strain coils. Increments of load were applied to the fabric and the relation between the outputs from the gauge and strain coils is presented in Figure 7. A calibration figure of 2.15 mV for 0.5 percent strain was obtained for the gauge, but beyond this steady readings were difficult to obtain because the fabric tended to creep.

Figure 5. Calibration of pressure cell in crushed limestone.

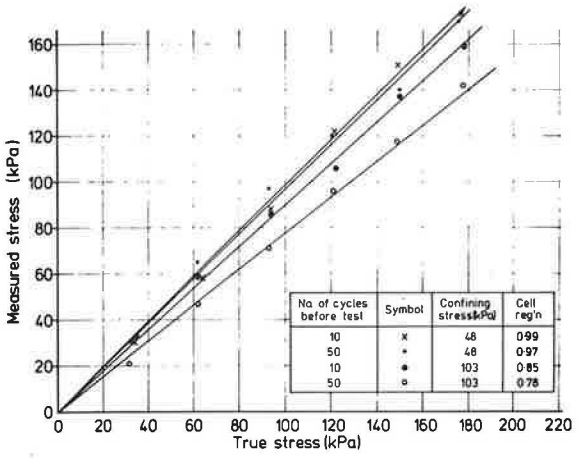

Figure 6. Comparison of theoretical and experimental cell registrations for pressure cell in asphalt.

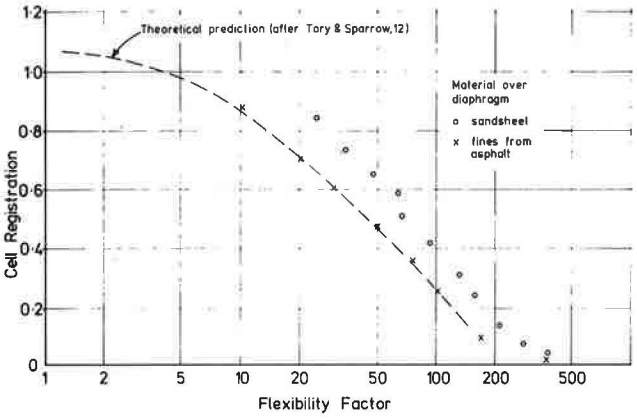

Figure 7. Calibration of strain gauge on fabric.

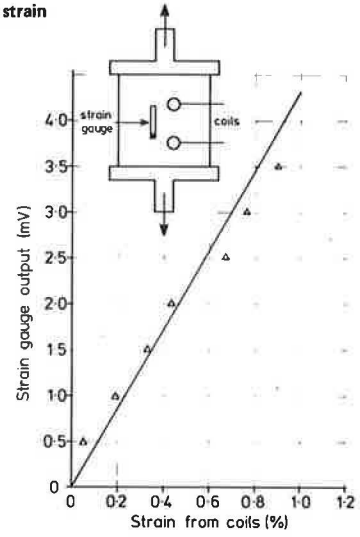

INSTALLATION PROCEDURES

A typical layout of instruments in a three-layer pavement constructed in the pavement test facility (2) is shown in Figure 8. The apparent overcrowding is a function of the reduced horizontal scale since

Figure 8. Typical instrumentation layout in pavement test facility.

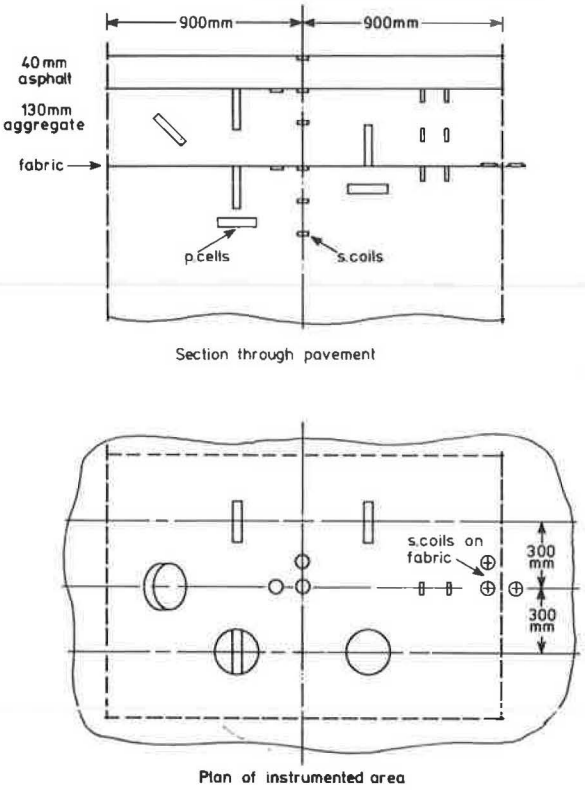

Figure 9. Tools for installation of instruments.

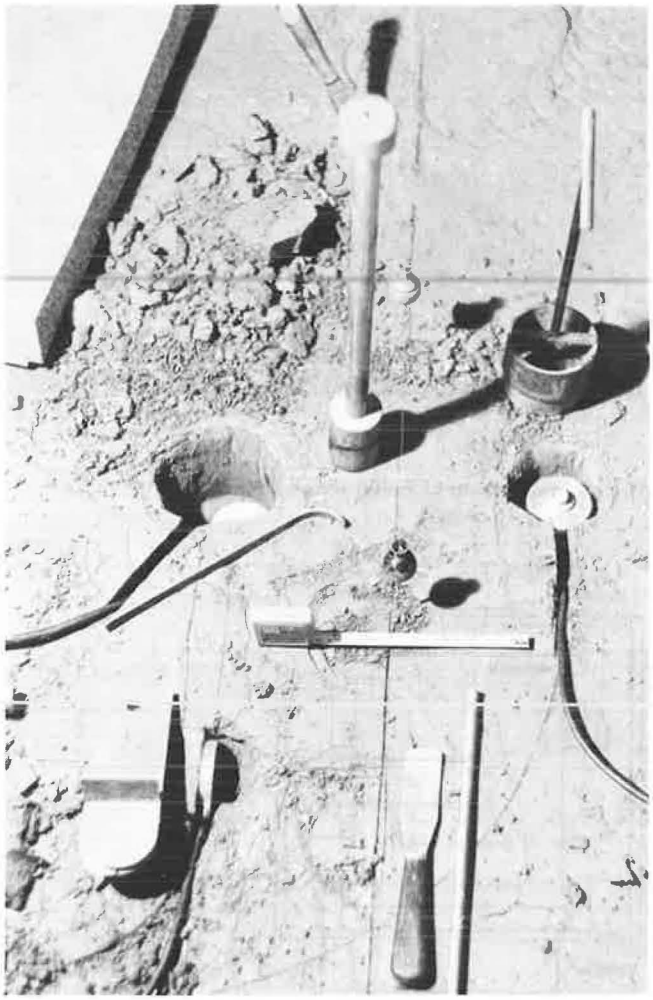

all pressure cells are separated from each other and the strain coil stack by at least 200 mm. Interaction between cells only occurs when they are within two to three diameters of each other (13).

The strain coil stack consists of 25-mm coils separated by approximately 50 mm. Only one pair of coils is energized at a time and the effect of the inactive adjacent coils was found to be negligible during calibration. A set of tools has been developed to bring a measure of consistency to the installation procedure, and these are shown in Figure 9.

Pressure Cells

Because of the destructive nature of the clay subgrade-compaction procedure, the instruments could only be installed on completion of this operation. Holes were then prepared by using special tools (Figure 9) to accept the cell with enough working clearance for backfilling. This is particularly important for the vertically installed cells (for measuring horizontal stresses), as it is necessary to select the soil for placement against the diaphragm. This involves removal of large particles and careful compaction against the diaphragm. The sides of the holes and any backfill layers are scarified to maintain continuity with the undisturbed soil. Attempts were made to achieve the same density in the backfill as in the main soil mass by using the correct amount of soil for the unfilled volume of the hole.

The crushed limestone base was compacted by vibration in layers to a level that only required a shallow hole to accommodate the instrument prepacked with fines held in position over the diaphragm with a thin polythene sheet. Excavations of holes to a specific size are not possible in granular materials and only the minimum amount of material was removed. More fines were used to position the cell in relation to a suspended plumb bob and then the excavated aggregate was carefully placed and hand tamped against these fines before compaction of the next layer of base.

Pressure cells were only used in the asphalt layer for the full-depth tests (10). They were positioned at a layer interface during paving. A hot-hand-compacted sandsheet mix covered the diaphragms for the horizontally placed cells. The vertically oriented cells were positioned in a mound of sandsheet. A quantity of the actual pavement mix was immediately compacted with a ram over the sandsheet in order to integrate the two materials. Paving operations were commenced as soom as possible to establish the satisfactory bond with the interface materials. Calibration tests specifically relating to this installation procedure and the appropriate test conditions yielded a cell registration of 0.97.

Strain Coils

Figure 10 illustrates the installation arrangements for strain coils in various situations. Generally, 25-mm coils were used, but 50-mm coils were occasionally adopted for the coplaner mode since it was felt that they were more likely to resist reorientation during compaction and testing.

A hole was cut in the subgrade with a 37-mm diameter sharpened tube to a depth of 100 mm and then an

Figure 10. Installation of strain coils.

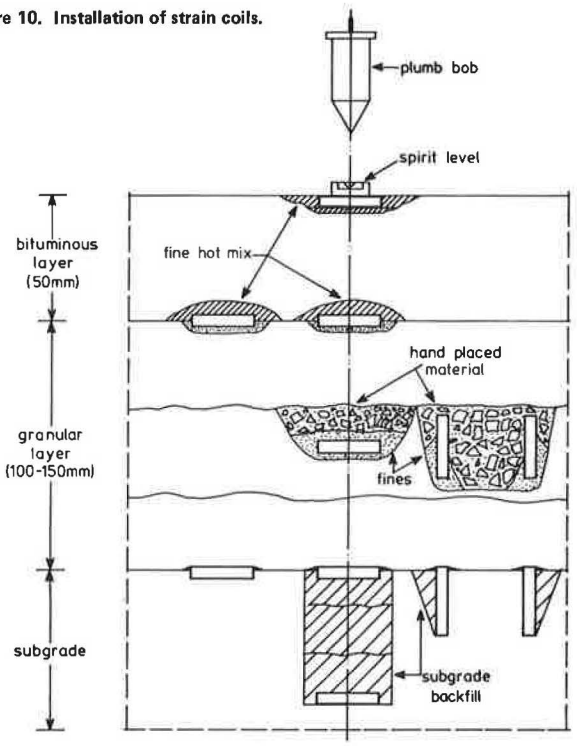

Table 1. In situ performance of instruments.

Instrument	Output	Pavement Layer	Cell Registration	Accuracy
Pressure cells, not amplified	0.5 μV/kPa per V DC	Subgrade	0.95	±10 kPa
		Aggregate	0.98	±30 kPa
		Asphalt	0.97	±30 kPa
Strain coils	Typically 1 percent strain = 2V	Subgrade	1.0	±50 με
		Aggregate	1.0	±100 με
		Asphalt	1.0	±50 με
Strain gauges	0.43 mV/1000 με	Fabric	Direct calibration	±20 με

angled slot that leads to the bottom of this hole was excavated for cable entries. The base of the hole was flattened and a strain coil was gently pressed into this base being positioned by a plumb bob. A circular spirit level was laid on the coil to ensure horizontal placement. Soil from the tube was then tamped in layers over the coil to give 50-mm cover and then the next coil was installed. The sides of the holes and layer interfaces were scarified and an attempt was made to achieve the same backfill compaction, by touch, as the surrounding soil. A third coil was installed level with the subgrade surface and two further coils were placed longitudinally and laterally to provide a coplanar measurement of horizontal strain at the interface. Subgrade material was pressed around the perimeters to lock them into the soil. An alternative to the coplanar arrangement was provided for measuring horizontal strain by placing the coils vertically, in coaxial and parallel alignment (i.e., with the strain coils on edge in slots) (Figure 10).

The strain coils were placed in the granular layer as each lift was completed. It was necessary to set the coils on a bed of fines below the surface of the lift and then add further fines and some larger aggregate as protection from the effects of compaction of the next layer. The final set of coils on the surface of the granular layer was covered with selected fine mix from the hot asphalt just after delivery.

The thickness of the bituminous layer, for the three-layer pavements, was approximately 50 mm, and it was only necessary to glue the top coil of the stack into a recess cut into the surface after the mix had cooled. Grooves for the cables were chiseled out and a fine hot asphalt mix was run in to cover the cables and exposed coils.

Protection of Cables

It is very important to protect instrument cables. They were usually separate or in small groups set in trenches leading to a larger trench away from the test area. Trenches are more difficult to cut in the granular layer and exposed cables can be covered with a mound of fines prior to placement of subsequent material. Braided copper-sheathed cables are normally connected to the instruments and these are inherently robust. Poly-tera-fluoro-ethylene (PTFE)-coated cables are recommended for applications in high temperature. Polyvinylchloride (PVC)-coated cables will melt in hot asphalt but they have been known to survive if protected by a covering of a sandsheet mix that is given time to cool before the next layer is placed.

INSTRUMENT PERFORMANCE

Table 1 summarizes performance data on all the instruments in the pavement test facility. The estimated accuracies were based on work with 11 pavement installations in which the consistency of the readings was examined. Permanent strain accumulated by the strain coils was checked from measurements during pavement excavations (14).

The potential accuracy of these instruments is much greater than the figures indicate in Table 1. The figures in Table 1 take account of the typical scatter obtained from in situ readings obtained in the pavement test facility (1), where stress levels were somewhat higher than may be expected in a full-scale road.

DATA ACQUISITION

To obtain the maximum benefit from pavement instrument installations, a considerable amount of data will be generated. This needs to be converted to stresses, strains, and deformations in a convenient way. The system developed at Nottingham produces results on a printer in appropriate units. Improvements that involve microprocessors or minicomputers could be added later.

Originally, the strain-gauged pressure cells had a DC supply and, because of current limitations, low outputs were obtained. The type of amplifiers that were introduced not only increased these outputs but gave considerable flexibility in terms of the required size of output signal. They were connected to the ultraviolet (UV) recorders by means of galvanometer matching units. The sensitivities of all the pressure cells were then adjusted to an identical level during calibration so that the recorded pulses could be conveniently, quickly, and easily converted to stresses.

Users of the Bison-strain-coil equipment will be familiar with the nonlinear relation between strain and amplitude dial reading. Although this characteristic does not present problems when reading permanent strains, it is a major difficulty for measuring transient values, as the sensitivity varies with the amplitude dial reading. A linearizer unit was developed to overcome this difficulty by providing a constant sensitivity of 1 V for 1 percent strain,

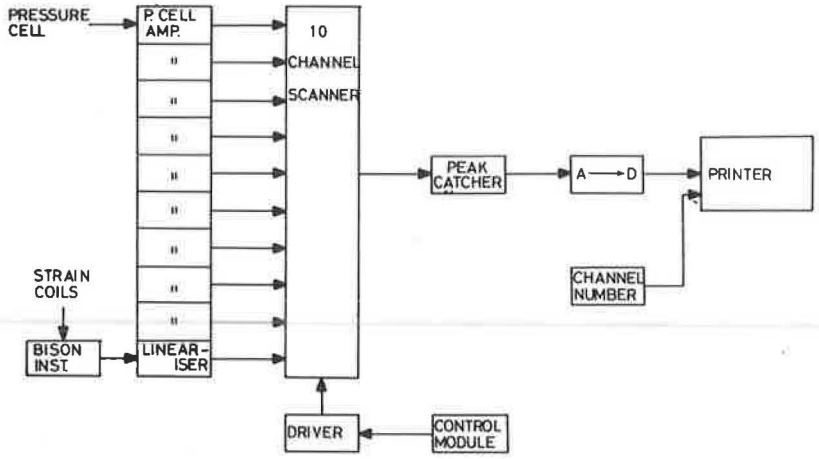

Figure 11. Schematic of data-acquisition system.

although this could be increased to 1 V for 0.1 percent strain if required. Full details of this device are presented elsewhere (12).

This initial processing of signals from pressure cells and strain coils forms the first stage of the data-acquisition systems shown in Figure 11.

The scanner moves automatically or manually from one instrument circuit to the next. In the automatic mode, a pulse from the wheel loading control equipment (1) moves it on so that readings are taken for consecutive wheel passes. Thus, for one pass of the wheel, the output of one transducer will be amplified, caught on a peak catcher, the peak voltage will be converted to a digital signal, and then printed as a stress or strain. It is for this last operation that scale factor controls are necessary to produce a convenient reading such as 600 mV for 600 kPa. Calibration can be carried out through the system and adjustments made to compensate for installation effects. In the tests that we have performed, transient stresses and strains reached reasonably uniform values after about the first 5000 wheel passes and so did not change significantly over the 10 or 20 passes required during scanning by the instrumentation.

CONCLUSIONS

Pressure cells for transient stress measurements in pavements can be used in cohesive soils, crushed rock, and asphalt when suitable techniques are adopted. Pressure cell diaphragms should be protected from the action of large aggregate particles. In crushed rock, this may be done by prepacking the instrument with fine material held in position by a thin plastic film. In asphalt, a fine mix may be compacted over the diaphragm.

The Nottingham pressure cell had a registration close to unity at low confining stresses (48 kPa) but underregistered under greater confinement. The response of the pressure cell placed in asphalt was very similar to that predicted theoretically by Tory and Sparrow (11).

Post-yield electrical resistance strain gauges may be used on fabrics to determine in situ strains. This arrangement was shown to operate successfully up to 1 percent strain and should be capable of measuring higher values up to 10 percent.

Techniques have been developed for the installation of pressure cells, strain coils, and strain gauges in various layers of test pavements by using special tools that cause a minimum of disturbance to the material. Measurement accuracies have been estimated for the various instruments. These depend on the material in which the instrument is to be placed. An electronic unit has been developed to linearize the output from Bison strain coils, thus data acquisition is made easier. A peak hold, scanning, and printing facility has been used to determine transient stresses and strains in pavement experiments.

ACKNOWLEDGMENT

The pavement tests that involved the instrumentation discussed in this paper were carried out in the University of Nottingham's Civil Engineering Laboratories under contract to the European Research Office of the U.S. Army Corps of Enginers and ICI Fibres, Ltd. We are grateful for this financial support and that of our own department under R.C. Coates. The assistance of the electronics workshop staff in the Faculty of Applied Science is also acknowledged with gratitude.

REFERENCES

1. S.F. Brown. State-of-the-Art Report on Field Instrumentation for Pavement Experiments. TRB, Transportation Research Record 640, 1978, pp. 13-28.
2. S.F. Brown. The Measurement of In Situ Stress and Strain in Soils. Field Instrumentation in Geotechnical Engineering, Pt. 1, Butterworths, England, 1973, pp. 38-51.
3. E.T. Selig and O.H. Grangaard. A New Technique for Soil Strain Measurements. Materials Research and Standards, ASTM, Vol. 10, No. 10, 1970, pp. 19-36.
4. S.F. Brown. The Performance of Earth Pressure Cells for Use in Road Research. Civil Engineering and Public Works Review, Vol. 66, 1971, pp. 160-165.
5. E.T. Selig. Soil Strain Measurement Using Inductance Coil Method. Proc., ASTM Symposium on Performance Criteria and Monitoring for Geotechnical Construction, 1974.
6. S.F. Brown and B.V. Brodrick. The Performance of Stress and Strain Transducers for Use in Pavement Research. Science Research Council, Univ. of Nottingham, Nottingham, England, 1977.
7. W.D.O. Paterson. Measurement of Pavement Deformation Using Induction Coils. Road Research Unit, National Roads Board, Bull. 13, Wellington, New Zealand, 1972.
8. Department of Transport. Specification for Road and Bridge Works. Her Majesty's Stationery Office, London, 1976.
9. T. Kallstenius and W. Bergau. Investigations of Soil Pressure Measuring by Means of Cells.

Proc., Royal Swedish Geotechnical Institute, No. 12, 1956.
10. S.F. Brown and C.A. Bell. The Prediction of Permanent Deformation in Asphalt Pavements. Proc., Assn. of Asphalt Paving Technologists, Vol. 48, 1979, pp. 438-474.
11. A.C. Tory and R.W. Sparrow. The Influence of Diaphragm Flexibility on the Performance of an Earth Pressure Cell. Journal of Scientific Instruments, No. 44, 1967, pp. 781-785.
12. S.F. Brown, B.V. Brodrick, and J.W. Pappin. Permanent Deformation of Flexible Pavements. European Research Office, U.S. Army, Univ. of Nottingham, Nottingham, England, Final Rept., June 1980.
13. R. Collins, K.J. Lee, G.P. Lilly, and R.A. Westmann. Mechanics of Pressure Cells. Experimental Mechanics, Vol. 12, No. 11, 1972, pp. 514-519.
14. S.F. Brown, C.A. Bell, and B.V. Brodrick. Permanent Deformation of Flexible Pavements. Report to U.S. Army, Univ. of Nottingham, Nottingham, England, 1977.

Publication of this paper sponsored by Committee on Soils and Rock Instrumentation.